From Gases and Evaporators risk assessmeNt towards an Integrated management of sea and land pollution incidentS

MANIFESTS is a project co-funded by the European Union Civil Protection - DG-ECHO, developed in cooperation with RBINS, CETMAR, IMT Mines Alés, INTECMAR, IST, the UK Security Agency as associated partner and coordinated by CEDRE.

D2.1 Experimental study on evaporation and dissolution

31/03/2026

Work Package 2	
Task 2.1	
Date	31/03/2026
Version	V5
Author/s	JULIE METZGER AND LAURA COTTE
Partners	CEDRE

ACKNOWLEDGEMENT

The work described in this report was supported by the Directorate-General for European Civil Protection and Humanitarian Aid Operations (DG-ECHO) of the European Union through the Grant Agreement number No AMD-101140390-3 corresponding to the Call objective "Enhancing prevention and protection from the effects of maritime disasters" under priority 1: "Developing response capacity for marine pollution".

TABLE OF CONTENT

SUMMARY

This study aimed at generating new experimental data on key transport and fate mechanisms through a series of experimental tests conducted at various scale on methanol, ammonia, methane, cyclohexane and butyl acetate. Specifically, the study focused on the:

1. Evaporation of chemicals from a slick on the water surface (surface release);
2. Dissolution of chemicals as they rise through the water column (underwater release);
3. Partitioning behaviour of chemicals between the air, water column, and surface compartments.

The main findings are:

- Increasing wind speed enhances the mixing of soluble compounds such as methanol into the water column. In contrast, for immiscible substances like cyclohexane, stronger winds primarily accelerate evaporation. For butyl acetate, the effect of wind is more moderate, as the compound remains at the surface with limited dissolution and evaporation.

- Methanol and butyl acetate evaporate faster when pure than when spilled on seawater; cyclohexane shows similar rates in both conditions. This highlights the influence of hydrosolubility on the evaporation process.

- Methanol dissolution in seawater causes a measurable increase in liquid temperature. Additional experiments are required to more precisely quantify the effects of salinity and temperature on the evaporation process.

- The experiments allowed to identify several areas for improvements for CEDRE's wind tunnel and chemistry bench, especially on the spillage systems or overall equipment design.

- The tests confirmed the theoretical behaviours described by the SEBC for cyclohexane (E), methanol (DE) and butyl acetate (FED).

- At low leak rates, methane dissolves nearly completely during its ascent in water, with any bubbles reaching the surface consisting predominantly of N_2 and O_2 from the water. At high leak rates, rapid local saturation significantly reduces dissolution, allowing methane-rich bubbles to reach the surface. Clear differences emerged between bubbles of different sizes: dissolution kinetics depend strongly on the initial bubble volume, with larger bubbles dissolving more slowly.

Operational key points

- High wind speeds significantly increase evaporation rates for all volatile chemicals, raising the risk of toxic or flammable vapor clouds downwind and personnel exposure during response operations.

- Wind direction and speed become critical decision variables for exclusion zones, responder positioning, and air monitoring.

- Methanol (hydrosoluble – DE behaviour): Rapid dissolution into the water column under wind mixing, increases risk of water column contamination rather than surface slicks. Complicated detection and tracking. Priority on water sampling and subsurface monitoring, not only surface surveillance. Risk of evaporation from the water column in case of calm weather conditions.

- Cyclohexane (not soluble in water – E behaviour): Stronger wind leads to faster evaporation: risk of flammable vapor formation, short persistence on the water surface but high atmospheric hazard. Emphasis on air monitoring, ignition source control, and exclusion zones. Cyclohexane evaporates at the same rate in freshwater and seawater.

- Butyl Acetate (Floating, slightly soluble in water – FED behaviour): Moderate wind sensitivity as floating slick persists while slowly evaporating and dissolving. Prolonged surface presence increases risk of chronic exposure, wider spread by currents. Combined surface containment and vapor monitoring required over longer periods.

- Methane underwater gas release: assessment of plume size, rate and depth of the leak is essential for defining safety zones and ignition control.

- Relative vapour densities of the cyclohexane, methanol, butyl acetate are above 1, suggesting that vapours tend to remain above the slick at low wind speed. Hence, care must be taken in case of incidents that would occur in low ventilated places (e.g., inside a ship), especially with cyclohexane regarding its high evaporation rate.

1.Introduction

1.1. Context

Shipping incidents involving Hazardous and Noxious Substances (HNS) that behave as gases or evaporators can pose significant risks to both the environment and public health, particularly when located in ports or coastal waters. New propulsion fuels for ships are being introduced into the maritime industry as cleaner, more sustainable alternatives to traditional fuel oils, in response to growing environmental concerns and increasingly stringent international regulations. Alternative fuels such as ammonia, methanol and Liquefied Natural Gas (LNG), are increasingly being considered and transported, either by bulk carrier or pipeline. As an example, according to the 2024 edition of the world LNG report, global LNG trade grew by 2.1% between 2022 and 2023 to about 401.42 million tonnes (MT). The world's first ammonia bunkering operation was completed in Singapore in March 2024[1], accompanied by studies that provided initial data on hazards and required safety mitigations.

Recent events have emphasised the need to improve preparedness and response measures for managing incidents involving gas clouds.

In 2022, a deadly ammonia leak happened on a Galician fishing boat as two mechanics lost their lives and eight sailors were also injured by inhalation of ammonia[2]. Additionally, the LNG leaks on the Nord Stream pipelines in September 2022[3] are noteworthy, with bubbles at the sea surface ranging from 200 to 1000 metres in diameter and a risk of explosion requiring an exclusion zone of 9 kilometres. These leaks can result in toxic or explosive clouds with the potential to impact multiple bordering States. Given their potential to form toxic, flammable or explosive gas clouds upon accidental or deliberate release, it is of paramount importance to provide accurate information on these substances (e.g., physical and chemical properties, evaporation kinetics, vapour density, etc.). This information is essential in defining appropriate response techniques and guidance, especially in cases of water and air pollution that could affect shoreline communities and the environment at a transboundary level.

[1] Oceans of Opportunity Supplying Green Methanol and Ammonia at Ports Oceans of Opportunity, global maritime forum
[2] Los tripulantes del Albacora Cuatro murieron intoxicados por el amoníaco
[3] https://www.cnbc.com/2022/10/11/nord-stream-gas-leaks-what-happened-and-why-europe-suspects-sabotage.html

1.2. Objectives of the study

The objective of this work is to assess the behaviour and impacts of volatile and gaseous HNS – including new propulsion energies – when released in coastal marine and fresh waters. Two scenarios will be considered: 1) a leakage at the water surface near the shoreline and 2) an underwater leak from a pipeline. The main focus will be on volatile or gaseous HNS releases that may form hazardous gas clouds – flammable, explosive, or toxic to humans.

Different environmental conditions can influence the behaviour of chemicals when they are spilled into the sea, and subsequently the measures taken by responders. The concentration of the chemical in solution, wind speed and ambient turbulence are important factors to be taken into account. Moreover, Corruchaga et al. (2022) used wind speed as one of the parameters in modelling to assess safety distances when responders intervene in the event of an accident involving a toxic pool.

This study aimed at generating new experimental data on key transport and fate mechanisms through a series of experimental tests conducted at various scale on methanol, ammonia, methane, cyclohexane and butyl acetate. Specifically, the study focused on the:

1. Evaporation of pure chemicals and chemicals released onto the water surface (surface release);
2. Dissolution of chemicals as they rise through the water column (underwater release);
3. Partitioning behaviour of chemicals between the air, water column, and surface compartments.

For the water surface release experiment, the evaporation kinetics of each chemical were monitored over time at various wind speeds using the wind tunnel developed in the previous MANIFESTS project (2021-2023). The wind tunnel enables the collection of quantitative data on the evaporation process, i.e., measurements of the evaporation rates for each environmental conditions tested. For the underwater leak experiment, CEDRE's Experimentation Columns (CEC and C^3) were used to assess the rising speed and the percentage of solubilisation of volatile and gaseous HNS, including new fuels. Finally, the partitioning behaviour of chemicals between evaporation and dissolution was assessed using CEDRE's chemistry test bench. The chemistry bench allows the study of the overall fate of spilled chemicals, providing qualitative insights.
The experimental data collected will be used to feed the MANIFESTS HNS database, to improve existing prediction models and to enhance knowledge of chemicals behaviours under different environmental conditions.

2. Material and methods

2.1. Chemicals

The list of chemicals studied is provided in **Table 1**. They were selected based upon their SEBC behaviour, the frequency of transport and the potential hazards associated with transport and storage, as well as the risks for human health. The selected compounds may serve as 'proxies' for other substances with analogous chemical functions. Chemicals identified as 'evaporators' (E) in the Standard European Behaviour Classification (SEBC; Bonn Agreement 1994) in their short-term fate were given priority.

Table 1. List of HNS studied in the lab and associated properties at atmospheric pressure, 20°C.

Chemicals	CAS number	SEBC	Boiling point (°C)	Water solubility (mg/L)	Vapour pressure (kPa)	Density ($Kg.m^{-3}$)	Relative vapour density
Ammonia aqueous (32%)	1336-21-6	DE	38	-	47.4	880	-
Anhydrous ammonia	7664-41-7	DE	-33.33	531000	881.5	681.8 (at -33°C)	0.6
Butyl acetate	123-86-4	FED	126	7240	1.16	881	3.7
Cyclohexane	110-82-7	E	80.7	55	10.3	778	2.9
Methane	74-82-8	G	- 161.52	22	448	0.671	0.55
Methanol	67-56-1	DE	64.6	10000000	12.3	793	1.1

Methane gas was chosen to study the dissolution of chemicals while rising into the water column. The characteristics of the gas are specified in Table 2.

Table 2. Specific characteristics of the gas cylinders used.

	Methane
Purity (%)	≥ 99,995 %
Impurities	H_2O ≤ 5 ppm mol O_2 ≤ 5 ppm mol C_2H_6 ≤ 15 ppm mol C_nH_m autres que C_2H_6 ≤ 5 ppm mol CO_2 ≤ 1 ppm mol N_2 ≤ 15 ppm mol H_2 ≤ 1 ppm mol

2.2. Experimental tools used

2.2.1. Wind tunnel

Assessing the impact of wind speed on the evaporation kinetics requires the establishment of a steady airflow with a controlled mean speed and a known velocity profile. The wind tunnel was built by CEDRE for this purpose.

The experimental set up is displayed in Figure 1. It consisted of a $3000 m^3.h^{-1}$ centrifugal hood fan with a cross-section of 25.4 cm x 29.2 cm placed at the entrance of a plywood tunnel of approximately 4 m long. The fan speed was controlled using a frequency three-phase converter. A 30 cm-thick aluminium honeycomb (Euro-Composites) ensured that the airflow was homogenised with a fully developed turbulent flow. The honeycomb grid shape and porosity had to be selected carefully to ensure that the turbulence generated by the fan was reduced (Cattafesta et al. 2010; Decelle and Nicolas 2017): a hexagonal grid with cell size of 6.4 mm appeared as a good compromise (Hamzah et al. 2021). An opening was built in the floor to accommodate various dimensioned cuvettes inside the tunnel (up to 18 x 23 x 4 cm in which up 1 L of liquid could be evaporated).

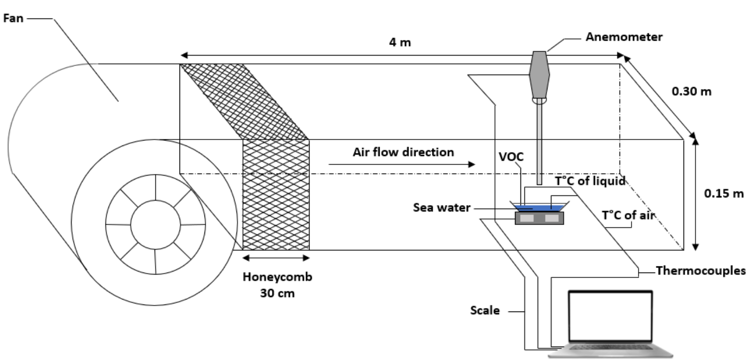

Figure 1. Scheme of the wind tunnel adapted from Heymes et al. (2013).

Tests were carried out in order to compare the results initially collected for pure chemicals during the previous MANIFESTS Project (CEDRE 2023).

In the present study, the evaporation kinetics of the chemicals were assessed following their release at the seawater surface. A 1 L-PP cuvette (surface of $0.036 m^2$) was filled with around 850 mL of seawater and placed on top of the 0.001 g-precision scale (Mettler – Toledo XS1203S) inside the tunnel. A 150 mL volume of chemical was then gently released onto the seawater surface. For pure chemicals, 60 mL of chemical were placed inside a petri dish (diameter of 10 cm, surface of $0.0064 m^2$) and the wind from the wind tunnel was then set on.

The evaporation of the chemical was assessed by recording its mass loss over time. The liquid and air temperatures were measured by four K-type thermocouples (Figure 2).

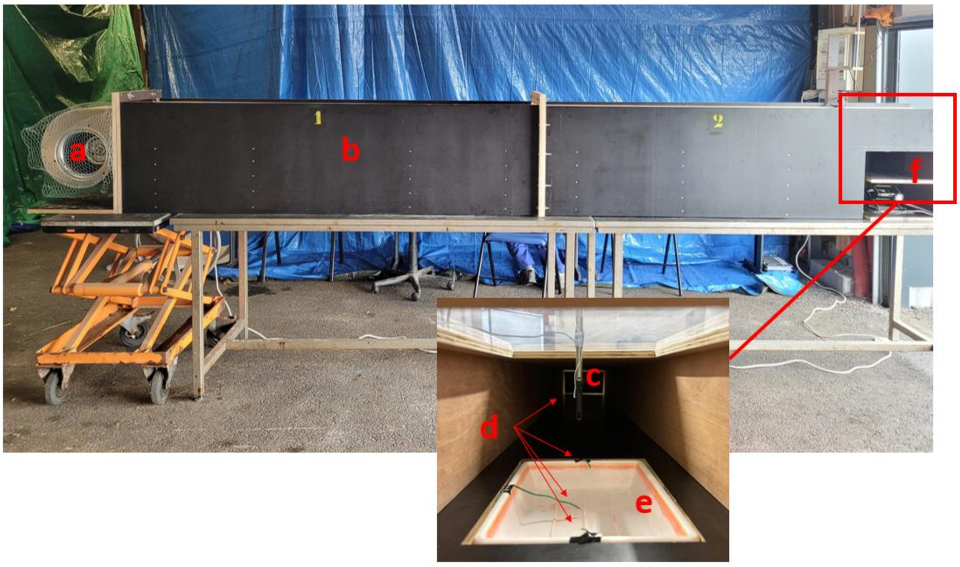

Figure 2. Wide shot of the wind tunnel with a zoomed-in image of the PP-cuvette and the operating sensors inside the gallery (temperature probes and anemometer): a) fan; b) tunnel; c) anemometer; d) thermocouples; e) cuvette and f) room for weighing scale.

Mass and temperature data were recorded in real time at 2 Hz and 1 Hz, respectively. The airflow mean speed was measured using a hotwire anemometer (SEFRAM 9862) placed at 6 cm above the petri dish. Experimental air flow velocities were 3 $m.s^{-1}$, 6 $m.s^{-1}$ and 9 $m.s^{-1}$. No turbulence measurement was performed. However, the dimensionless Reynolds number Re was ranging from 6,300 to 190,000 which is typical of a turbulent flow in a tunnel (CEDRE 2023).

2.2.2. CEC

Experimental setup

The experiments on methane were carried out using CEDRE's Experimental Column (CEC) (Figure **3**). This equipment is used to study the behaviour and fate of gas bubbles, oil droplets or chemicals while rising (or settling down) in the water column. It is a hexagonal column 5 metres in height and 0.8 metres in diameter. The CEC is equipped with four glass windows along its entire height, allowing observations to be made through a camera system used to record the morphological characteristics of the bubbles or droplets.

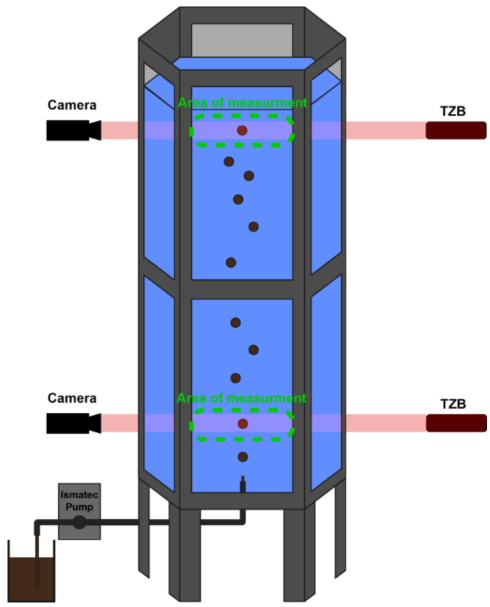

Figure 3. Experimental device for studying the rise of gas bubbles in the CEC – Direct parallel light ombroscopy technique.

For these experiments, the CEC was filled with filtered and UV-treated seawater with a salinity of 33‰. The gas was injected at the bottom of the column by connecting the injection pipe to a pressurised gas cylinder equipped with a pressure regulator and a pressure gauge to control the injection pressure. The optical device is based on the technique of direct parallel light shadowgraphy. This optical technique relies on the visualisation of variations in refractive indices in the medium, revealing non-uniformities in transparent media and thus allowing gas bubbles to be clearly visualised. The device consists of two SVS340 MUGE GigE monochrome cameras with a resolution of 640 x 480 pixels, which are coupled with tele-centric lighting (TZB95-R red LEDs). These cameras have been programmed to record videos at a frequency of 50 frames per second. The resolution of these cameras provides a pixel size of approximately 40 nm and a field of view of approximately 3.3 cm by 2.5 cm.

Experimentation plan

Two injectors of different sizes were used. The aim was to investigate the influence of the initial bubble diameter on the dissolution dynamics within the water column.
In addition, in order to obtain more comprehensive information, the top camera was positioned at two different heights. A series of experiments was carried out with a distance of 72 cm between the two cameras, using only half of the CEC. The second series of experiments was carried out in the entire CEC with a distance of 340 cm between the cameras. For the experiments conducted over the entire height of the CEC, only the 4 mm diameter injector was used to ensure that bubbles diameter remained sufficient at the top of the column for accurate characterisation. The experimental conditions are summarised in Table 3.

Table 3. Experimental conditions used.

# Test	Gaz	Injector internal diameter (mm)	Distance between cameras (m)	Seawater temperature (°C)
1	CH_4	2	0,72	19
2	CH_4	4	0,72	19
3	CH_4	4	3,40	19

2.2.3. Counter-current column (C^3)

The counter-current column (C^3) is a CEDRE tool designed to study the behaviour of particles as they rise through an infinite column of water (Figure 4). Oil droplets or gas bubbles injected at the bottom of the C^3 encounter a downward current coming from the top of the column at the same speed as their ascent. The injection capillary has a calibrated internal diameter of 200 µm in order to generate bubbles with a diameter of approximately 2 mm.

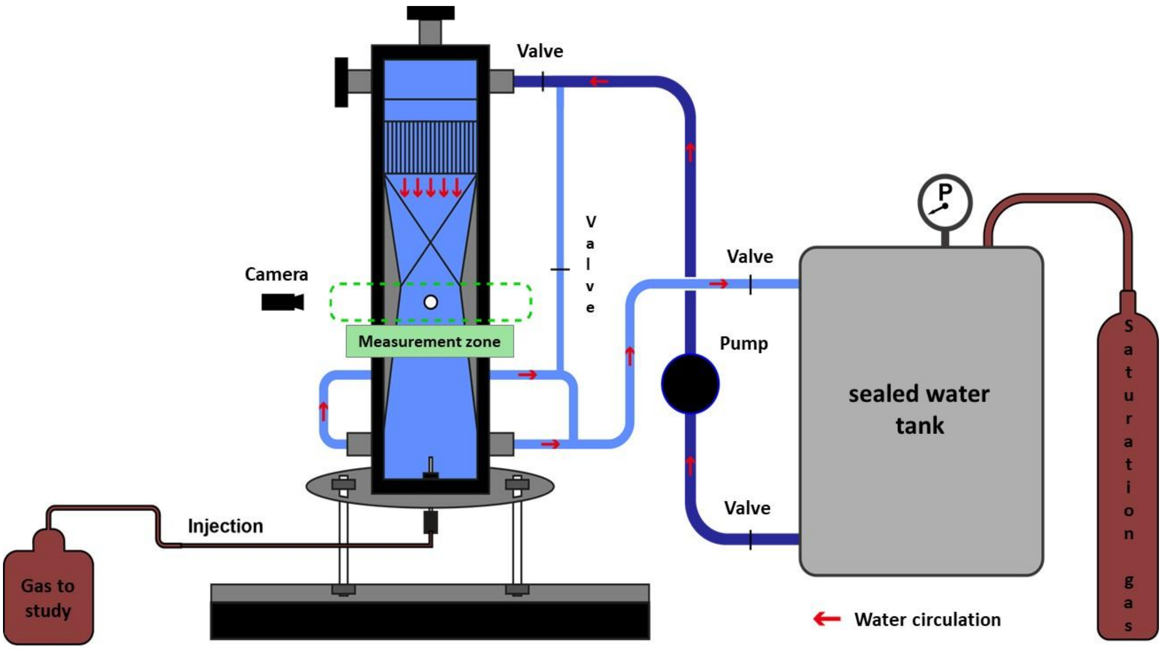

Figure 4. Diagram of the C^3 experimental set up.

The particles immobilised in the measurement zone are characterised using an optical system consisting of a high-frequency camera and a collimated light laser ("shadowgraphy" principle).

The experiments were conducted at a temperature of 15°C. This temperature was maintained constant using a thermoregulator (Teco TC 20 cooling unit). The pump used to create the counter-current is an Eheim submersible pump with a flow rate ranging from 2,500 to 5,000 litres per hour.

2.2.4. Chemistry test bench

This experimental device was used to study the mass transfer kinetics of chemicals from the water surface to both the atmosphere and the aquatic environment under controlled environmental conditions (Giraud et al. 2017). The system enables characterising the evaporation and dissolution processes occurring simultaneously and to identifying which one is predominant. It is designed to recreate the effects of several environmental parameters (water temperature, wind speed and surface agitation). The device is equipped with a 50 cm diameter 316 L cylindrical stainless-steel tank. Part of the tank is made of tempered glass that enables the observation of HNS slicks during experimentations (Figure 5). All tests were performed in filtered and UV-treated seawater. Three chemicals were studied: methanol, butyl acetate and cyclohexane.

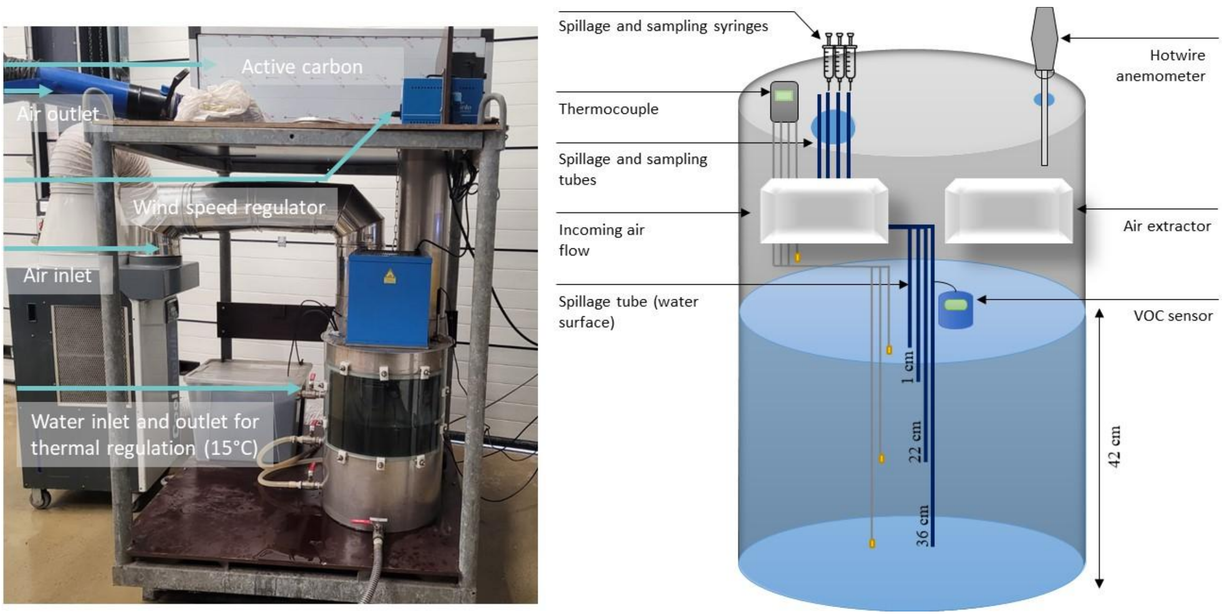

Figure 5. Chemistry test bench.

The volume of seawater introduced in the reactor was of 80 L. The temperature of seawater was set using a SIEBEC M15 external pump connected to a TECO TR20 cooling unit and monitored using three K-type thermocouples immerged in water at various depths (1,22 and 36 cm). The set point temperature was adjusted in order to obtain a temperature of 15 ± 1 °C in the water column. A constant velocity of wind was applied using a ventilation unit and an

Atlantic IP 65 regulator. A hotwire anemometer (SEFRAM 9862) was placed at 5 cm above the water surface to check wind speed during the experiment. It was placed at this height to prevent any splashing onto the hot wire. Air temperature was regulated using a mobile reversible air-conditioning unit CoolMobile E25. A fourth K-type thermocouple was used to monitor the air temperature. Due to the high volatility of the chemicals tested, the UV lamp available to simulate solar radiations was not used. Indeed, the power of the lamp is not adapted to this type of product, and the resulting heat tends to strongly accelerate the evaporation process of the HNS slick.

Three wind velocities (0 m.s^{-1}, 3 m.s^{-1} and 6 m.s^{-1}) were tested. Note that it was not possible to reach zero for the wind speed because of the constant evacuation of the vapours emanating from the slick outside the tank. For information purpose a wind velocity of 6 m.s^{-1} corresponds to 4 on the Beaufort scale and enables reproducing a moderate breeze. As soon as the temperature was stable in the tank, 150 mL of HNS (15 mL for methanol) were poured at the surface of seawater. Concentrations of VOC in the atmosphere were continuously monitored above water using a Photo Ionization Detector (PID) MiniRAE 3000 equipped with a lamp of 10.6 eV. The calibration of the PID was performed with isobutylene and a correction factor was applied, depending on the HNS studied. The air admission tip was placed 10 cm above water surface and VOC concentrations recorded every 10 seconds. The evaporation of the HNS slick was considered as ended as soon as the signal of the PID had reached zero. For methanol, a specific Dräger sensor (Pac Series 8000) was used to monitor the concentration in air.
Water sampling was performed at different times to monitor the solubilisation of the chemical over time (**Table 4**). As methanol is the most soluble compound of the list, samples were collected at higher frequency in the first hour following the spill. Ventilation was let on during each sampling. Samples were simultaneously collected at three different depths using an automatic pump for further analyses by HS-GC-MS as described in 2.3.

Table 4. Sampling times after chemical release.

Chemical	T_1	T_2	T_3	T_4	T_5	T_6	T_7	T_8	T_9	T_{10}	T_{11}	T_{12}
Butyl Acetate	30 s	5 min	15 min	30 min	1 h	2 h	3 h	4 h	5 h	6 h	7 h	8 h
Cyclohexane	30 s	5 min	15 min	30 min	1 h	2 h	3 h	4 h	5 h	6 h	7 h	8 h
Methanol	30 s	2 min	4 min	6 min	8 min	15 min	0.5 h	1 h	2 h	4 h	6 h	8 h

2.3. Analytical method

2.3.1. Methanol - Headspace GC-MS - ALIVION detector

The detection principle involves sampling the gas phase above the sample liquid phase (headspace), followed by separation on a Tenax TA column. Detection of methanol was then performed using a chemo-resistive gas sensor made of SnO_2 particles doped with Pd[4]. The Tenax TA column selectively retains methanol and limits interference from compounds such as ethanol, acetone and hydrogen. The measuring range is of 10 – 999 ppm with an accuracy of 5% and a LOD of 1 ppm. For each analysis, 2 mL of sample was introduced into a vial previously filled with an absorbent. The vial was then screwed on and the extraction was initiated automatically. Following extraction, the sample underwent separation and analysis, a procedure lasting around 2 minutes. The vial was then removed to complete the process. Results are provided in ppm (or mg.L^{-1}).

2.3.2. Analytical method for butyl acetate and cyclohexane

The gas chromatograph (Agilent 7890A, USA) used for the analyses was equipped with a Combipal MPS2 multifunction injector (Gerstel, Switzerland) in split mode. The analysis was performed without any dilution of samples. Briefly, 10 mL of liquid sample were placed in a sealed vial and heated at 60°C until the equilibrium was reached between the liquid and vapor phases. A volume of 1 mL of the vapor-phase mixture was then withdrawn through a 1 mL-gas-tight syringe and transferred to the chromatograph for separation and analysis of the components (Poole 2005). A Rxi-5ms capillary column (Restek) of 30 m length, 0.25 mm in inner diameter and 0.25 µm in film thickness was used. Standard were prepared for the different chemicals. Blanks consisted of natural seawater collected prior to spillage. The limit of quantification (LOQ) was calculated using the accuracy profile method, and the LOD was defined as one-third of the LOQ. The standard ranges were prepared in seawater, and the sample were run without any dilution. The analytical methods for cyclohexane and butyl acetate are presented in **Table 5** and Table 6 respectively.

Table 5. Cyclohexane analytical method.

Analysis method	HS/GC-MS
Internal standard	Methylcyclohexane, 1 mg/L
Standard range	0 to 5 mg/L
Column	HP 5-MS 30m*0.25mm*0.25µm
Detection limit (mg/L)	LOD = 0.03
Quantification limit (mg/L)	LOQ = 0.09

Table 6. Butyl acetate analytical method.

Analysis method	HS/GC-MS
Internal standard	Propyl acetate, 1 mg/L
Standard range	0 to 50 mg/L
Column	HP 5-MS 30m*0.25mm*1µm
Detection limit (mg/L)	LOD = 0.09
Quantification limit (mg/L)	LOQ = 0.31

3. Results and discussion

3.1. Evaporation kinetics studies

The evaporation kinetics of the HNS listed in Table 1 were investigated at pilot-scale using the wind tunnel described in 2.2.1. Tests were performed with pure chemicals and then after being released onto seawater surface. For pure chemicals, the experimental data were fitted with the Brighton's model and showed good agreement with a relative error in the range of 12 to 24 %. The model generally provided lower evaporation rates compared to the experimental ones (Lepers et al. 2023). The different tests conducted and the associated experimental conditions are reported in appendices 0, 4.2, 4.3 and 4.4.
For each experiment, the evaporation fluxes were assessed by dividing the slopes of the mass curves (in g/s) by the surface of the petri-dish or the cuvette where the chemical evaporated (2.2.1).

Evaporation is an endothermic process that absorbs energy, or heat, from the environment, thus lowering the energy level of the medium (Gonczi 2005). For the experiments conducted in this work, the heat loss was not compensated by sufficient heat exchange from the environment (air, solar intake, etc.). This transiently led to a drop in liquid temperature that tended to reduce vapour pressure and, hence, evaporation. This feature was systematically observed, in agreement with previous works (Braconnier et al. 2008; Heymes et al. 2013; CEDRE 2023).

3.1.1. Experimental wind velocity profile

The wind speed profile can generally be described by a logarithmic curve in neutral atmospheric conditions (Laporte 2010; Oke 1987). In other words, the horizontal wind speed increases with increasing altitude – being generally slower near the ground or sea surface – and reaches its maximum at the atmospheric boundary layer (Oke 2002). Such velocity profile depends on the roughness of the terrain and directly impacts mass transfer mechanisms at the surface of HNS slicks (Figure 6): the higher the wind speed over the HNS slick's surface, the faster the mass transfer to the atmosphere. In order to know where to monitor wind speed during the experiment, the experimental wind velocity profiles inside the wind tunnel were investigated.

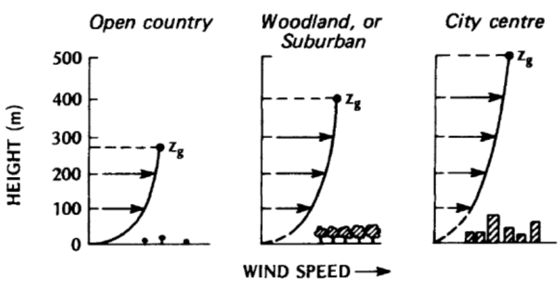

Figure 6. Variation of the wind velocity profile with surface roughness Z0 (Davenport 1965; Oke 2002).

The results showed parabolic profiles, resembling the effect of two ground surfaces, where two logarithmic regions developed and converged at the tunnel's centreline. Inside the tunnel, the maximum wind speed was reached between 6 and 8 centimetres above the cuvette (Figure 7). The flow pattern generated was typical of a turbulent flow (2.2.1).

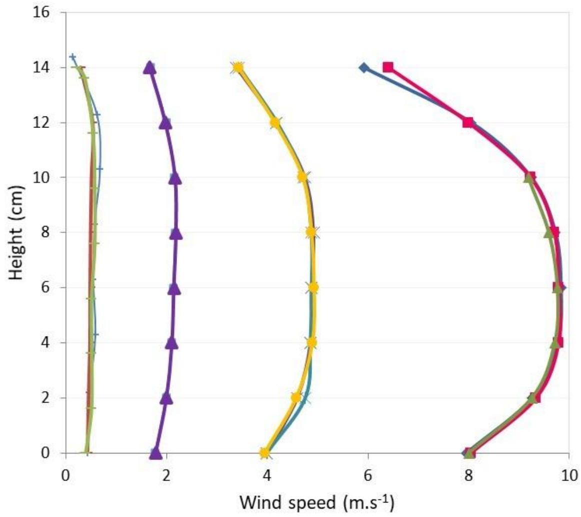

Figure 7. Experimental wind velocity profile in CEDRE's wind tunnel.

To prevent potential damage from splashes, the anemometer was thus placed at 6 centimetres high, where the wind speed was maximum. The wind perceived at the surface of the chemical slick was therefore slower than the measurement recorded by the anemometer. The margin of error was calculated based on the experimental wind profile and reached 18 % on average, and the experimental wind speeds corrected accordingly (Table 7).

Table 7. Actual wind speed above the slick in the wind tunnel.

Anemometer measurement (m/s)	Error (%)	Observed wind (m/s)
3	17	2,5
6	18	4,9
9	18	7,4

3.1.2. Seawater evaporation

A volume of 1 L seawater was left evaporating at different wind speeds: 3, 6 and 9 m/s corresponding to 2,5; 4,9 and 7,4 m/s respectively. A linear mass loss was observed for all the three conditions ($R^2 \geq 0.97$; Figure 8).

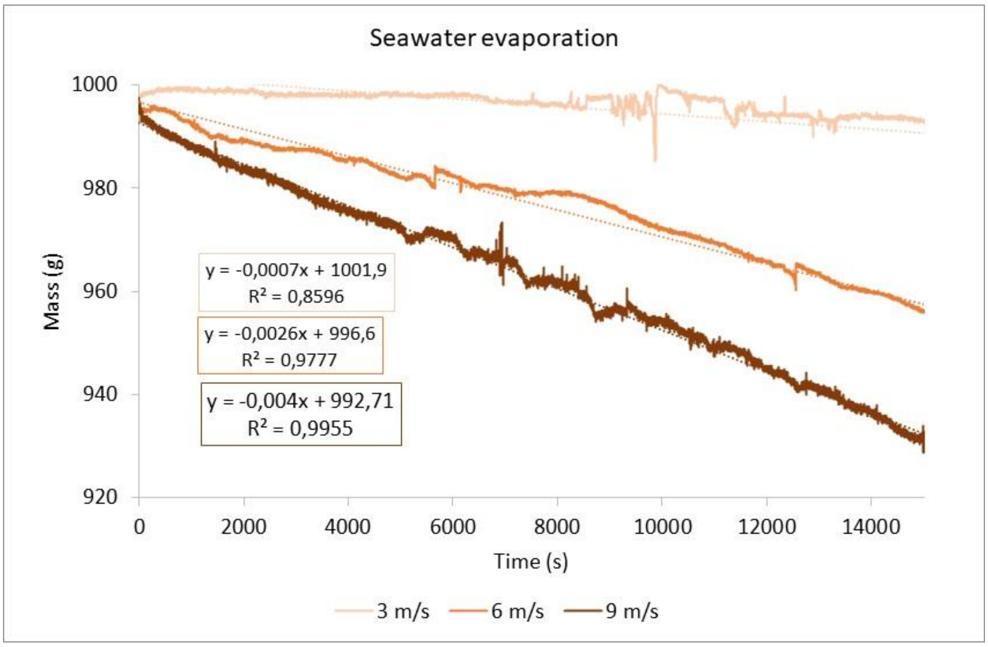

Figure 8. Evaporation of 1 L of seawater under different wind conditions (3, 6 and 9 m/s) in CEDRE's wind tunnel.

The evaporation fluxes were calculated by dividing the experimental slopes by the cuvette surface. Results are reported in Table 8.

Table 8. Evaporation fluxes of seawater alone under different wind speeds.

Wind (m/s)	Evaporation flux (g/m²/s) x 10^{-1}
3	0.2
6	0.7
9	1.1

The evaporation fluxes were 0.2×10^{-1} g/m²/s, 0.7×10^{-1} g/m²/s and 1.1×10^{-1} g/m²/s at 3, 6 and 9 m/s, respectively. No decrease in liquid temperature attributable to evaporation was observed. The experiments were conducted at an average air temperature of 20 °C. Overall, seawater evaporation remained moderate; however, wind speed had a clear influence on the evaporation rate, with stronger winds promoting faster evaporation, consistent with previous tests (CEDRE 2023).

3.1.3. Methanol

Pure methanol evaporation

The evaporation of pure methanol was studied by pouring 60 mL into a glass petri dish (10 cm diameter) positioned inside the wind tunnel with the wind set at three different velocities: 3, 6 and 9 m/s. The mass loss of methanol as well as its temperature were recorded continuously as described in 2.2.1. The gaps observed in mass curves correspond to automatic internal adjustments carried out by the weighting scale during the experiments (Figure 9).

At a wind speed of 3 m/s, a 12°C temperature decrease was observed for the liquid at the beginning of the experiment (Figure 9). This corresponds to the strongest phase of the evaporation process. Similarly, a temperature drop of 15°C was recorded at 6 and 9 m/s (Appendix 4.1.1.).

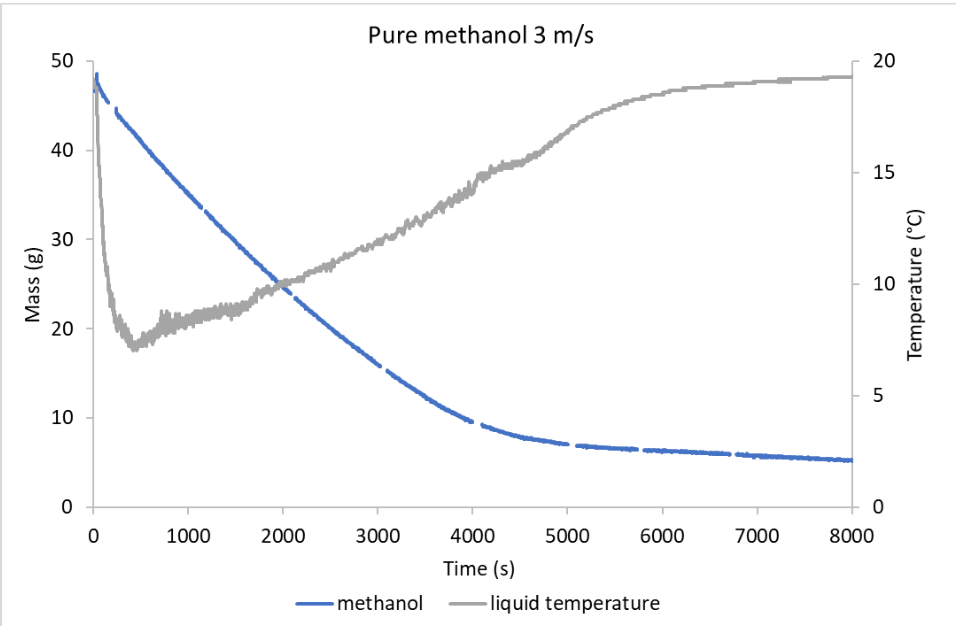

Figure 9. Evaporation of pure methanol (60 mL) at a wind speed of 3 m/s. Liquid temperature drops by 12 °C in the first 500 s, due to methanol evaporation.

Pure methanol generally exhibited a linear mass loss over time, which eventually reaches an inflection point, indicating a progressive reduction of the evaporation rate.
When only 20 to 30 % of the methanol volume remains in the dish, the evaporation rate indeed decreases due to the reduced surface area of methanol in contact with air. The residual methanol tends to adhere to the sides of the dish, further slowing the evaporation process. Additionally, the decreasing temperature contributes to a further reduction in the evaporation rate. The evaporation process can be divided into two stages – separated by the inflection point – which

corresponds to the volume of methanol becoming too low to behave like an ideal pool in contact with air. The initial portion of the evaporation curves were fitted using a linear model (Figure 10).

Mass also decreased faster with increasing wind velocities as evidenced by steeper slopes (Figure **10**). This shows that an increase in wind velocity generally involves higher evaporation rates (Table 9). The inflection point is also reached faster with increasing wind speeds. At 3, 6 and 9 m/s, the inflection point is reached after 4 000 s, 3 000 s and 2 200 s, respectively.

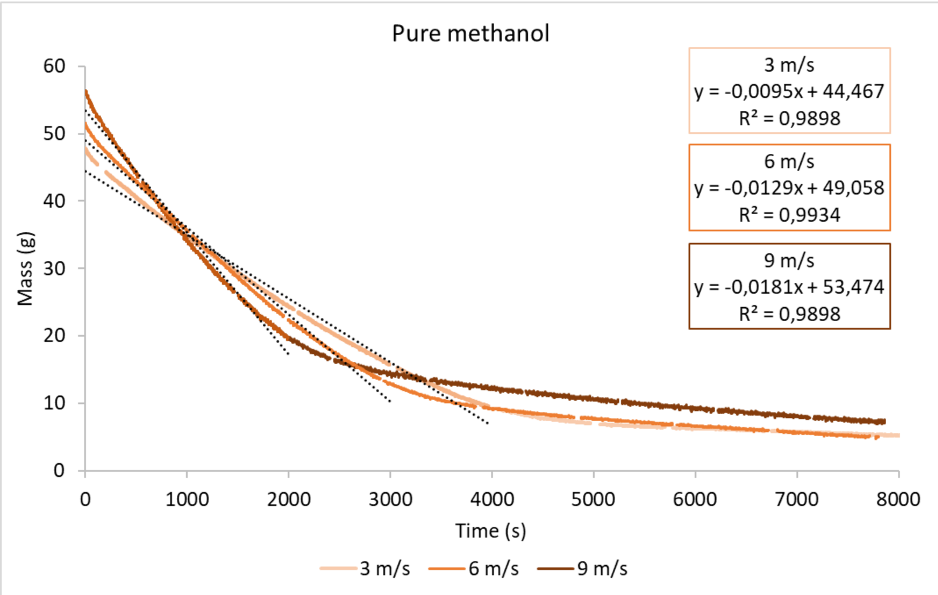

Figure 10. Pure methanol evaporation (60 mL) at 3, 6 and 9 m/s wind speed.

In all cases, the evaporation of pure methanol is significant during the first hour, and enhanced by higher wind speeds. The experimental evaporation rates (Table 9) were calculated by dividing the experimental slopes of mass loss by the surface area of the petri dish.

Table 9. Experimental evaporation rates for pure methanol at different wind speeds.

Wind (m/s)	Evaporation flux (g/m²/s)
3	1,48
6	2,02
9	2,83

Methanol evaporation when released in seawater

According to the SEBC Code (Bonn Agreement 1994), methanol is a DE (dissolver evaporator) which is fully soluble in water and remains in subsurface due to its very low density (0.791) compared to seawater. This section focuses on the evaporation of a water-methanol mixture, prepared by pouring 150 mL of methanol into approximately 800 mL of seawater. When the methanol is released at seawater surface, both solubilisation and evaporation happen. Solubilisation causes the liquid temperature to increase, while evaporation leads to its cooling. The two processes are competing at the initial stage of the experiment. Different increases in temperature were observed depending on the wind speed. Under wind conditions of 3 m/s (Figure 11) and 6 m/s (Appendix 4.1.2), a similar rise of around 10 °C was observed both at the bottom and at the surface immediately after methanol was spilled. Then, the temperature decreased and homogenised between the surface and the bottom.

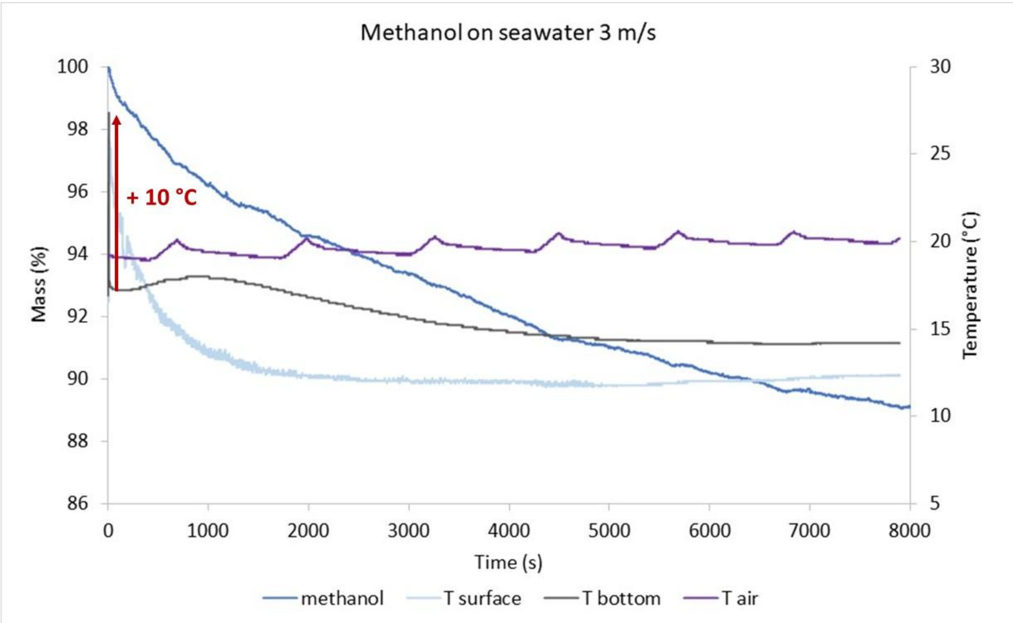

Figure 11. Evaporation of 150 mL of methanol released at seawater surface at a wind speed of 3 m/s. The increase of liquid temperature at the surface and bottom (+10°C) can be attributed to methanol solubilisation.

At a wind speed of 9 m/s (Appendix 4.1.2), methanol solubilisation initially causes the surface temperature to rise by 8 °C (from 18.5 °C to 26.5 °C). A smaller increase of 0.7 °C also occurs at the bottom of the mixture, 1 000 s after the spill. As the wind is stronger than in the two previous experiments, it is likely that evaporation of methanol is favoured in the early stages, delaying its solubilisation in water. Then, the temperature drops and becomes uniform between the surface and the bottom, as observed at 3 and 6 m/s.

As with pure methanol, the evaporation is faster with increasing wind speeds, especially in the first seconds of the experiments, where the evaporation rates are the highest (Figure 12). Some methanol may evaporate directly after being spilled, followed by the evaporation of the seawater-methanol mixture, with further methanol volatilization.

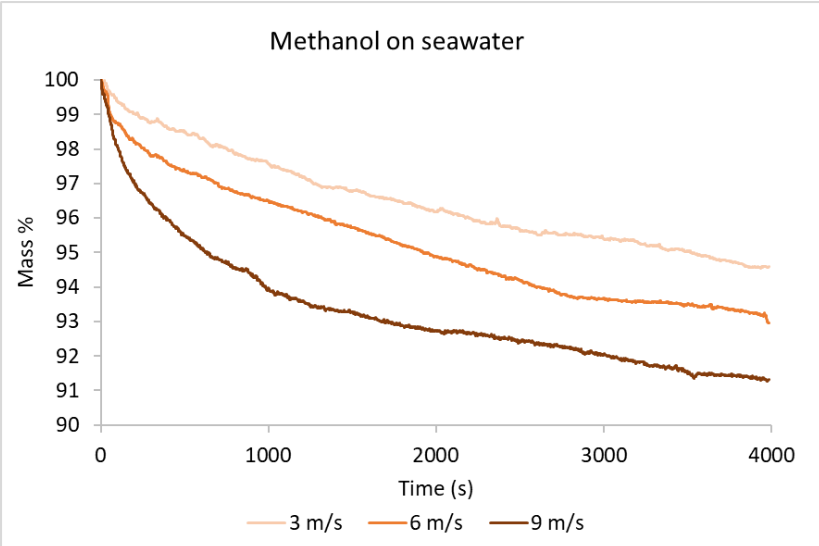

Figure 12. Evaporation of 150 mL of methanol released onto seawater surface at three different wind speeds (3, 6 and 9 m/s). The impact of wind is greater during the first seconds of the experiments.

It was assumed for each experiment that the initial segment of the mass loss curve (grey portion on Figure 13) most likely corresponds to pure methanol evaporation. The slope of this segment was divided by the cuvette surface area to calculate the experimental evaporation flux in g/m²/s. When this segment could not be distinguished and the overall mass loss displayed a linear trend, the entire curve was used to estimate the evaporation rate. The evaporation fluxes are of 1.2, 2.4 and 7.2 g/m²/s for 3, 6 and 9 m/s, respectively (Table 10).

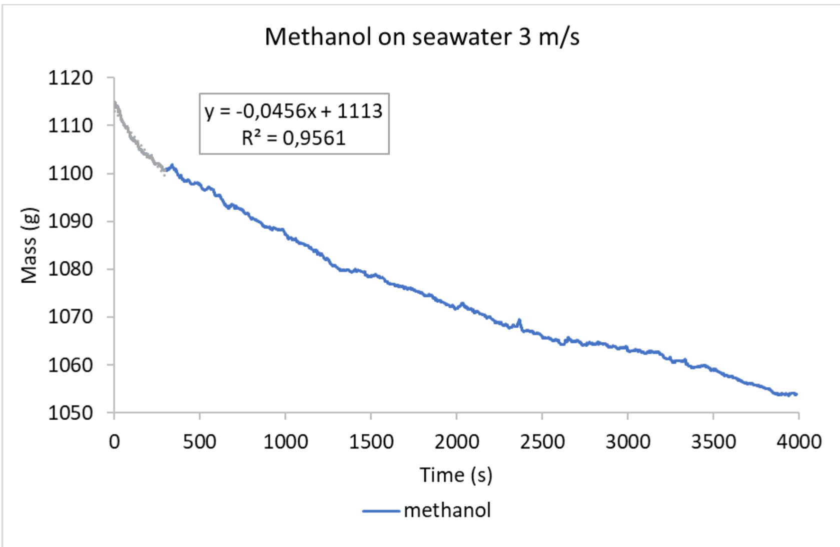

Figure 13. Example of evaporation rate calculation: the slope of the grey part (g/s) is divided by the cuvette surface to obtain the experimental evaporation flux in g/m²/s.

Table 10. Experimental evaporation fluxes (g/m²/s) of 150 mL of methanol on seawater.

Wind (m/s)	Evaporation flux (g/m²/s)
3	1,2
6	2,4
9	7,2

The evaporation fluxes are greater with increasing wind speeds, in agreement with the previous tests presented above.

Comparison Pure - On seawater

To assess the effect of seawater on methanol evaporation, 60 mL of methanol were poured onto the seawater surface and allowed to evaporate (see Appendix 4.1.3), and the results were compared with the evaporation of 60 mL of pure methanol. The evaporation fluxes are displayed in Figure 14, with the corresponding numerical values summarized in Table 11. On average, the evaporation rate of pure methanol was found to be 74 % higher than that of methanol released in seawater. This result suggests that dissolution is the dominant process occurring against evaporation when methanol is poured on seawater.

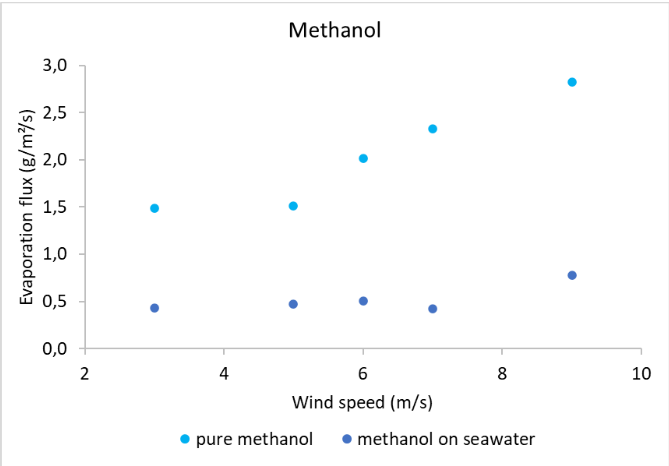

Figure 14. Evaporation rates of 60 mL methanol pure (light blue) and on seawater (dark blue).

Table 11. Evaporation fluxes of 60 mL methanol on seawater or pure.

Wind speed (m/s)	Evaporation flux	Evaporation flux pure	difference %
3	0,43	1,5	71
5	0,50	1,5	66
6	0,47	2,0	77
7	0,42*	2,3	82
9	0,78	2,8	72

*Average value from two experiments.

Methanol evaporation when released in freshwater

Additional tests were conducted in freshwater to compare the evaporation rates with those measured in seawater. To do so, 60 mL of methanol were released in freshwater and put to evaporate under 3, 6, 9 m/s wind speed, with air temperature around 20 °C. The results were compared with the same experiments realised with 60 mL methanol poured onto seawater. Mass curves can be found in appendix 4.1.4.

As observed for methanol released in seawater, both the surface and bottom liquid temperatures increased in all experiments, rising by 1-4°C. It can also be seen that the bottom temperature rise is the highest (+ 4 °C) and fastest at 9 m/s (Figure 15), supporting the fact that a stronger wind promotes the solubilisation of methanol.

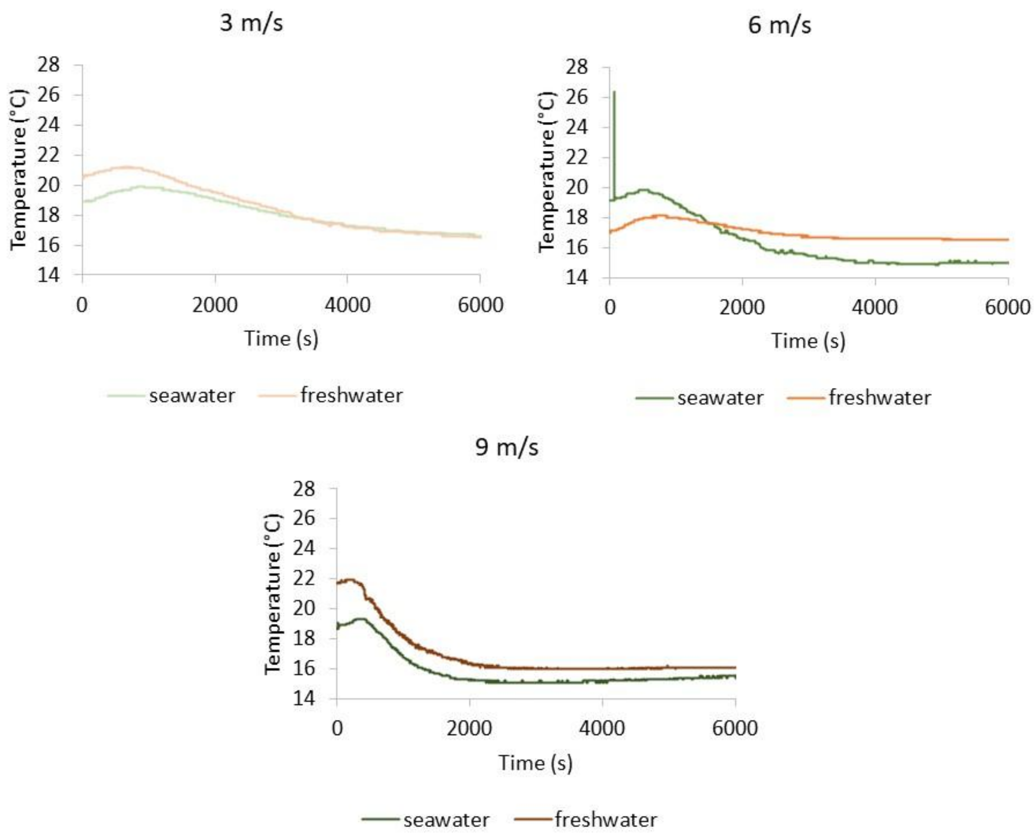

Figure 15. Bottom temperatures of 60 mL methanol poured onto freshwater (red shades) and seawater (green shades) at different wind speeds.

The increases in liquid temperature are relatively similar in freshwater and seawater (Table 12), suggesting that water salinity has little effect on methanol dissolution.

Table 12. Temperature increases for 60 mL methanol poured in freshwater or seawater.

wind (m/s)	surface temperature in freshwater (°C)	surface temperature in seawater (°C)	bottom temperature in freshwater (°C)	bottom temperature in seawater (°C)
3	+7.3	+6.6	+0.7	+1
6	+6.7	+6.8	+1.1	+0.7
9	+6.8	+6.5	+0.5	+0.6

Regarding the evaporation fluxes, the experiments did not show any clear trend indicating that water salinity affects methanol evaporation (Figure 16).

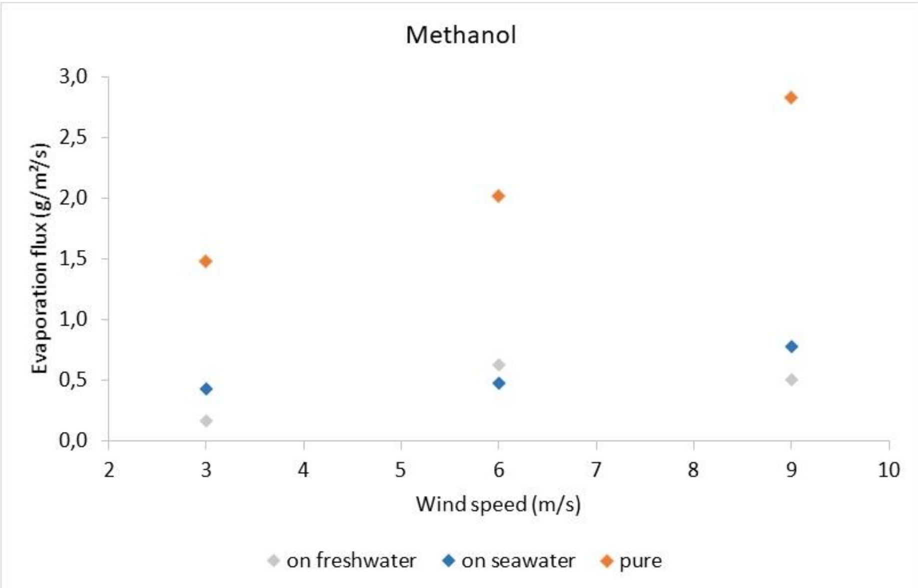

Figure 16. Evaporation rates of 60 mL methanol on seawater (blue), freshwater (grey) and pure (orange).

Yet, a greater solubilisation of methanol would be expected in freshwater, meaning a lower evaporation rate than in seawater. This was observed for two of the three experiments conducted (3 and 9 m/s wind), whereas the experiment at 6 m/s showed relatively close evaporation rates (**Table 13**; Figure 16). Some uncertainty in the evaporation rate estimates may also indues minor errors.

Table 13. Evaporation fluxes of 60 mL of methanol on seawater or on freshwater.

Wind (m/s)	Evaporation flux on freshwater	Evaporation flux on seawater
3	0.166	0.434
6	0.629	0.474
9	0.502	0.781

3.1.4. Cyclohexane

Pure cyclohexane evaporation

A volume of 60 mL of cyclohexane was left evaporating at 1, 3, 5 and 7 m/s wind speed (Appendix 4.2.1). For all the experiments, the cyclohexane temperature dropped in the first 200 s and kept decreasing over time. Temperature drops were in the range of 11 to 14 °C. Except at a wind speed of 1 m/s, where cyclohexane cooled by 9 °C, the temperature drop was such that it reached a temperature close or below 6 °C, i.e. below cyclohexane's melting point (6.5 °C, HNS-database). Once again, the evaporation fluxes increased linearly with the wind speed (R^2 = 0.92), consistently with previous observations (Figure 17).

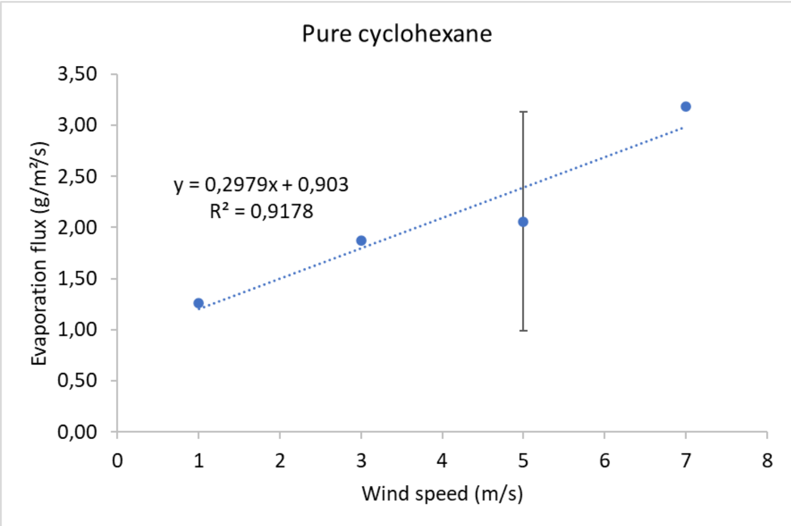

Figure 17. Pure cyclohexane evaporation rates at different wind speeds (60 mL). The evaporation rates follow a linear trend (R^2 = 0.92) with increasing wind speeds.

The experimental fluxes are reported in Table 14. The average value at 5 m/s was calculated as 2.06 ± 1.07 g/m²/s from the evaporation rate values obtained in three experiments. The relatively large uncertainty can be attributed to limitations in the experimental setup, particularly the weighing scale, which did not ensure high repeatability of the measurements.

Table 14. Experimental evaporation fluxes of 60 mL pure cyclohexane.

Wind (m/s)	Experimental flux (g/m²/s)
1	1,26
3	1,87
5	1,24
5	4,18
5	0,76
7	3,18

Cyclohexane evaporation on seawater

A volume of 150 mL of cyclohexane was poured onto seawater surface at 3, 6 and 9 m/s. Due to its low solubility in water (0.055 g/L) and its high vapour pressure (10.3 kPa), the chemical is expected to form a slick onto the sea surface, and evaporation is likely to be the dominant process controlling its fate. Tests were also carried out with 60 mL of cyclohexane released onto seawater at 1, 3, 5 and 7 m/s. The results are presented in appendix 4.2.2.

When a volume of 150 mL of cyclohexane is released, it appears that higher wind speeds lead to a greater and more transient decrease in surface temperature, occurring over a shorter timescale. A decrease in surface temperature due to evaporation was indeed observed across all three wind speeds tested, ranging from 8 to 10 °C (10 °C at 3 m/s, 8 °C at 6 m/s, and 9 °C at 9 m/s), with the surface temperature reaching 5.1, 3.5 and 3.7 °C at 3, 6 and 9 m/s, respectively (Appendix 4.2.3.).

The freezing of the cyclohexane surface slick also affected bottom temperatures, which decreased by 6 °C at 3 m/s and by 4 °C at 6 and 9 m/s, consistent with observations for pure cyclohexane. The bottom temperature changes appear more important at the lowest wind speed, likely because the slick freezes more slowly than at higher wind speed (lower evaporation rate). This slower freezing prolongs the evaporation of the slick and cyclohexane crystals formation, allowing the cooling effect to last longer and to propagate to the bottom of the cuvette.

Regarding the evaporation rates, the mass loss curve seems to be divided in two distinct phases (Figure 18). In theory, the first phase of mass loss would correspond to cyclohexane alone, while the second phase – highlighted by the inflection point – would involve the evaporation of a mixture of cyclohexane and seawater as the slick fragments, with the share of seawater evaporation increasing over time. This theory is further explored in the following section.

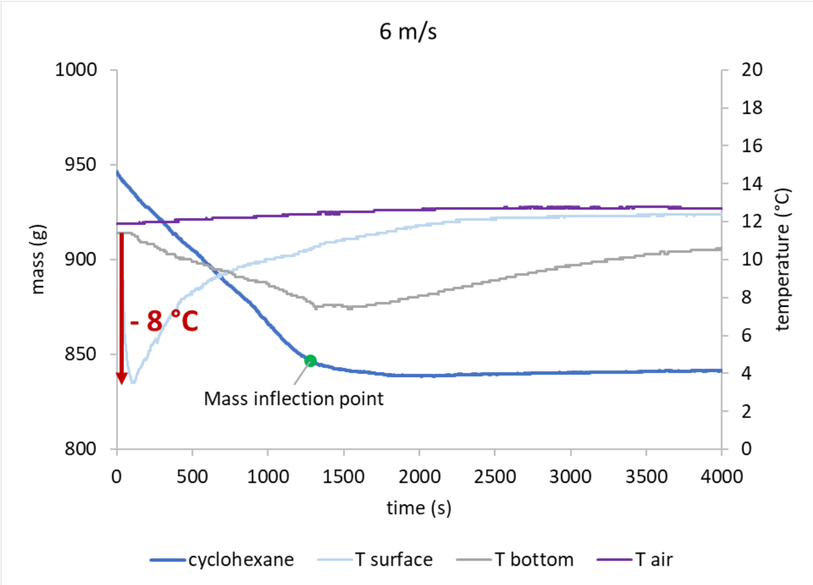

Figure 18. Evaporation of 150 mL cyclohexane on seawater, at a wind speed of 6 m/s. Cyclohexane's slick freezing cause surface temperature to decrease in the first seconds of the experiment, followed by the bottom temperature as the deeper water progressively cools down.

The evaporation fluxes were calculated by dividing the slope of the first part on the mass curve (from 0 to 1000 s) by the cuvette surface and are reported in Table 15. Evaporation fluxes increase with wind speed.

Table 15. Evaporation fluxes (g/m²/s) of 150 mL cyclohexane on seawater at different wind speeds.

Wind speed (m/s)	Evaporation flux (g/m²/s) before inflection point	Seawater experimental flux (g/m²/s) $*10^{-1}$
3	2.06	0.2
6	2.16	0.7
9	3.31	1.1

Slick study with colouring agent

To test the above hypothesis, a colouring agent (Red Organol) was added to cyclohexane prior to the spill to monitor the evolution of the slick surface – specifically its fragmentation – over time using video footage to estimate changes in slick surface coverage. The wind conditions tested were 3 m/s, 6 m/s and 9 m/s.

As noticed in experiments without colouring agent, the cyclohexane cooled to temperatures near or below 6 °C i.e., below its melting point (6.5 °C). Similar to the case of pure cyclohexane evaporation, crystals were formed in the cuvette and the surface slick started freezing. Consistently with the other experiments performed on cyclohexane, a greater and more transient decrease in surface temperature was observed at higher wind speeds (light blue curve; Figure 19).

Bottom temperatures also decreased (grey curve; Figure 19) and reached 6 °C (drop of 5 °C) for 3 m/s, 10 °C (drop of 4 °C) for 6 m/s and 9 °C (drop of 4 °C) for 9 m/s. It confirmed that seawater gradually cools down under the influence of the freezing cyclohexane layer. Moreover, as being denser due to the colouring agent, cyclohexane reaches the bottom of the cuvette by capillarity along the thermocouple probe. This could also induce a decrease of liquid temperature at the bottom.

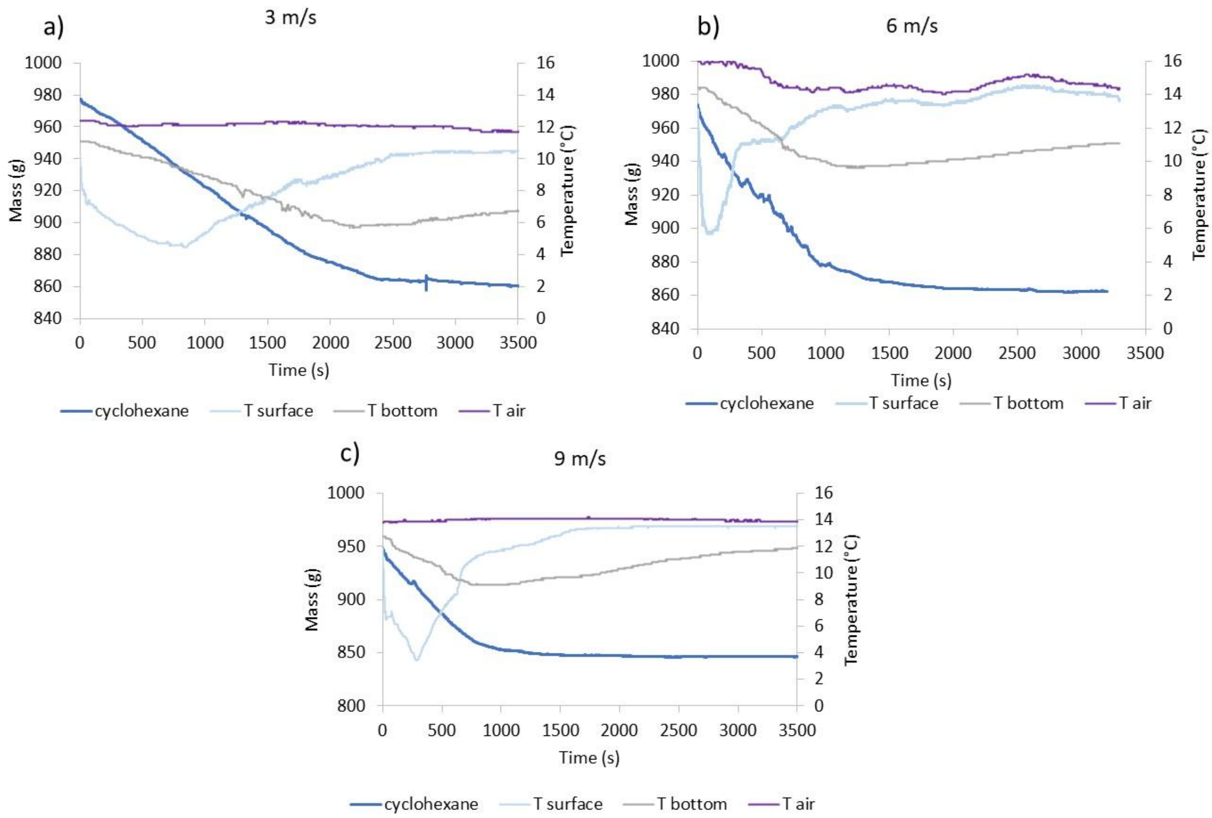

Figure 19. 150mL cyclohexane evaporation on seawater with Red Organol at a) 3 m/s; b) 6 m/s and c) 9 m/s. The decrease in surface temperature is faster and sharper with increasing wind speeds.

Overall, the initial phase of the experiment following the release shows that the cyclohexane slick initially covers the entire surface of the cuvette, before breaking into several fragments that evaporate independently (Figure 20). Hence, it can be hypothesized that during the initial phase where the slick of cyclohexane entirely covers the cuvette, the exchanges at the interface occur primarily between cyclohexane and air (Figure 20a). In the second phase, the cyclohexane slick fragments into several pieces (Figure 20b) that gradually evaporate independently along seawater. Then, some frozen residues remain on the edges of the cuvette until the end of the experiment, suggesting that evaporation at this point is primarily due to seawater (Figure 20c).

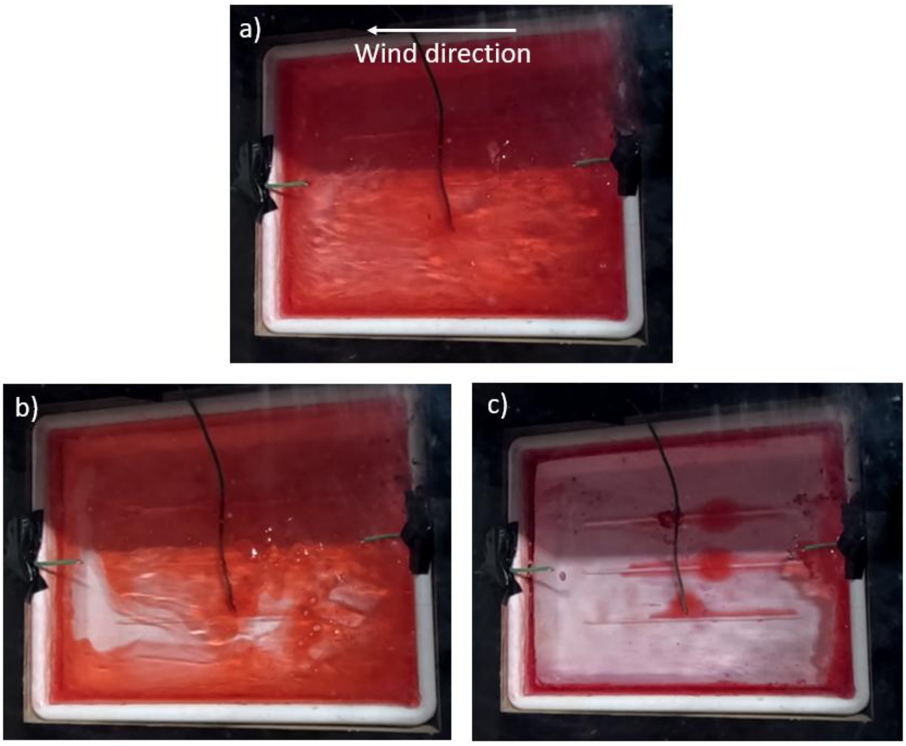

Figure 20. Cyclohexane with Red Organol colouring agent spilled on seawater at 6 m/s: a) 30 s after the spill: the slick is completely covering seawater; b) 13 min after the spill: the slick starts to fragments; c) 20 min after the spill: frozen pieces remain on the edge of the cuvette.

At a wind speed of 3 m/s, the slick starts to break out 1 615 s after the spill (red dots in Figure **21**). By 3 000 s after the spill, only 12 % of the slick persist. The inflection point in the mass curve occurs around 2 420 s (green dot in Figure 21), corresponding to the fragmentation stage, when roughly 22 % of the slick remains.

At 6 m/s, the slick starts to break out 620 s after the spill. Then, after 1 336 s, only few fragments of slick persist, corresponding to 15% of the initial slick surface. The inflection point in the mass curve occurs around 1 000 s, corresponding to the fragmentation stage, when about 20 % of the slick remains on the cuvette.

At 9 m/s, the slick starts to break out 570 s after the spill and only few pieces of slick persist after 1 632 s. The inflection point in the mass curve occurs around 2 400 s when about 18 % of the slick remains on the cuvette. At this speed, the wind has a stronger influence and favours the movement of the slick leading to its faster fragmentation.

In these experiments at three different wind speeds, no inflection point on the mass curve was observed when the slick starts to break into pieces. An inflection point on the mass curve was only observed when about 20 % of the slick remained on seawater.

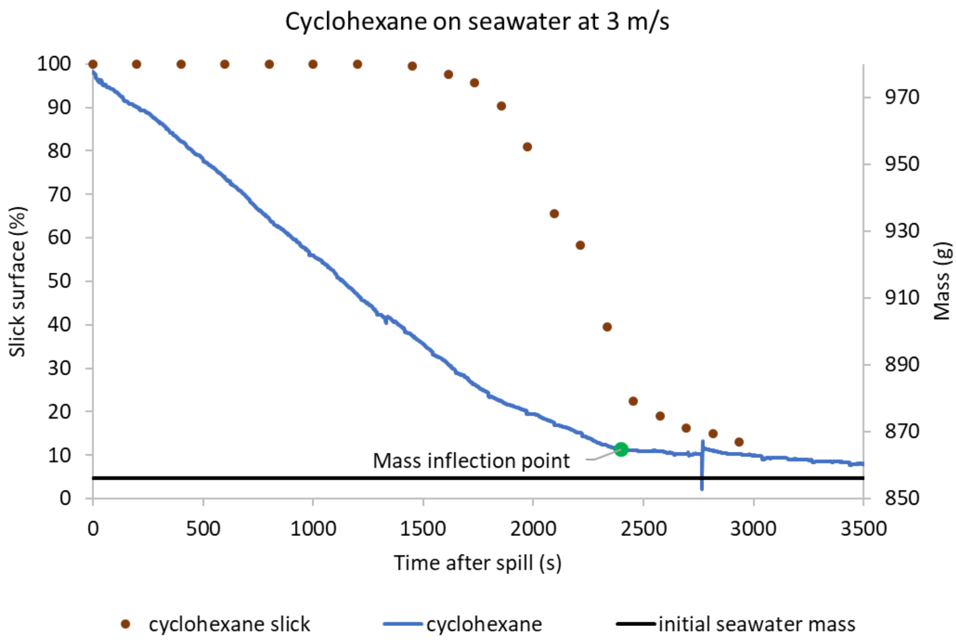

Figure 21. Mass variation of cyclohexane with colouring agent spilled on seawater at 3 m/s wind. Only cyclohexane evaporates until 1 615 s after the spill, before that the slick breaks out. Beyond this point, a mixture of seawater and of the remaining piece of slick evaporates. An inflection point on the mass curve is observed when the slick percentage reaches 20%.

Once the cyclohexane slick has disappeared, only the evaporation of seawater would be expected. Nevertheless, the remaining slick pieces on the cuvette (about 15 % of the slick mass) imply changes in the evaporation. Both the remaining volume of cyclohexane and seawater evaporate simultaneously once the slick starts to break out.

In conclusion, different processes are competing: the cyclohexane slick freezes, while wind promotes its fragmentation through mechanical action. Cyclohexane mostly evaporates in the first 2 000 s after the spill, and the remaining pieces of slick evaporates alongside the seawater. In case of a larger spill in open sea, the freezing of cyclohexane is not likely to happen as the slick will not be constrained inside an enclosed tray as in the experiment.

Comparison Pure - On seawater

Additional tests were conducted to assess the influence of seawater on cyclohexane evaporation. The evaporation of 60 mL of cyclohexane (Appendix 4.2.1) was compared under two conditions: pure and when poured onto seawater. As shown in Figure 22, There is no significant change in the evaporation rates of cyclohexane between experiments on pure chemical and when released into seawater. These results support the conclusion that cyclohexane evaporates predominantly during the initial phase of the water–cyclohexane mixture, without significant dissolution.

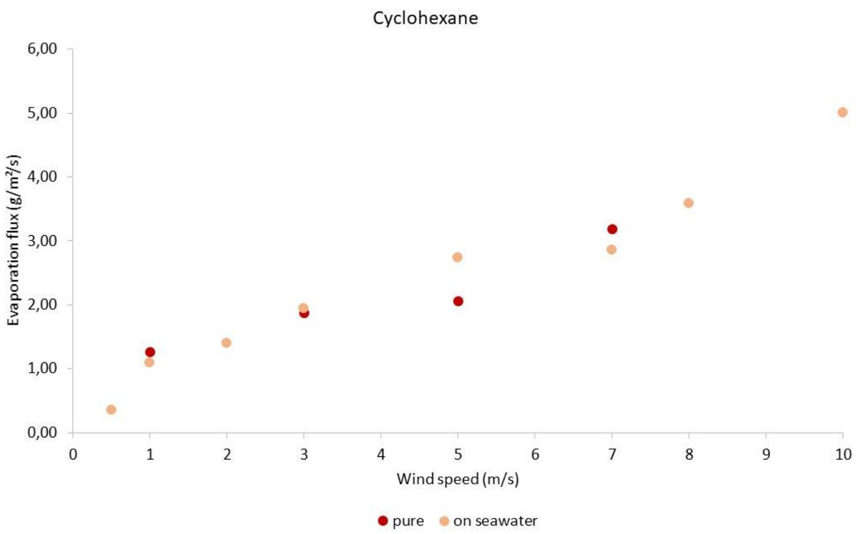

Figure 22. Comparison of pure/on seawater cyclohexane evaporation. There is no significant change in the evaporation rates of cyclohexane whether pure or released in seawater.

The evaporation fluxes of pure cyclohexane and cyclohexane poured onto seawater differ by only 4% to 24 %. The highest difference of 24 % occurs at a wind speed of 5 m/s (Table 16). Some errors may also occur, partly due to limitations in the experimental set up, which does not always ensure perfect repeatability.

Table 16. Evaporation fluxes of pure or on seawater 60 mL of cyclohexane.

Wind speed (m/s)	Evaporation flux cyclohexane on seawater ($g/m^2/s$)	Evaporation flux pure cyclohexane ($g/m^2/s$)	Difference %
0,5	0,36	-	-
1	1,10	1,26	15
2	1,40	-	-
3	1,95	1,87	4
5	2,74	2,06*	25
7	2,86	3,18	11
8	3,59	-	-
10	5,01	-	-

*Average value from three experiments

3.1.5. Butyl acetate

Pure butyl acetate evaporation

A volume of 10 mL of pure butyl acetate was left evaporating at different wind speeds: 1, 2, 3, 5, 7, 8, 10 m/s. As the product evaporates, a decrease in liquid temperature is observed. The drop in temperature was in the range of 2 to 3 °C for all wind speeds tested. **Erreur ! Source du renvoi introuvable.** illustrates the mass loss over time at 7 m/s. The mass loss of butyl acetate seems to follow a polynomial law (R^2 = 0,9998). For the sake of simplification and to assess the evaporation flux in g/m²/s, the evaporation fluxes were calculated using linear relationships (Figure 23) as in the previous experiments, with the slope of the mass curve (in g/s) divided by the surface of the petri dish. The other results are provided in Appendix 4.3.1.

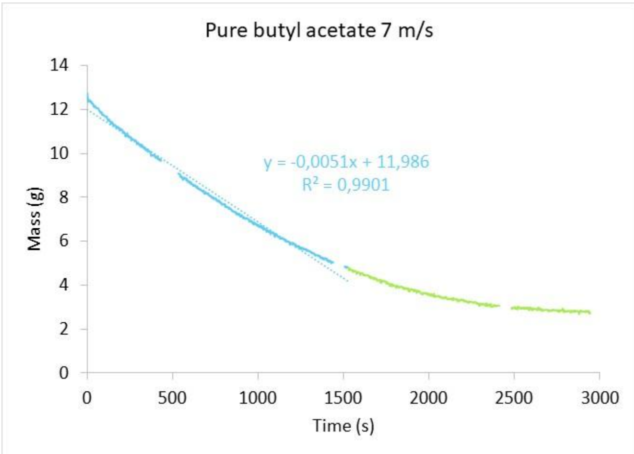

Figure 23. Linear relationship used to calculate the evaporation flux of pure butyl acetate at 6 m/s. The slope (in g/s) is divided by the surface (in m²) of the petri dish.

The evaporation fluxes of pure butyl acetate are reported in Table 17. Without surprise, higher wind speeds generally correspond to higher evaporation fluxes. A slightly lower evaporation rate can nonetheless be observed at 8 m/s, probably because the ambient air temperature was 4 °C lower than in the other experiments.

Table 17. Evaporation fluxes (g/m²/s) of pure butyl acetate.

Wind speed (m/s)	Evaporation flux (g/m²/s)
1	0,18
2	0,26
3	0,45
5	0,67
7	0,83
8	0,78
10	0,89

Butyl acetate evaporation on seawater

A volume of 60 mL of chemical was poured onto seawater and three wind speeds were tested: 3, 5 and 7 m/s. As soon as butyl acetate is spilled onto seawater, both surface and bottom temperatures gradually decrease by around 3 °C across all wind speeds tested. The mass loss curve seems to be divided into two linear phases (Figure 24).

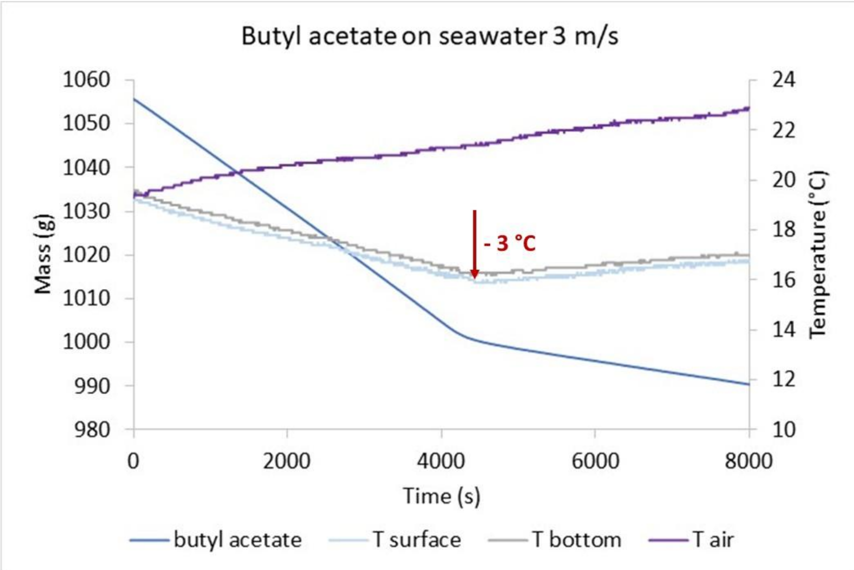

Figure 24. 60 mL of butyl acetate poured onto seawater at 3 m/s wind speed. The first part of the mass loss (until 4200 s) might correspond to the evaporation of the water-butyl acetate mixture but mostly concentrated with butyl acetate, whereas the following part should be mainly seawater.

At 3 m/s, the inflection point is reached 4 300 s after the spill, and is reached faster for the two other wind speeds: 3 600 s after the spill for 5 m/s and 1 800 s after the spill for 7 m/s (Appendix 4.3.2). As butyl acetate displays low water solubility (5.7 mg/L), is lighter than water (density of 0.881 g/mL) and has moderate vapour pressure (1.16 kPa), the chemical is classified as a FED under the SEBC classification. Hence, part of the chemical is expected to dissolve within the subsurface layer of seawater, whereas another part is likely to evaporate or volatilize. The wind will promote the evaporation of the closest layer of butyl acetate to the surface, but could also favour the dissolution of the chemical in seawater as observed with the chemistry test bench (3.3.2 Butyl acetate).

The first linear phase might correspond to the evaporation of the water-butyl acetate mixture, primarily enriched in butyl acetate, which could remain just below the surface due to its density. The evaporation rate of the second part is $7.61*10^{-2}$ g/s/m² (R^2 = 0,99), while seawater alone at 3 m/s evaporates at $2.0*10^{-2}$ g/s/m² (see 3.1.2 Seawater evaporation), suggesting that butyl acetate is still evaporating in the second phase. As previously observed, evaporation fluxes increase linearly with the wind speed (Table 18).

Table 18. Evaporation fluxes (g/m²/s) of 60 mL of butyl acetate poured onto seawater (first phase mainly composed of butyl acetate).

Wind speed (m/s)	Evaporation flux (g/m²/s) *10^{-2}
3	36.1
5	44.8
7	72.7

Following the previous experiment on seawater, the influence of the spill volume on the evaporation kinetics was tested at a wind velocity of 5 m/s, with spill volumes of 5 mL, 10 mL and 60 mL of butyl acetate (Figure 25). Regardless of the volume spilled, the overall trend of the curves is similar, with two parts separated by an inflection point. Still at the same wind speed, the slope of the second segment of each curve closely matches that of seawater alone, reflecting a comparable evaporation rate and implying that evaporation is predominantly from the seawater. This can be explained by the low volume of butyl acetate spilled (5 and 10 mL) The numerical values of the evaporation fluxes calculated for the 2 phases are presented in **Table 19**.

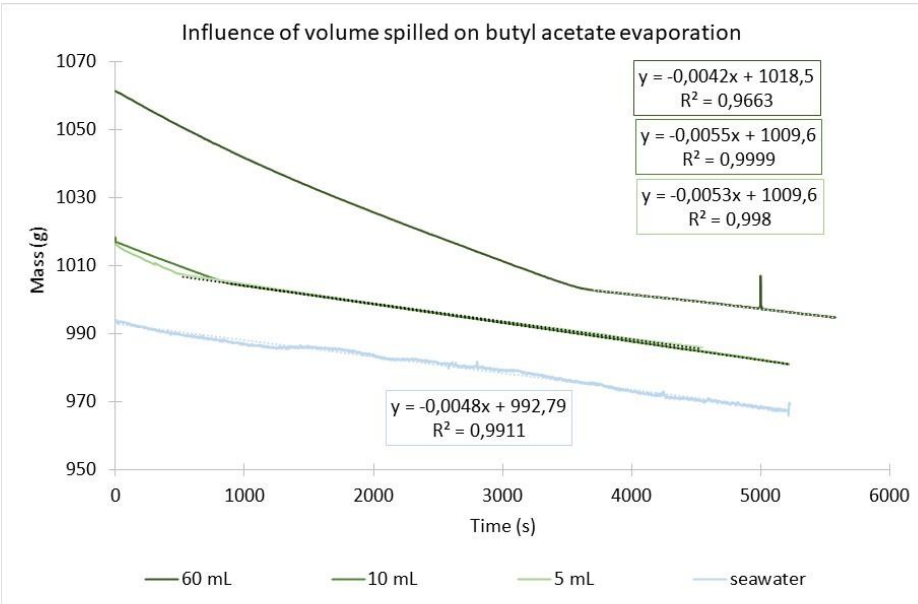

Figure 25. Evaporation of butyl acetate with different volumes spilled. At the same wind speed, the slope of the second segment of each curve closely matches that of seawater alone (light blue curve).

The larger the amount of butyl acetate spilled, the longer it takes to reach the inflection point. For a 5 mL spill (corresponding to 4.4 g), the inflection point occurs after 11 g of the total mass has evaporated, indicating that the mixture, rather than the pure chemical, is evaporating, as previously suggested.

A similar feature is observed for the other volumes: with 60 mL spilled (corresponding to 52 g), the inflection point is reached after a mass loss of 58 g, and with 10 mL spilled (8.81 g), the inflection point occurs at 14 g of mass loss. Since the mass loss exceeds the amount initially introduced, it shows that seawater has to evaporate simultaneously with the butyl acetate.

The evaporation fluxes from the linear sections (2nd phase) are quite similar between the different volumes tested, with a standard deviation of 0.05×10^{-2} g/m²/s. At 5 m/s wind speed and 20 °C, seawater evaporates with an evaporation rate of 1.41×10^{-2} g/m²/s (light blue curve in Figure 25). This corresponds to the evaporation rates of the second parts of the experiments using 5, 10 and 60 mL of butyl acetate (Table 19).

Table 19. Experimental evaporation rates of the two different parts.

Volume of spill (mL)	First part evaporation rate, mostly butyl acetate (g/m²/s) $*10^{-2}$	Second part evaporation rate, mostly seawater (g/m²/s) $*10^{-2}$
5	48.8	1.41
10	38.9	1.41
60	44.8	1.13

A variation in volume spilled would therefore lead to greater changes in the duration of evaporation rather than in the evaporation flux. Additional tests were carried out with 150 mL of butyl acetate on seawater, results are provided in Appendix 4.3.3.

Comparison pure – On seawater

The evaporation of 10 mL of pure butyl acetate was compared with 60 mL butyl acetate poured on seawater. The comparison between these experiments with two different volumes was made possible thanks to the results of the previous section, in which it was observed that the volume poured had negligible effect on the evaporation rate.

The evaporation rates are reported in Figure 26.

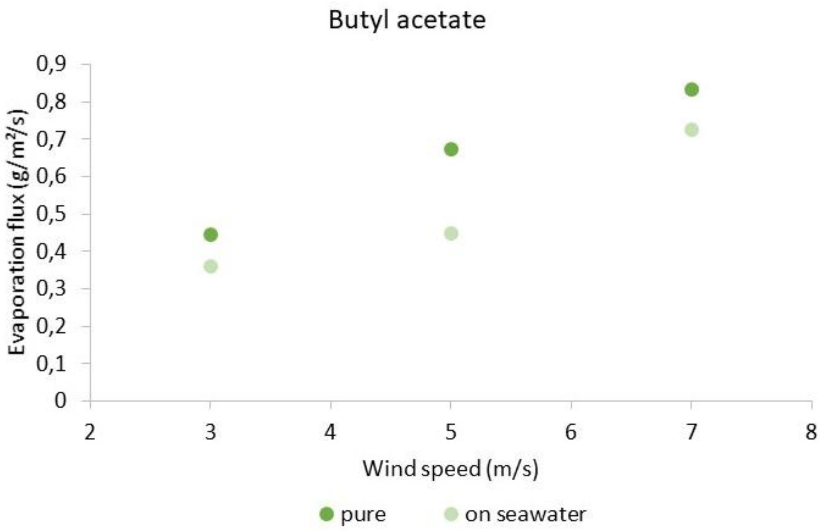

Figure 26. Evaporation rates of 60 mL of butyl acetate on seawater compared to the evaporation rates of 10 mL of pure butyl acetate.

At wind speeds of 3, 5 and 7 m/s, evaporation fluxes are between 15-50 % lower when butyl acetate is poured onto seawater compared to the pure chemical (Table 20). Butyl acetate's solubility in seawater could limit its evaporation. Additionally, the liquid temperature decreases more rapidly for the pure chemical, while the decrease is more gradual when the chemical is released in seawater. A higher decrease in temperature highlights a more significant evaporation.

Table 20. Evaporation fluxes of butyl acetate either pure (10 mL) or poured on seawater (60 mL).

Wind speed (m/s)	Evaporation flux 60 mL on seawater ($g/m^2/s$)	Evaporation flux 10 mL pure ($g/m^2/s$)	Difference (%)
3	0,361	0,446	23
5	0,448	0,673	50
7	0,727	0,833	15

3.1.6. Aqueous ammonia

The influence of solution concentration on ammonia evaporation rates was investigated. To do so, three aqueous ammonia solutions were prepared at concentration of 7, 14 and 21 % in distilled water and were exposed to a constant wind speed of 6 m/s. Solutions of identical concentrations were also prepared in seawater to compare and to assess the additional effect of salinity on the evaporation process. The corresponding mass loss curves are reported in Figure **27** and Figure 28.

An aqueous ammonia solution contains free ammonia (NH_3) in acid-base equilibrium with the ammonium ion (NH_4^+), according to equation (1):

$$NH_3 + H^+ \leftrightarrow NH_4{}^+ \quad (1)$$

At a pH above 9.5 and temperatures between 15 and 20 °C, the equilibrium shifts to the left, making NH_3 the dominant species in solution (Alleman 1998; Edwards et al. 2024). When the solution is discharged into seawater, the NH_3 reacts with water to form ammonium hydroxide (NH_4OH), following equation (2):

$$NH_3 + H_2O \leftrightarrow NH_4{}^+ + OH^- \quad (2)$$

The hydration and subsequent protonation of NH_3 release energy in the form of heat (an exothermic reaction) and generate hydroxide ions (OH^-). Therefore, discharging the ammonia solution is expected to cause mass loss through volatilization of ammonia, together with an increase in both temperature and pH.

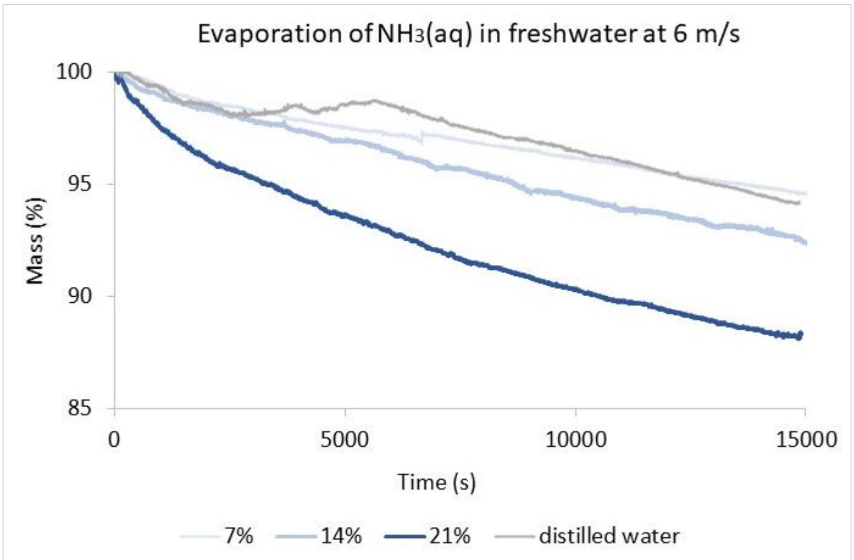

Figure 27. Evaporation of aqueous ammonia solutions in freshwater at 6 m/s. Three concentrations were tested: 7, 14 and 21%.

The evaporation fluxes of the ammonia solutions are reported in Table 21. It was observed that higher ammonia concentrations generally led to greater evaporation fluxes. To further investigate the influence of salinity on the evaporation process, a 14% ammonia solution was prepared in seawater, with aquarium salts added to restore the salinity reduced by dilution with the freshwater-based commercial solution. The solution was evaporated at 6 m/s, and the pH was monitored throughout the process (Figure 29). Overall, the results indicate that salinity has little impact on the evaporation of aqueous ammonia, as the measured evaporation fluxes were comparable in freshwater and seawater (Table 21). In both media, ammonia solutions evaporated more rapidly than water alone, whereas the 7% ammonia solutions exhibited evaporation rates similar to those of water, likely due to their relatively low ammonia content. This conclusion is further supported by the observed temperature data.

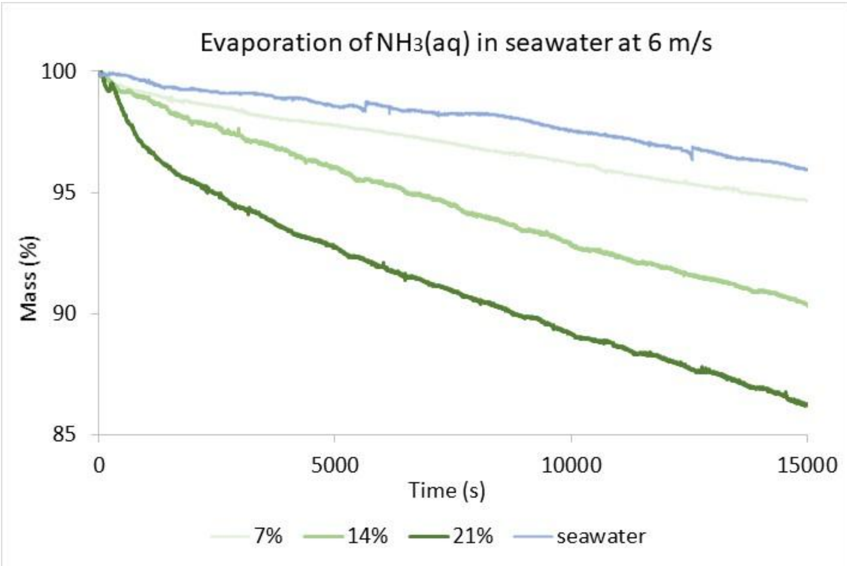

Figure 28. Evaporation of aqueous ammonia solutions in seawater at 6 m/s. Three concentrations were tested: 7, 14 and 21%.

Contrary to expectation, no significant increase in temperature was observed upon release. However, in all experiments, the ammonia solution temperature steadily decreased over the first 1,500 seconds (25 minutes), with nearly identical temperature drops for solutions of the same concentration – whether in freshwater or seawater (Appendices 4.4.1 and 4.4.2). However, temperature drops increased with ammonia concentration: at 7%, the decrease ranged from −6.7°C at the liquid surface to −8.4°C at the bottom. For 14% solutions, the drops were of −11.6°C at the surface and −11.3°C at the bottom. At 21%, the temperature uniformly fell by about −16°C, both at the surface and the bottom (Appendices 4.4.1 and 4.4.2).

Table 21. Evaporation fluxes of aqueous ammonia (in distilled water and in seawater).

Ammonia solution concentration	Evaporation flux in distilled water ($g/m^2/s$)	Evaporation flux in seawater ($g/m^2/s$)
7%	0.085	0.087
14%	0.118	0.152
14% with salts	-	0.127
21%	0.175	0.192
Distilled water only	0.096	-
seawater only	-	0.073

The pH reached a maximum value of 12.01 and then gradually decreased to 10.84 over the 6 hours following release, confirming ammonia evaporation (Figure 29).

In seawater, high pH conditions promotes the conversion of bicarbonate (HCO_3^-) into carbonate ions (CO_3^{2-}), thereby altering solubility equilibria and facilitating carbonate precipitation (Dong et al. 2017). This feature was observed in all experiments performed in seawater with the systematic formation of a milky white precipitate after release. This phenomenon, which has already been reported in previous studies (Morse, 1979; Shand, 2006), was also observed repeatedly in a series of laboratory tests (CEDRE 2024). Tests and spectroscopic analysis (CEDRE 2025a) suggest the presence of mixed calcium-magnesium carbonates, such as dolomite ($CaMg(CO_3)_2$). This hypothesis needs to be confirmed through multi-element analysis using ICP-AES or ICP-MS; tests are currently underway.

The presence of the precipitate did not appear to hinder ammonia evaporation, as evidenced by the very similar evaporation rates observed in freshwater and seawater (Table 21).

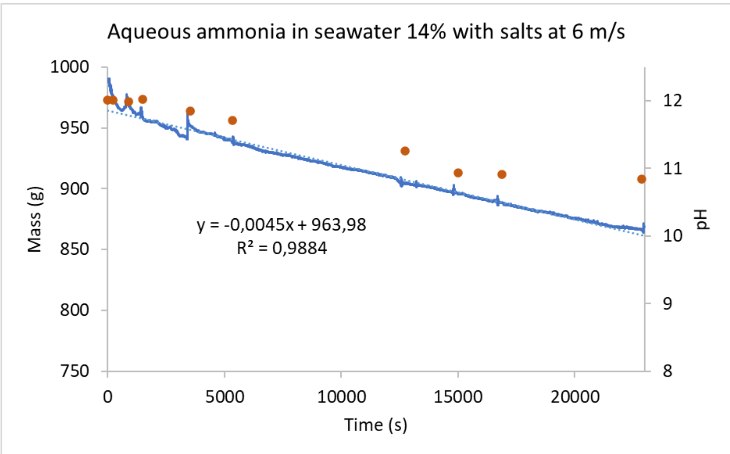

Figure 29. Evaporation of a 14% ammonia solution in seawater. pH was monitored during the evaporation, and its decrease shows the ammonia evaporation from the solution.

3.1.7. Comparison between cyclohexane, butyl acetate and methanol

According to the SEBC classification, all chemicals investigated in this study undergo evaporation, but exhibit different secondary behaviours, which depend on their inherent physical and chemical properties. Specifically, compounds with higher vapour pressures and lower boiling points evaporate more quickly. Their behaviour is also influenced by molecular interactions. Upon release into seawater, the relative contribution of evaporation, dissolution, and floating to the behaviour of those chemicals was studied. This section explores how seawater and wind influence the overall fate of the chemical studied.

Pure chemicals

Based on their vapour pressure values (Table 1), cyclohexane and methanol are expected to evaporate at comparable rates, while butyl acetate is anticipated to evaporate more slowly. Experimental observations confirmed this trend: pure cyclohexane exhibited the highest evaporation rates; followed by methanol and butyl acetate (Figure 30). Additionally, the evaporation rate of each chemical rose with increasing wind speed. It should be noted that the reported value for cyclohexane at 5 m/s is an average value (3 repetitions), whereas the other experiments were conducted only once.

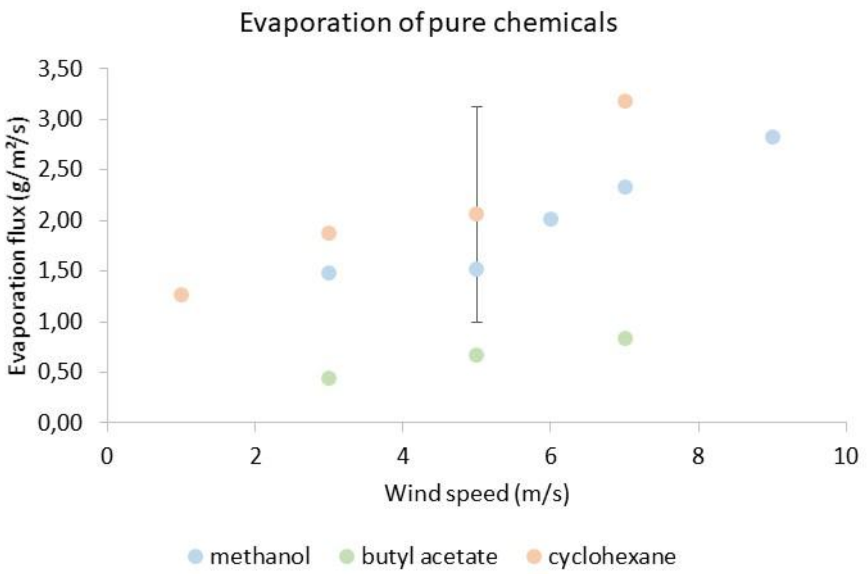

Figure 30. Evaporation fluxes of pure cyclohexane, methanol and butyl acetate at wind speeds ranging from 1 to 9 m/s.

Chemicals on seawater

In theory, methanol is the most hydrosoluble of the compounds studied, followed by butyl acetate and cyclohexane (**Table 1**).

As observed in experiments with pure chemicals, releasing 150 mL of each substance onto seawater under identical wind conditions showed that butyl acetate consistently had the lowest evaporation rates (Figure 31). Although cyclohexane – classified as an “Evaporator” in the SEBC system and known for its very low water solubility – was expected to evaporate the fastest, this behaviour was only evident at a wind speed of 3 m/s and not at higher speeds.

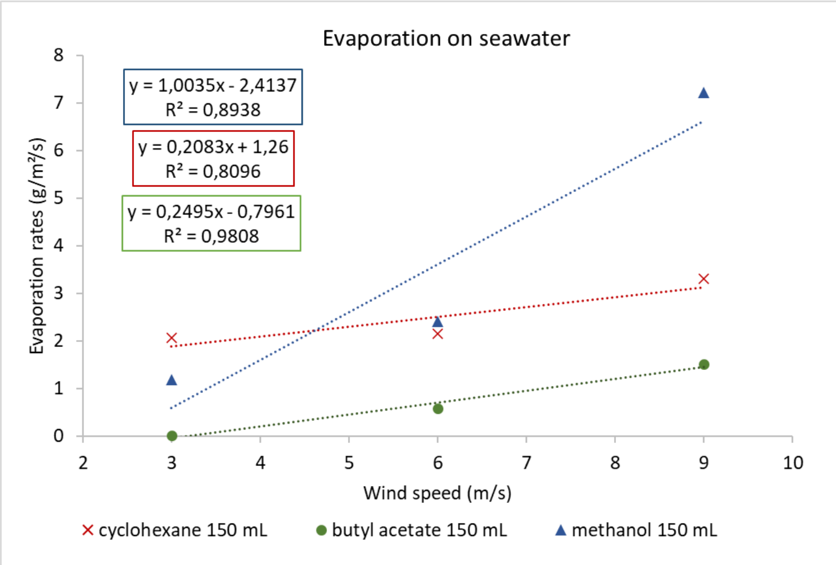

Figure 31. Evaporation of 150 mL of cyclohexane, butyl acetate, methanol at 3, 6 and 9 m/s. All evaporation fluxes increase linearly with the wind speed, and butyl acetate exhibits the lowest evaporation rates.

As observed in the 'Slick study with colouring agent' section, the slower evaporation of cyclohexane at higher wind speeds may be attributed to the freezing of its slick, which likely inhibits evaporation. Additionally, the evaporation flux of methanol at 9 m/s may have been overestimated.

When 60 mL of each chemical was released onto seawater under identical wind conditions, butyl acetate again displayed the lowest evaporation rates (Figure 32). While the evaporation fluxes of cyclohexane and butyl acetate increased linearly with wind speed, methanol's evaporation did not follow a linear trend—though its evaporation rates still rose with higher wind speeds.

These findings indicate that the linear correlation between evaporation rate and wind velocity does not hold for highly water-soluble chemicals like methanol. Nevertheless, as seen with pure chemicals, evaporation rates for all substances still increased with rising wind speeds.

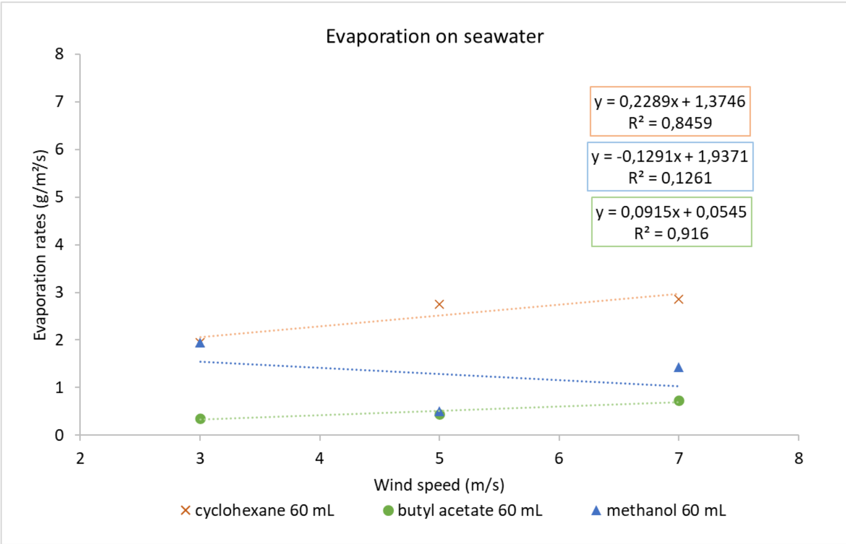

Figure 32. Evaporation of 60 mL of cyclohexane, butyl acetate, methanol at 3, 6 and 9 m/s. Only the evaporation fluxes of cyclohexane and butyl acetate increase linearly with the wind speed.

Upon release into seawater, distinct surface temperature responses were recorded for each chemical: methanol caused a temperature rise, cyclohexane caused rapid cooling due to slick freezing, and butyl acetate resulted in a gradual temperature decline over time (Figure 33). These variations highlight the specific interactions between each chemical and water.

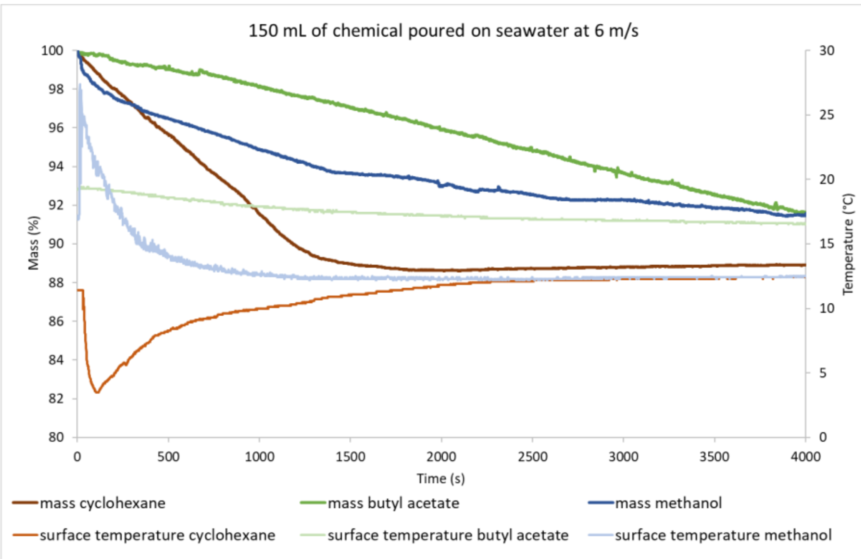

Figure 33. Surface temperatures of 150 mL of cyclohexane, butyl acetate and methanol poured onto seawater at 6 m/s. Surface temperature of cyclohexane shows a sharp decrease as the product evaporates fast (significant mass loss until 1300 s), while surface temperature of methanol rises and the one of butyl acetate stays stable.

Methanol's hydroxyl group enables strong hydrogen bonding with water molecules, releasing energy as heat and raising the solution's temperature upon release. This interaction may also contribute to hinder methanol evaporation process[4]. In contrast, cyclohexane is a non-polar molecule with no hydrogen-bonding capability. As a result, its interactions with water molecules are limited to weak London dispersion forces, which could explain the high evaporation rate and the rapid cooling of the solution observed (Figure 34).

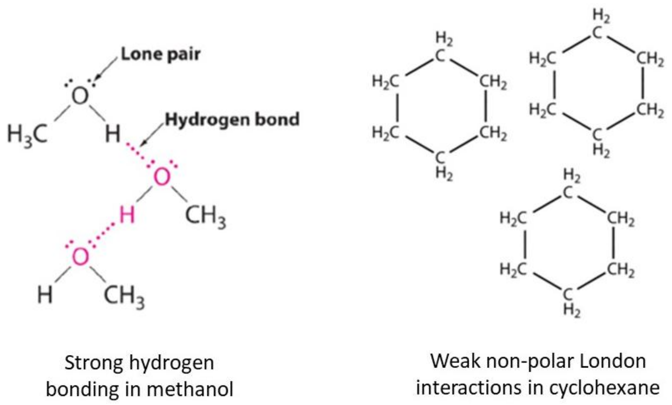

Figure 34. Illustration of hydrogen bonding in methanol and non-polar interactions in cyclohexane (adapted from [4]).

The gradual temperature decrease observed for butyl acetate is most likely due to evaporation. In water, butyl acetate will undergo hydrolysis reactions to form acetic acid and butanol at a rate determined by the pH of the solution (Johannes et al. 1997; World Health Organization 2005). However, this reaction is slow in neutral environment such as seawater (pH ~ 8). At 20°C, the half-life calculated for n-butyl acetate indeed ranges from 11.4 days at pH 9 to 114 days at pH 8 and up to 3.1 years at pH 7. Moreover, only 37% of n-butyl acetate degrades via hydrolysis and biodegradation after 20 days in seawater. Hence, without a catalyst, hydrolysis is minimal in the short term, making evaporation the dominant factor in its environmental behaviour (Price et al. 1974; World Health Organization 2005).

In general, interaction with seawater reduced the evaporation rates of all chemicals compared to their pure forms, with the exception of cyclohexane, whose evaporation rate remained unaffected due to its low water solubility. Methanol demonstrated significant solubilisation in seawater, as evidenced by the observed temperature increase. Butyl acetate, despite its higher water solubility compared to cyclohexane, showed moderate temperature change, which does not preclude solubilisation but rather indicates that the process is not exothermic.

[4] CHEMISTRY 103 PRINCIPLES OF CHEMISTRY, Carlisle J. E. D'Souza, SUNY Adirondack.

Experiments with cyclohexane containing the colouring agent (see Slick study with colouring agent) confirmed that it forms a surface slick and does not dissolve in seawater. These findings align with the evaporation fluxes data: seawater involved reduced cyclohexane fluxes by only ~14%, while fluxes of butyl acetate and methanol decreased by ~30% and 74%, respectively. Figure 35 illustrates the relationship between water solubility and evaporation rates, logically showing that higher solubility corresponds to lower evaporation.

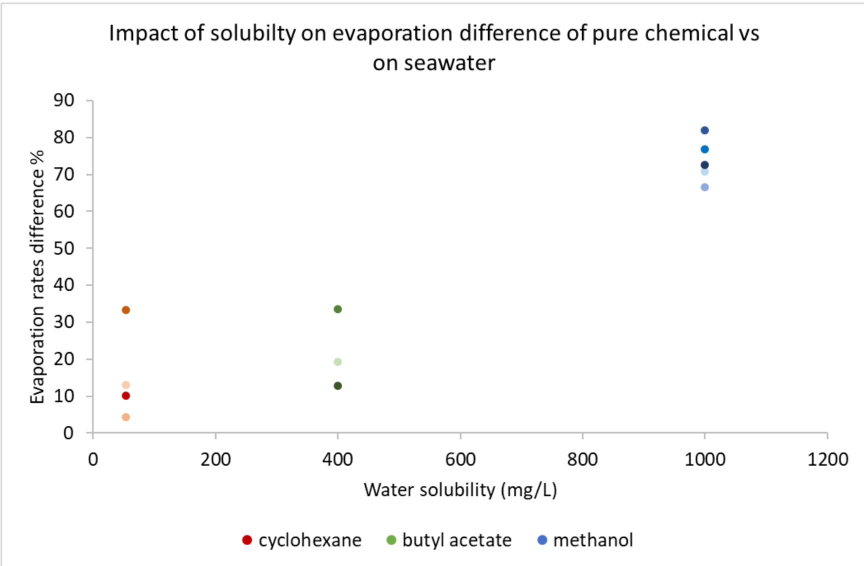

Figure 35. Impact of water solubility on evaporation rate difference between pure chemical and poured on seawater. Each shade corresponds to a different wind speed, with the colour darkening as the wind speed increases. As a product is more soluble in water, the difference between the evaporation rates increases.

The evaporation rate of a chemical becomes increasingly influenced by seawater conditions as its solubility in water rises. Table 22 summarises the different evaporation fluxes.

Table 22. Evaporation fluxes (g/m²/s) of 60 mL of cyclohexane, methanol and butyl acetate either pure or poured and seawater.

Substance	Wind speed (m/s)	On seawater	Pure (g/m²/s)	Difference (%)
Methanol	3	0,434	1,48	71
	5	0,507	1,52	67
	6	0,470	2,02	76
	7*	0,424	2,33	82
	9	0.781	2,83	72
Cyclohexane	0,5	0,36	—	—
	1	1,10	1,26	15
	2	1,40	—	—
	3	1,95	1,87	4

	5*	2,74	2,06	25
	7	2,86	3,18	11
	8	3,59	—	—
	10	5,01	—	—
Butyl acetate	3	0,36	0,45	24
	5	0,45	0,67	50
	7	0,73	0,83	15

*Average value from three experiments.

3.1.8. Future improvements

Several improvements of the wind tunnel are being considered to enhance the robustness of the experiments. When the wind tunnel was operated in CEDRE's garage, the ambient air temperature could increase by up to 4°C over the course of an experiment. Figure 36 illustrates this effect, showing the ambient air temperature rising from 24.9 to 30 °C during the evaporation of butyl acetate at a wind speed of 1 m/s.

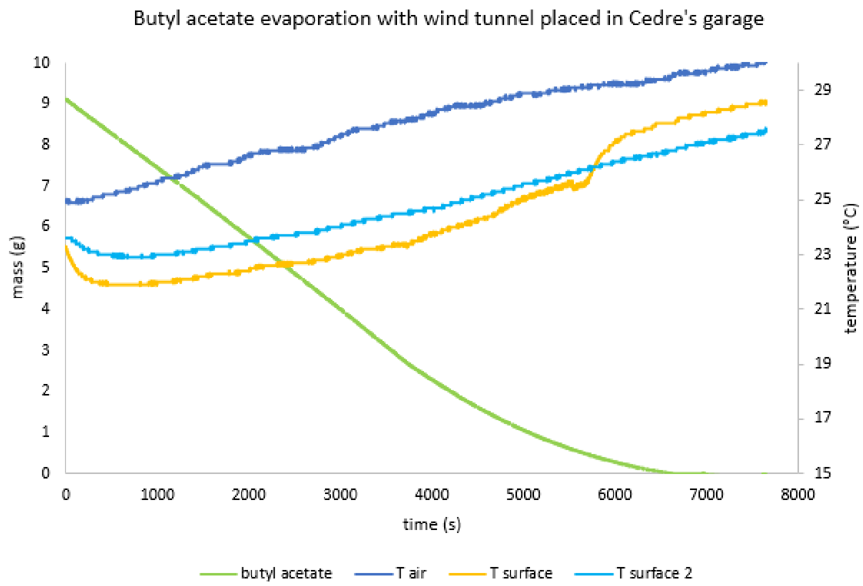

Figure 36. Uncontrolled ambient temperature increases in CEDRE's garage.

Relocating the wind tunnel in a thermoregulated-room would avoid any uncontrolled temperature variations that could impact evaporation and would enable reliable comparisons between experiments at varying wind speeds, e.g., for one chemical. While the "Ecotox" room was used for this purpose, its temperature still remains dependent on that of the adjacent Polludrome®, highlighting the need for improved insulation between these two rooms to maintain stable temperature conditions. Furthermore, activation of the Ecotox room's ventilation causes periodic temperature fluctuations while reaching the set point, which affects evaporation, as reflected in the mass curve (Figure 37).

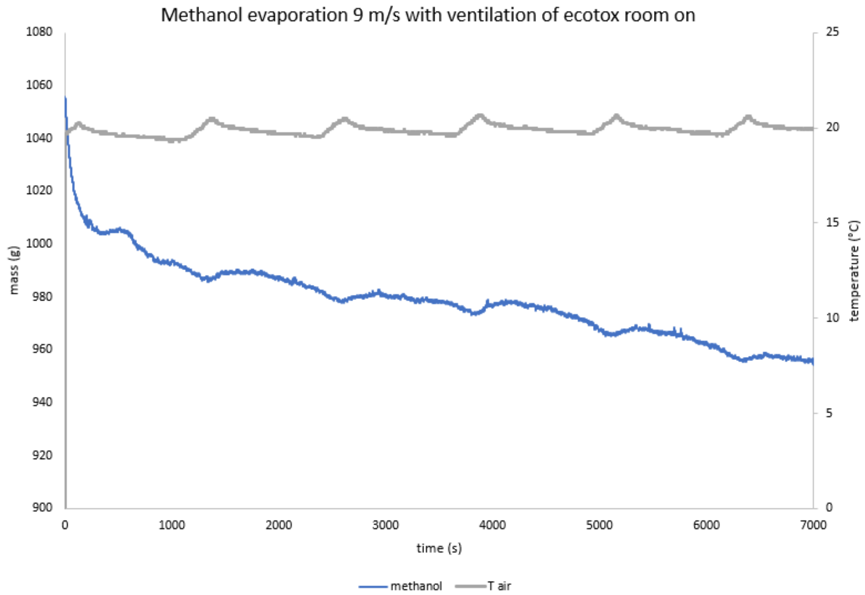

Figure 37. Uncontrolled temperature drops influence on methanol mass loss in the ecotox room.

In addition, the spill procedure and the design of the wind tunnel could be improved. The temperature probes are only secured with adhesive tape, which can come off during the experiment or after the spill. If the probes are replaced manually, this induces factice changes in the initial mass. A tray equipped with tubes in which to insert the probes in advance would prevent this problem and ensure that the temperature probes are always placed in the same location (Figure 38).

Figure 38. Scheme of the scale with suited holes to place temperature probes, two on the surface and one at the bottom.

The wind tunnel scale randomly performs internal adjustment during the experiments, which induces gaps in the mass measurements, as shown on the mass curve in Figure 39.

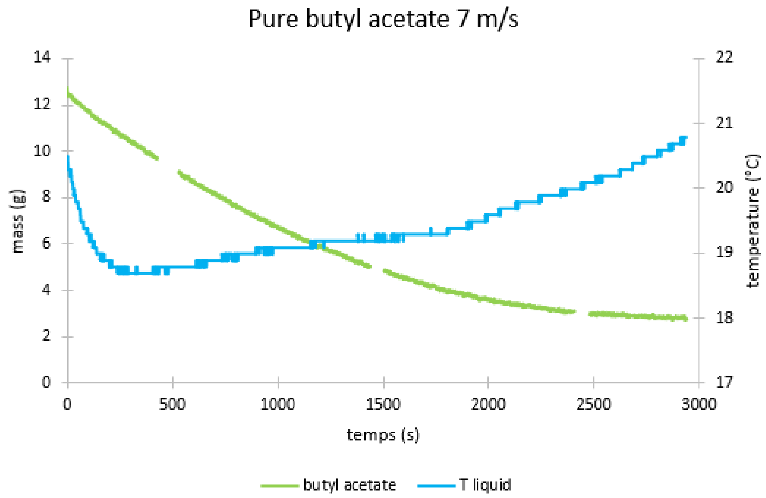

Figure 39. Gaps in the mass curve (green) are due to the scale making internal adjustments.

In addition, a study conducted by The French Aerospace Lab ONERA using thermal imaging revealed that some of the gas escapes through the open side of the wind tunnel, where the balance is located (Figure 40). While this gap should not affect significantly the accuracy of mass loss measurements, installing a removable panel to cover this gap, while maintaining access to the scale, would prevent this issue.

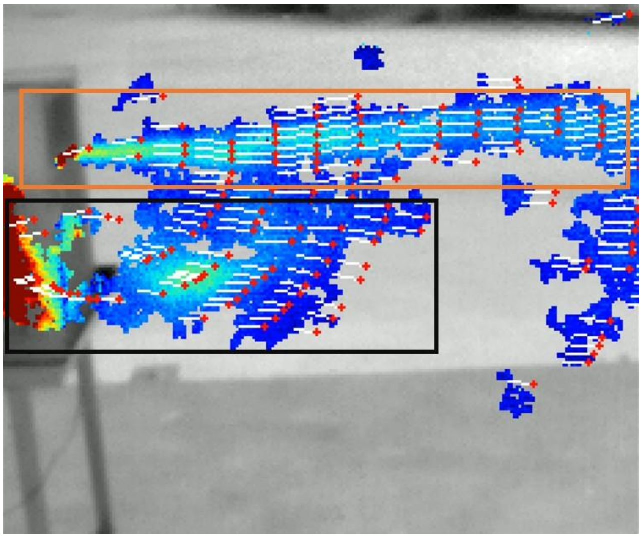

Figure 40. Gas flow of acetone from the wind tunnel. Part of the gas comes out from the upper part of the wind tunnel (orange frame) as intended, but some gas also through the open space on the side of the wind tunnel (dark frame).

To prevent wind flow disturbances, the liquid surface must be precisely aligned with the airflow, necessitating that the dish be filled to its maximum capacity. Currently, the available containers – a 60 mL glass Petri dish (10 cm diameter) and a 1 L cuvette – limit experimental flexibility. The absence of a dish with an intermediate volume has made it impossible to test 150 mL of pure chemical, hindering direct comparison with experiments involving 150 mL of chemical released onto seawater. With the existing setup, pure chemical tests are restricted to 60 mL, while smaller volumes (5 – 10 mL) result in a liquid surface below the wind flow, compromising the accuracy of open-sea spill simulations.

To address this limitation, the protocol could be revised to standardize all experiments at 60 mL for consistent comparisons. Alternatively, the setup could be modified by introducing an adjustable platform for the dish, ensuring alignment with the airflow and eliminating gaps that affect simulation accuracy.

3.2. Dissolution of methane while rising into the water column

This section focuses on providing and analysing experimental data on methane dissolution and behaviour in the water column using the CEDRE Experimental Columns CEC (2.2.2) and C^3 (2.2.3).

3.2.1. Methane solubilisation in fresh water (C^3)

The first experiments involving methane were conducted using the C^3 to characterise its behaviour and fate in freshwater. The methane bubble diameter was measured by taking 10 - second readings every 3 minutes. The experimental data collected show that methane dissolves during the first 5 minutes following injection (**Erreur ! Source du renvoi introuvable.**). The bubble diameter then stabilises at around 80% of its initial value and remains unchanged until the end of the acquisition. The standard deviation in the measurements is mainly due to the accuracy of the acquisition system, in which each pixel corresponds to 0.069 mm for this series of experiments.

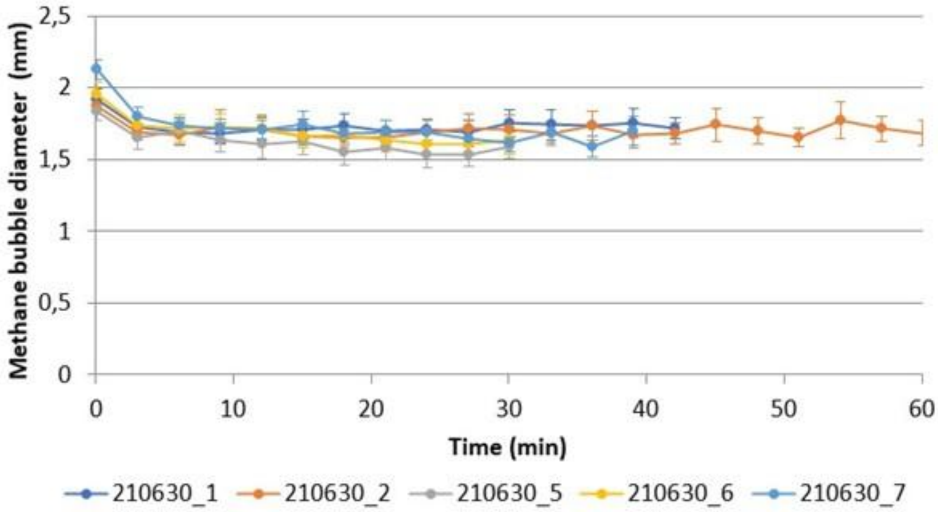

Figure 41. Change in methane bubble diameter over time in fresh water at 15°C.

Two distinct phases are suggested to characterize the dissolution of methane (Figure 42). The first phase could correspond to rapid diffusion of methane into the surrounding water due to the absence of dissolved methane in the environment, resulting in a decrease in the diameter of the bubble. The second phase can be described as the stabilisation of the bubble and the equilibrium between the dissolution of methane and the concomitant absorption of dissolved gases from the surrounding water. The bubble, which is rapidly depleted of methane, will gradually be composed mainly of nitrogen and oxygen dissolved in the water. This explains why the diameter of the bubble remains stable over time.

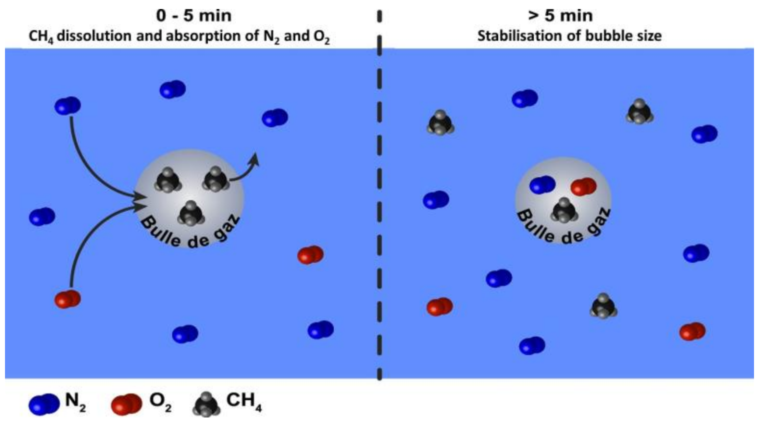

Figure 42. Illustration of the phenomena occurring at the methane bubble level.

This hypothesis is corroborated a former study (Olsen et al. 2017), which showed that methane from a 0.5 mm bubble dissolves into the surrounding water within approximately 3 minutes and is subsequently replaced by dissolved nitrogen and oxygen from the medium.

Our experimental results suggest that, in the event of a deep-water spill, methane is unlikely to reach the surface in large quantities. With an estimated average speed of 25 cm/s (Metane Project – CEDRE 2014), it takes 100 minutes for the gas plume to reach the surface if the release occurs at a depth of 1,500 metres. For a low leak rate, methane is highly likely to dissolve in the water column, and the bubbles reaching the surface would consist solely of dissolved gases from the environment (N_2 and O_2). In contrast, when the leak flow rate is very high, the saturation of the water mass with methane substantially reduces its dissolution, allowing bubbles with significant methane content reaching the surface. However, the risks associated with methane dissolving in water from an underwater leak also depend on the depth of the leak and the diameter of the plume.

3.2.2. Rising speed of a methane bubble (CEC)

Building on the observations of methane dissolution and bubble composition, the second experiment consisted of tracking the rise of a methane bubble in the CEC using cameras spaced 72 cm apart, and with two different diameter gas injectors (2 and 4 mm). The aim was to obtain information on the fate of bubbles in a limited volume and to assess whether their dissolution could be quantified in this interval. Bubbles were initially injected using a 2 mm – diameter injector to ensure a small initial diameter.
The Student's t-test was used to compare the means and determine whether the differences observed between the means of the two groups are likely to be due to chance or whether they are statistically significant. This test calculates a dimensionless value, the coefficient t, which, if less than 0.01, allows to conclude that the means are significantly different, or not.

First experiment: 2 mm diameter injector - cameras spaced 72 cm apart
With the 2 mm diameter injector, the distribution of droplet sizes is similar at the bottom and top of the water column. The diameter of the bubbles measured at the top of the water column is slightly larger than that obtained at the bottom, with a bubble size distribution slightly shifted towards larger diameters (Figure 43).

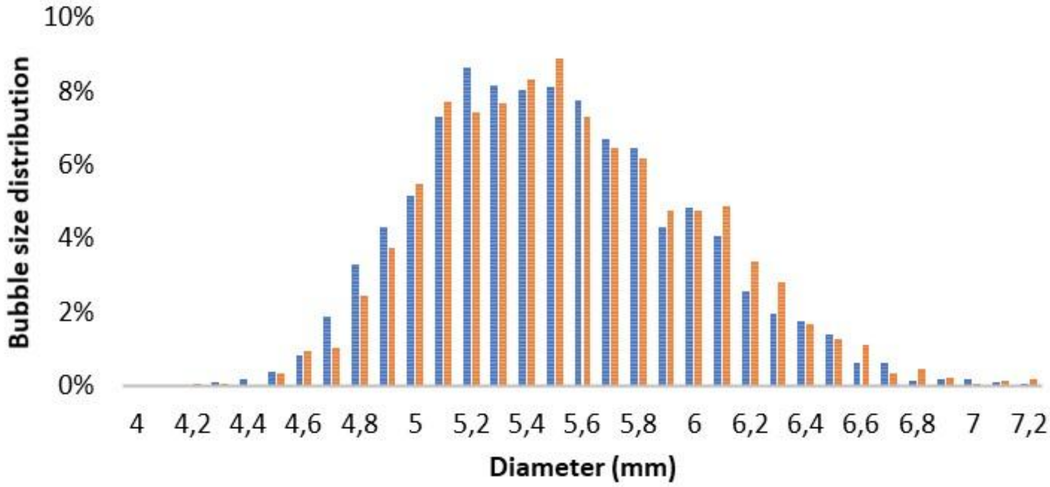

Figure 43. Distribution of methane bubble sizes at the bottom (■) and at the top (■) of the CEC (2 mm diameter injector).

Second experiment: 4 mm diameter injector - cameras spaced 72 cm apart

Larger methane bubbles were then generated using the 4 mm diameter injector. The distance between the two cameras was the same as in the first experiment, i.e., 0.72 metres. In agreement with the results from the 2 mm injector experiment, the bubble size distribution at the bottom and top of the water column is similar. However, the distribution of bubble sizes at the top of the column displays a more marked shift towards larger bubble diameters (Figure 44).

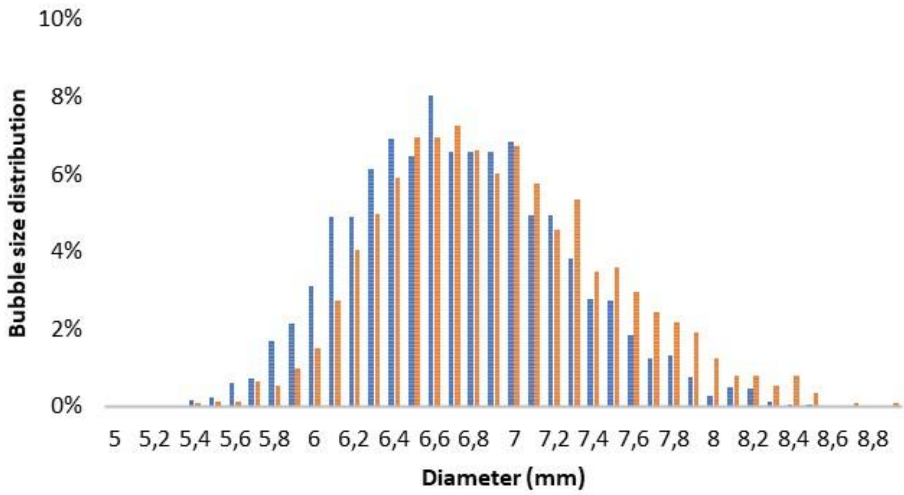

Figure 44. Distribution of methane bubble sizes at the bottom (■) and at the top (■) of the CEC (4 mm diameter injector).

In this experiment, bubbles at the top of the column expanded by 9.5% in volume compared to the initial bubbles injected at the bottom of the CEC. This corresponds to a volume increase of 15 µL.

Comparison between the 2- and 4-mm diameter injectors - cameras spaced 72 cm apart

The experiment with the 2 mm injector shows that the average volume is significantly lower at the top of the column than at the bottom (Student coefficient t = 4.5×10^{-9}). This result shows that some of the methane in the bubble was solubilised during its ascent. The phenomenon of methane dissolution is therefore clearly observed in this case, and the decrease in diameter is estimated at 6% per metre of ascent. The results of the experiment with the 4 mm injector show that there is no significant difference between the average volumes at the top and bottom of the column (t = 0.018), suggesting that there is very limited methane dissolution in the water column under these experimental conditions. The use of a 4 mm diameter injector generates larger bubbles than in the first experiment. This increased volume makes the bubbles more susceptible to expansion as they rise, which partly explains the similarity between the two bubble populations at the bottom and top of the CEC.

Furthermore, gas dissolution in the water column is directly dependent on the surface area available for exchange between the bubble and the medium. Bubbles with larger volumes will have slower dissolution kinetics than those with smaller diameters. This phenomenon can be better understood by considering the equation for gas dissolution kinetics, where dissolution kinetics is directly proportional to the exchange surface between the bubble and the surrounding medium, as provided by equation (4):

$$\frac{dn}{dt} = KA(C_S - C_0) \qquad (4)$$

With:

- n : amount of gas in the bubble in moles
- t : time in s
- K : mass transfer coefficient in m.s^{-1}
- A : surface area of the bubble in m^2
- C_S : saturation concentration of dissolved gas in mol.m^{-3} (gas solubility)
- C_0 : initial concentration of dissolved gas in mol.m^{-3}

It is also important to note that the surface-area-to-volume ratio is higher for a small bubble than for a large one. This means that, relative to its size, a small bubble has more surface available for gas exchange. This happens because surface area and volume do not scale in the same way: when a bubble gets larger, its volume increases much faster than its surface area. As a result, a small bubble ends up with much more surface area compared to its volume. Since dissolution occurs through the bubble's surface, this larger relative surface area makes a small bubble dissolve more quickly than a large bubble.

This point also explains why the experiment with the 4 mm injector shows no significant difference between the volumes measured at the top and bottom of the column. The height of 72 cm between the two acquisitions is too small to show the dissolution of methane in the water column of a bubble larger than 6 mm in diameter.

Third experiment: 4 mm diameter injector - cameras spaced 3.40 m apart

The last experiment concerning methane was carried out using the entire height of the CEC. In this case, the two cameras are spaced 3.40 metres apart and the injection is carried out, as in the previous experiment, using the 4 mm diameter injector.

The bubble size distribution follows the results obtained for the first two experiments (the ones with different injector diameters of 2 and 4 mm). The distribution at the top of the column is shifted towards larger diameters (Figure 45).

This experiment with a 3.40-metre water column involves a prolonged rise of the bubbles and therefore a longer presence time in the environment. The absorption of dissolved nitrogen and oxygen can thus counterbalance the dissolution of methane and explain the absence of difference between the bubble populations observed at the top and bottom of the CEC.

The initial decrease in bubble diameter between the second and third experiments can be explained by the increase in hydrostatic pressure at the injection point. Although the diameter of the injector remains unchanged, the bubbles generated have a smaller diameter when the pressure is higher, even with the same flow rate.

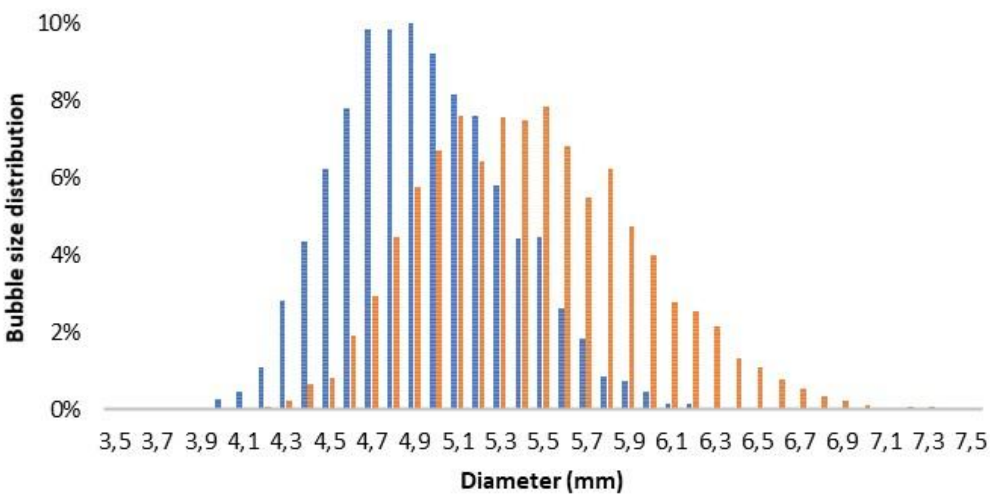

Figure 45. Distribution of methane bubble sizes at the bottom (■) and at the top (■) of the CEC.4 mm diameter injector - cameras spaced 3.40 m apart.

The average diameter of the bubbles at the bottom of the column is 4.897 ± 0.383 mm. The increase in bubble size is the most significant of the three experiments, as shown by the clear shift in the distribution of bubble sizes. The average diameter at the top of the column is 5.395 ± 0.500 mm.

In this third experiment, it was observed that the average volumes at the top and bottom of the column are not significantly different (t = 0.19). In this case, this lack of difference cannot be explained by the bubbles being too large and the dissolution kinetics being too slow. As studied in the experiment with the C^3 column (3.2.1), exchanges take place between the methane bubble and the gases dissolved in the water column. As it rises, the methane in the bubble can dissolve into the water column, but the nitrogen and oxygen dissolved in the water can also revert to gaseous form by re-entering the methane bubble (Figure 42).

Conclusion on methane behaviour

Experiments with methane (CH_4) showed that this poorly soluble gas dissolves slowly in the water column. The bubble populations observed at the top and bottom of the CEDRE Experimental Column (CEC) did not exhibit a significant decrease in diameter during ascent.
However, clear differences emerged between bubbles of different sizes: dissolution kinetics depend strongly on the initial bubble volume, with larger bubbles dissolving more slowly.

Although methane itself dissolves slowly, gas exchange at the gas-water interface is very active. Methane diffuses out of the bubble into the surrounding water in roughly 90 seconds, while dissolved nitrogen and oxygen diffuse into the bubble. As a result, by the time small bubbles reach the surface under low-flow conditions, most of the methane has already been replaced by environmental gases (N_2, O_2).

These findings indicate that methane released at great depth is unlikely to reach the surface unless the leak rate is high enough to saturate the water mass entrained by the bubble plume.

Because such methane-rich bubbles can form a flammable or explosive gas cloud at the surface, the safety risks associated with high-flow leaks must be considered, even at depths of up to 1,500 meters. These risks are consistent with past incidents where sudden releases of large volumes of methane generated hazardous surface gas clouds, such as the Baltic Sea pipeline explosion.

The experimental data obtained can now be used to calibrate and validate numerical models simulating deep-water leaks and their associated hazards.

3.3. Distribution between air, water column and surface compartments

The evaporation and dissolution of chemicals released at sea surface were studied simultaneously at various wind speeds (0, 3 and 6 m/s) using CEDRE's chemistry test bench, with cyclohexane, butyl acetate and methanol as test substances (150 mL released). The results are presented in the following sections. Concentrations in the water column can be found in Appendices 4.5, 4.6 and 4.7.

3.3.1. Cyclohexane

As cyclohexane is poorly soluble in water and lighter than water (solubility of 0.055 g/L and density of 0,779 g/mL), it is expected that the chemical forms a slick on the water surface without significant dissolution. However, traces of cyclohexane in the middle and bottom parts of the tank were observed even at wind velocity close to 0 m/s (Figure 46), suggesting a dispersion of the chemical throughout the water column.

At a wind velocity close to 0 m/s, the PID sensor recorded cyclohexane evaporation during the first hour following the spill, with concentrations rising up to 4 035 ppm. After 1 hour, no concentrations in air were detected anymore, perhaps because the vapours might have remained near the water surface, i.e., too low to be detected by the PID that was positioned well above the surface.

In seawater, the maximum cyclohexane concentration measured was 0.33 mg/L at the bottom compartment, 1 hour after the spill. After 8 hours, cyclohexane concentration seems to homogenises around 0.10 mg/L in the water column (Figure 46; Appendix 4.5). The concentration at sea surface is the lowest from the three compartments, suggesting exchanges with air.

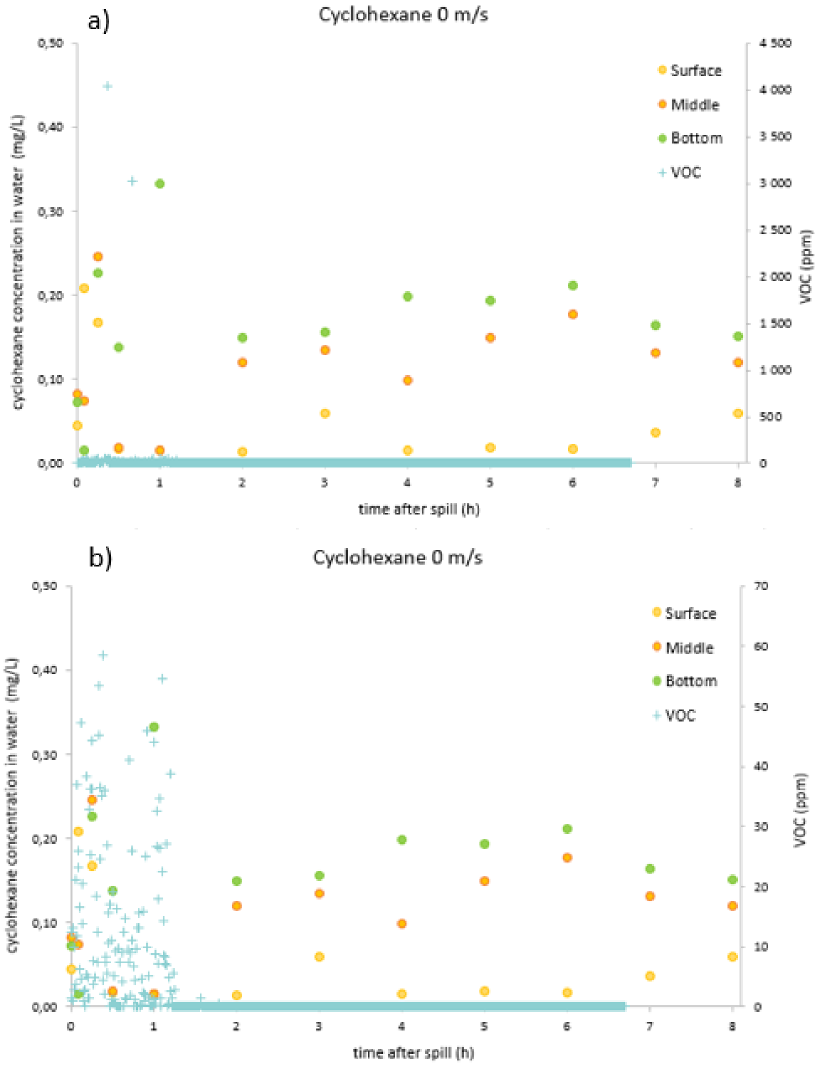

Figure 46. 150 mL of Cyclohexane poured into 80 L of seawater with wind velocity close to 0 m/s. Concentrations in air are detected in the first hour after the spill.
a) two peak concentrations were detected: 4 035 ppm 22 min after the spill and 3 020 ppm 40 min after the spill b) scale zoomed-in for VOC concentration.

In the two experiments conducted at wind speeds of 3 and 6 m/s, cyclohexane concentrations at the different sampling depths never exceeded 0,2 % of the theoretical solubility limit of 0.055 g/L, with maximum concentrations of 0.05 mg/L and 0.08 mg/L at 3 m/s and 6 m/s, respectively. After 8 hours, the water column concentrations homogenized to 0.03 mg/L in both experiments, corresponding to 0.05% of the theoretical concentration if all cyclohexane had dissolved. These low concentrations indicate that most of the cyclohexane evaporated within the first hour, consistent with the absence of detectable cyclohexane in the air afterward (Appendix 4.5).

At a wind speed close to 0 m/s, water concentrations of cyclohexane were higher than in the other two experiments. For instance, the concentrations in the middle compartment ranged from 0.02 to 0.25 mg/L, compared with 0.01 to 0.04 mg/L and 0.01 to 0.07 mg/L at 3 and 6 m/s, respectively. The highest concentrations were recorded at water surface, 5 and 15 minutes (0.21 and 0.17 mg/L) after the spill at a wind speed of 0 m/s, probably reflecting sampling directly within the cyclohexane slick prior to its evaporation. These results suggest that stronger winds will promote evaporation of cyclohexane when spilled into water. Nevertheless, no concentrations in air were detected at 3 and 6 m/s, likely because the PID might have been placed too high to capture any vapours.

The mass distribution of cyclohexane, butyl acetate and methanol within the water column were studied at the 3 sampling depths (Figure 47). For cyclohexane, results were similar at wind speeds of 3 and 6 m/s, with no more than 0.2 % of the theoretical mass detected at the different sampling depths. Less mass is found in the surface compartment than in the others due to cyclohexane evaporation. The downward dispersion of cyclohexane within the water column is also possible, as evidenced by some increasing concentrations in the middle compartment.

The upper compartment beneath the water surface is exposed to both air and water, resulting in simultaneous volatilisation and dispersion/solubilization. After dispersion/solubilisation occurs, the middle and bottom compartments maintain higher concentrations due to their greater distance from the air–water interface. It can also be noted that the samples collected 30 s after the spill do not contain any cyclohexane in any of the three experiments. Considering that the sampling tube was positioned 1 cm below the surface, these observations suggest that cyclohexane does not dissolve instantaneously, and that a thin slick is formed on the surface during the first minute. This is further supported by the air concentrations measured at the onset of the experiment at a wind speed of 0 m/s (Figure 46).

Future experiments at higher wind speeds could help determine whether enhanced water agitation promotes cyclohexane dissolution. Nonetheless, these results are consistent with the ones from the wind tunnel experiments (section 3.1.4), where evaporation was the predominant process and where no dissolution of cyclohexane in seawater was observed.

3.3.2. Butyl acetate

As previously mentioned, butyl acetate is classified as FED according to the SEBC scheme, suggesting a complex behaviour in water. Upon release into seawater, part of the chemical is expected to form a surface slick and to dissolve within the subsurface water layer, while another part is likely to evaporate and/or volatilize: both dissolution and evaporation are thus competing, with the relative rates governed by environmental conditions such as temperature and salinity.

Figure 47. Cyclohexane (first row), butyl acetate (second row) and methanol (third row) mass distribution (% of the theoretical mass if complete dissolution of the chemical) in the chemistry bench at 0, 3 and 6 m/s. For cyclohexane, more wind favours evaporation rather than dissolution and faster mass homogenisation in the water column.

At a wind speed close to 0 m/s, the surface-water concentrations are in the range of 41,61 mg/L to 589,50 mg/L (Figure 48). The highest concentration measured 30 s after release suggests a direct sampling within the butyl acetate slick. Then, surface concentrations showed no significant decrease nor increase over time. In the middle and bottom water compartments, concentrations range from 1,24 to 55,86 mg/L and from 0,29 to 41,93 mg/L, respectively, and are globally increasing over time (Figure 48; Appendix 4.6). This increase suggests that not only butyl acetate evaporates from the surface but also progressively diffuses into the deeper water layers. Around 3 hours after the spill, the concentrations homogenise throughout the water column, averaging 47 mg/L. Regarding air concentrations, butyl acetate vapours – denser than air – were probably too low and too close to water surface to be detected by the PID sensor positioned above.

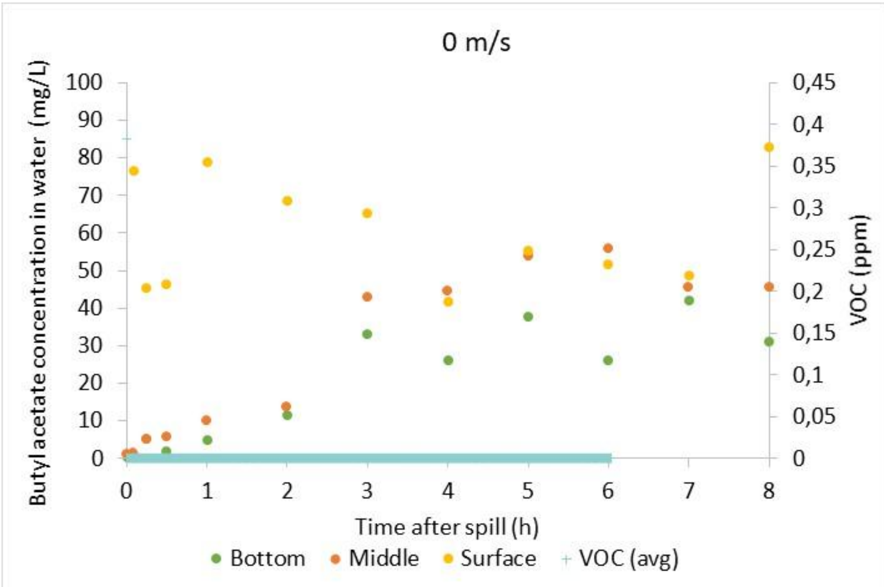

Figure 48. Water and air concentrations of 15 mL butyl acetate at wind close to 0 m/s in the chemistry bench. Concentrations in water homogenise 3 hours after the spill around 47 mg/L.

At a wind speed of 3 m/s, concentrations in the middle and bottom water layers increase during the first 4 hours following the spill (Appendix 4.6; Figure 66), indicating a progressive dissolution of the chemical. Concentrations in the middle and bottom layers range from 0.43 to 62.73 mg/L and from 11.88 to 79.87 mg/L, respectively. As observed above, the butyl acetate concentrations then become uniform across the water column, reaching an average value of around 51 mg/L.

At a wind speed of 6 m/s (Appendix 4.6: Figure 67), concentrations across the water column seem to homogenise approximately 5 hours after the spill, reaching an average of 79 mg/L. During the last 3 hours of the experiment, surface concentrations decrease by 36 %, the middle layer concentrations by 37 %, and bottom-layer by 41 %. The comparable decrease across all layers suggests relatively uniform volatilization of the chemical from the water. Higher wind speeds indeed accelerate both homogenisation volatilisation. In contrast, the duration of the experiment was surely too short to observe similar volatilization dynamics at wind speed close to 0 m/s or of 3 m/s.

The mass detected at the first sampling time (30 s after the spill), suggests that butyl acetate undergoes rapid dissolution into the subsurface upon release (Figure 47). The surface mass increases over time and is higher under low wind conditions (e.g., close to 0 m/s). Conversely, higher wind speeds promote evaporation, as observed the wind tunnel experiments, thereby limiting subsurface dissolution. Over time, the chemical also diffuses in the water column as evidenced by the increasing masses observed in the middle and bottom compartments.

3.3.3. Methanol

Due to its miscibility with water, methanol is expected to undergo more pronounced dissolution than evaporation. When methanol was spilled under a wind speed of 6 m/s, the surface temperature increased from 15.1 °C to 21.4 °C, and surface concentrations were in the range of 259 mg/L to 606 mg/L during the first 8 minutes after the spill (Figure 49). This shows the instantaneous methanol dissolution in water, in agreement with the experimental data observed using the wind tunnel (3.1.3).

Volatilization is also observed from 2 min to 8 min on the mass distribution (Figure 47) as indicated by the decreasing mass at the surface (especially at 0 m/s wind speed). The masses calculated in the middle and the bottom compartments start to increase 8 minutes after the spill, suggesting downward diffusion through the water column. The homogenisation of methanol in the water column is reached approximately one hour after the spill.

At an intermediate wind speed of 3 m/s, concentrations measured 30 s after the spill were of 124, 150 and 158 mg/L at the surface, and in the middle and bottom layers, respectively (Appendix 4.7). Wind-induced mixing, along with the pressure exerted during the introduction of methanol into the tube, could explain the presence of the chemical even in the lower compartments. During the first hour after the spill, the concentrations detected at the surface remained higher than those in the middle and bottom compartments, ranging from 137 to 360 mg/L at the surface compared with 34 to 74 mg/L in the bottom layer.

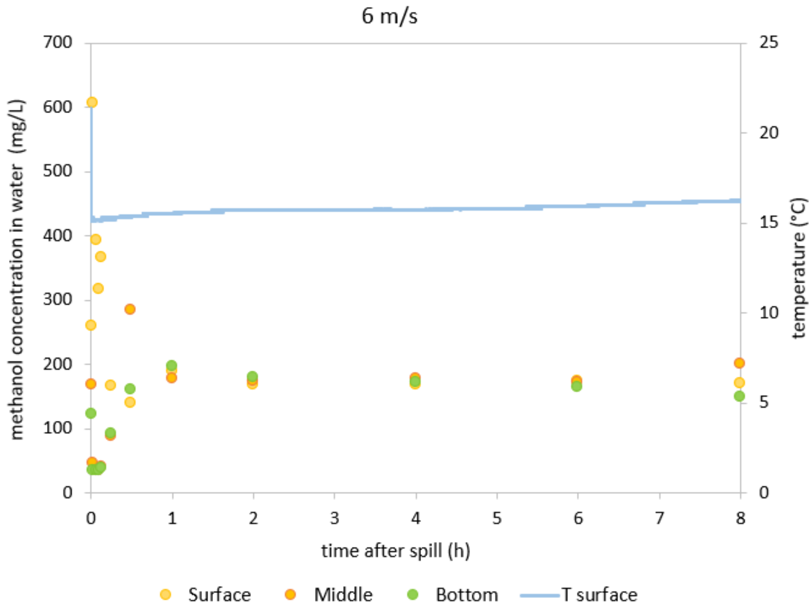

Figure 49. Water concentrations and surface temperature of 15 mL methanol released in 80 L seawater at 6 m/s wind speed. Increase of surface temperature by 6 °C due to methanol solubilisation in seawater.

Due to its lower density compared with water, methanol likely rose into the water column and remained predominantly in the subsurface layer. Methanol concentrations appear to homogenize approximately 4 hours after the spill, reaching around 158 mg/L. Given that the theoretical concentration if all the methanol would dissolve in 80 L of seawater is 148 mg/L, this suggests that homogenisation is not complete and that samples were still directly taken from areas of concentrated pure methanol at the surface.

As for the mass distribution (Figure 47) no relative masses are above 100%, suggesting a better mixing of methanol in seawater. The high mass on the surface at 2 min that decreases until 8 min show the volatilisation of methanol. Direct evaporation of methanol also happens at the moment of the spill, as detected with the Dräger sensor (from 2.7 to 13.9 ppm in the first 40 s after the spill, see Figure 50). After that, no concentrations in air are recorded anymore during the experiment. After 4 hours, the water column becomes homogenized as about 30 % of the mass is found in each compartment.

At a wind close to 0 m/s, no increase in surface temperature is observed, and the surface concentration is 35 mg/L 30 s after the spill. Surface concentrations then increase, ranging from 376 to 1 110 mg/L, and reach a maximum (1 159 mg/L) approximately 8 hours after the spill. During the whole experiment, concentrations detected in the middle and bottom layers remain within the ranges of 34 – 142 and 34 – 42 mg/L, respectively. In the absence of wind-driven mixing, methanol primarily remains dissolved in the subsurface layer. The mass distribution is presented in Figure 47: values exceeding 100% are attributed to sampling directly from areas of concentrated pure methanol at the surface. Between 2 min and 8 min, the subsurface mass decreases, showing evaporation and some diffusion into the water column as the middle mass is increasing at 6 min. Evaporation is the dominant process to occur, consistent with the concentrations detected in air that exceed 100 ppm one hour after the spill (Figure 50). It can be noted that methanol appears to stay close to the surface without reaching the bottom of the water column.

The behaviour of methanol is generally similar at wind speeds of 3 m/s and 6 m/s, with faster homogenisation of the concentrations across the water column with increased with speeds. As for the concentrations detected in air, measured values, reached 16 and 14 ppm during the first minutes at 3 and 6 m/s, respectively (Figure 50).

Given methanol's relative vapor pressure of 1.1, some vapours may have remained close to the water surface, below the detection height of the sensor, and subsequently dispersed by the wind. Nevertheless, it can be seen that the maximum of evaporation happens immediately upon the spill, whereas at near-zero wind speed, evaporation is more gradual, with most methanol volatilizing during the first three hours. A secondary peak in air concentration is also observed before 6 hours, reaching 19.6 ppm, suggesting on-going volatilisation. Without wind, methanol largely remains in the subsurface layer and is more likely to evaporate.

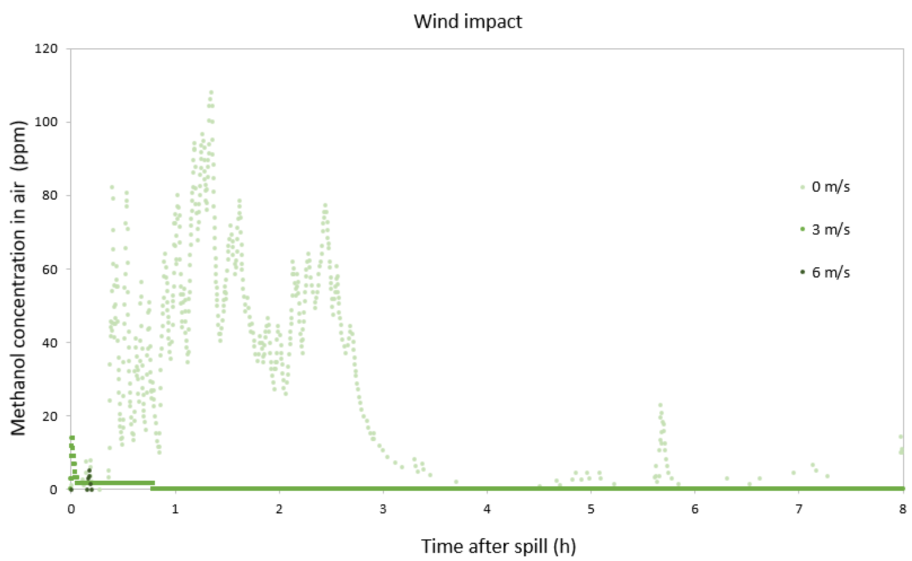

Figure 50. Methanol concentration in air at 0, 3 and 6 m/s wind velocities. Greater evaporation is observed at a wind speed of 0 m/s, while higher wind speeds promote the dissolution of methanol in seawater, hence reducing evaporation.

The behaviour of methanol was also investigated in freshwater (CEDRE 2025b). Experimental tests conducted as part of this study have enabled a more detailed characterisation of methanol behaviour in fresh water, with particular attention paid to the effects of temperature and surface agitation, two parameters that influence the volatilisation and dispersion of the pollutant. In summary, methanol dissolves almost instantaneously after spillage and moderate evaporation is observed. However, this evaporation becomes significant when hydrodynamics is limited, i.e., low water flow, and when water and air temperatures are summer-like. Conversely, in the presence of significant surface agitation, methanol will distribute throughout the water column and evaporation will only be observed in the first initial moments following the spill, consistent with observations from the experiments conducted with seawater.

3.3.4. Overall fate

For all chemicals, the evaporation process was generally faster with stronger wind velocities. This is in agreement with the observations made using the wind tunnel (Section 3.1). As an example, in a water at 15°C and without wind, the slick of cyclohexane disappeared around 3 hours and 40 minutes after the spillage. With 3 m/s wind, the slick only remained 30 min and disappeared instantly with 6 m/s wind speed. Indeed, wind induces air renewal that favours the evaporation process, but not the dissolution one.

Rise in liquid temperature was only observed when methanol was spilled, and not for the other chemicals. The same observation was made with the experiments of the wind tunnel (See section 3.1.7).

In the chemistry bench, methanol is the most impacted chemical by the wind: the surface concentration is more than 3 times higher with 0 m/s wind than for higher wind speeds. Consequently, the bottom and middle concentrations are higher with increasing wind speed as it promotes mixing into the lower compartments. For butyl acetate, a stronger wind means a greater dissolution, in every compartments. The effect of wind on methanol and butyl acetate is comparable in the middle and bottom compartments, where higher wind speeds meant higher concentrations.

Cyclohexane concentrations in water remain largely unaffected by wind velocity, with evaporation dominating as the primary process, consistent with both its SEBC classification and wind tunnel observations. Nevertheless, concentrations in the bottom compartment are slightly higher at 0 m/s (Figure 47, Figure 51), suggesting that increased wind promotes slick evaporation and reduces the time available for cyclohexane to penetrate deeper into the water column.

In summary, methanol rapidly dissolves in seawater, with dissolution further accelerated by wind followed by further volatilisation. Cyclohexane forms a surface slick that evaporates independently of wind speed; however, stronger winds enhance evaporation and reduce its dissolution. Butyl acetate, which floats at the surface, exhibits moderate wind sensitivity, characterized by limited dissolution and evaporation.

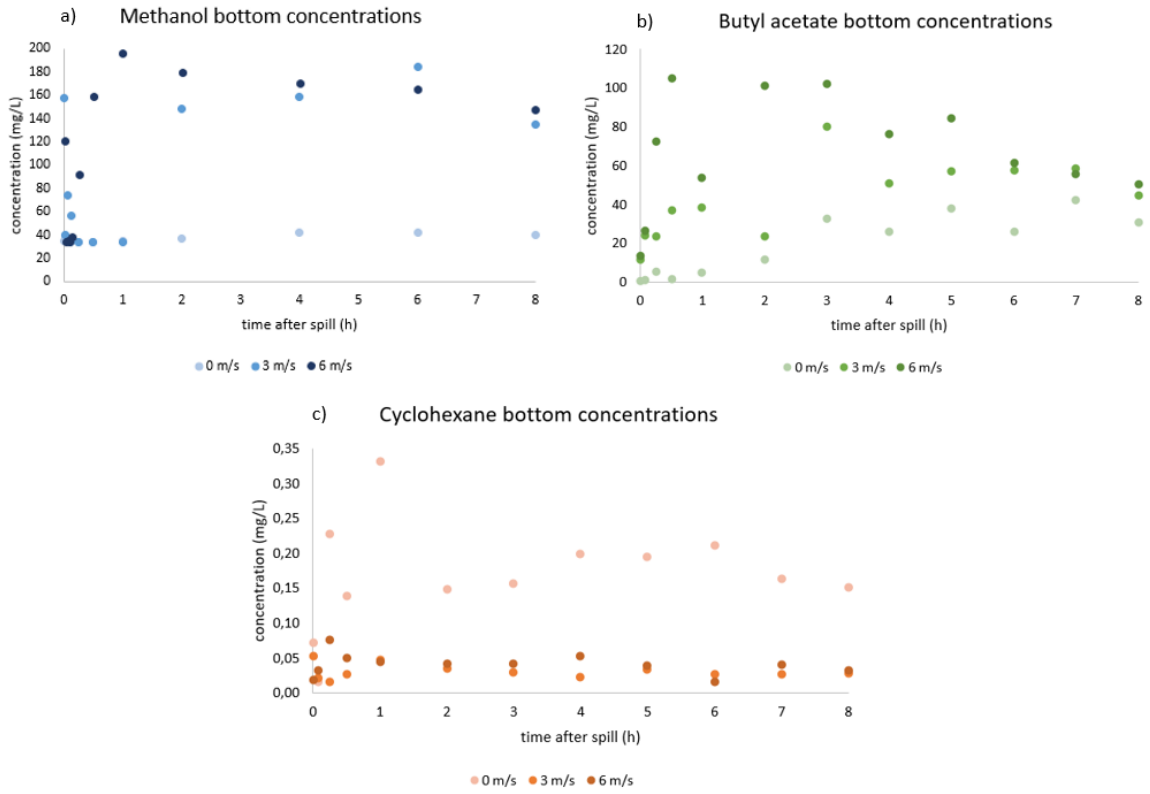

Figure 51. Concentrations in water at the bottom of the chemistry bench for a) methanol, b) butyl acetate and c) cyclohexane.

3.3.5. Future improvements

The experiments revealed opportunities to improve CEDRE's chemistry bench. The current UV lamp – intended to simulate solar radiation – was not used due to its excessive power, which would artificially accelerate evaporation of the chemicals tested. To address this, a lower-power lamp and a modified lid with openings for sensors and sampling tubes could be implemented. Additionally, replacing the spillage system with fixed stainless-steel tubes would ensure consistent sampling depths, while mounting temperature probes on these tubes would standardize measurement locations (Figure 52).

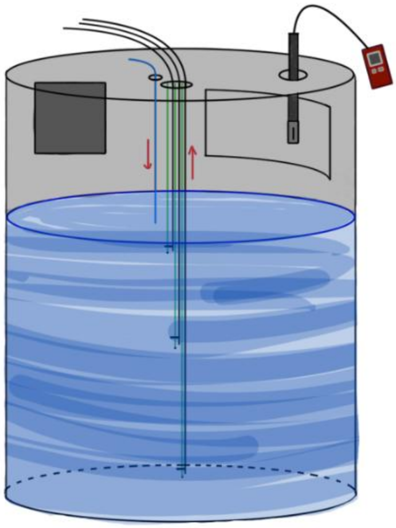

Figure 52. Chemistry test bench with adapted lid to place any captors or tubes. Sampling tubes could also be improved by adding a system to fix the temperature probes.

The gas detection to assess the evaporation of a chemical was also difficult with the existing set-up. The PID sensor was probably placed too high to capture any vapours. Placing the PID sensor in the hose where the vapours are escaping the water reservoir might solve this issue.

4. Conclusion and recommendations

This work provides experimental data on the evaporation and dissolution of various chemicals – cyclohexane, methanol, butyl acetate, and aqueous ammonia – in seawater and freshwater. Each chemical exhibited distinct theoretical SEBC behaviours, which were confirmed experimentally.

The wind tunnel experiments yielded evaporation rates under different experimental conditions, consistently showing that higher wind speeds promote evaporation.

Tests using CEDRE's experimental columns on methane demonstrated that at low leak rates and high depths, methane dissolves rapidly in water, with bubbles reaching the surface primarily composed of oxygen and nitrogen. At higher leak rates and larger plumes, methane is more likely to reach the surface, posing a fire risk of the gas potential gas cloud formed at the surface.

In accidental seawater spills, methanol is expected to dissolve quickly and subsequently evaporate. Butyl acetate floats and evaporates slowly while mixing with seawater, whereas cyclohexane evaporates rapidly without significant mixing.

Bibliography

Alleman, JE. 1998. 'Free Ammonia-Nitrogen Calculator & Information'. *Purdue University*. https://www.engineering.iastate.edu/%7Ejea/w3-research/free-ammonia/nh3.html.

Bonn Agreement. 1994. 'Hazardous Material Spills. Counter Pollution Manual for Incidents Involving Hazardous and Noxious Substances (HNS)'. *London*.

Braconnier, R, J Chaineaux, J Triolet, J.R Fontaine, and B Salle. 2008. 'Mesures Du Flux d'évaporation de Liquides Volatils Dans Des Ambiances de Travail - INRS'. *Hygiène et Sécurité Du Travail*, no. 212: 1–11.

Cattafesta, Louis, Chris Bahr, and Jose Mathew. 2010. 'Fundamentals of Wind-Tunnel Design'. *Encyclopedia of Aerospace Engineering*, 1–10.

CEDRE. 2023. 'D2.3 – Experimental Study on Evaporation from a Chemical Slick'. *MANIFESTS Project*, 1–63.

CEDRE. 2024. *Étude Bibliographique et Expérimentale Sur Les Nouvelles Énergies de Propulsion Des Navires. Rapport de Stage Interne, 44.* S.2024.08.

CEDRE. 2025a. *Étude Du Comportement Des Produits Chimiques Déversés En Mer. R.25.47.C/35025*. 1–67.

CEDRE. 2025b. *Fate of Methanol When Spilled in a River and Risk Analysis - Insights for Emergency Response. R.25.43.C/35923*. 1–51.

Corruchaga, Agustín, Oriol Casal, Adriana Palacios, and Joaquim Casal. 2022. 'Influence of Wind Speed and Ammonia Concentration on Its Evaporation Rate from Aqueous Solution Spills'. *Journal of Loss Prevention in the Process Industries* 76 (May): 104750. https://doi.org/10.1016/j.jlp.2022.104750.

Davenport, A.G. 1965. *The Relationship of Wind Structure to Wind Loading*. Proceedings of Conference 'Wind effects on buildings and structures' National Physical Laboratory 26-28 June 1963 HMSO, 53–102.

Decelle, Lucas, and Kevin Nicolas. 2017. 'Conception d'une Soufflerie de Démonstration.' *Projet de Fin d'étude Court. Polytech Lille*, 1–19.

Dong, Haoliang, Cise Unluer, En-Hua Yang, and Abir Al-Tabbaa. 2017. 'Synthesis of Reactive MgO from Reject Brine via the Addition of NH4OH'. *Hydrometallurgy* 169 (May): 165–72. https://doi.org/10.1016/j.hydromet.2017.01.010.

Edwards, Thea M., Holly J. Puglis, Douglas B. Kent, Jonathan López Durán, Lillian M. Bradshaw, and Aïda M. Farag. 2024. 'Ammonia and Aquatic Ecosystems – A Review of Global Sources, Biogeochemical Cycling, and Effects on Fish'. *Science of The Total Environment* 907 (January): 167911. https://doi.org/10.1016/j.scitotenv.2023.167911.

Giraud, William, Amélie Thomas, Pierre Richard, Sophie Chataing, and Stéphane Le Floch. 2017. 'An Innovative Experimental Device to Assess the Behavior of a Chemical under Controlled Environmental Parameters'. *International Oil Spill Conference Proceedings* 2017 (1): 1287–303. https://doi.org/10.7901/2169-3358-2017.1.1287.

Gonczi, Georges. 2005. *Comprendre La Thermodynamique*. Ellipses.

Hamzah, Hudhaifa, Laith M Jasim, Ali Alkhabbaz, and Besir Sahin. 2021. 'Role of Honeycomb in Improving Subsonic Wind Tunnel Flow Quality: Numerical Study Based on Orthogonal Grid'. *Journal of Mechanical Engineering Research and Developments* 44: 352–69.

Heymes, Frédéric, Laurent Aprin, Aurélia Bony, Serge Forestier, Stefano Cirocchi, and Gilles Dusserre. 2013. 'An Experimental Investigation of Evaporation Rates for Different Volatile Organic Compounds'. *Process Safety Progress* 32 (2): 193–98.

Johannes, L., L. Mölder, and H. Tamvelius. 1997. 'Hydrolysis of Butyl Acetate'. *Oil Shale* 14 (4): 579–90. https://doi.org/10.3176/oil.1997.4.03.

Laporte, David. 2010. 'A Surface Roughness Parameterization Study near Two Proposed Windfarm Locations in Southern Ontario'. *MSC Thesis*, August 24, 82.

Lepers, Ludovic, Ligia Pinto, Knut-Frod Dagestad, Vincent Gouriou, Sébastien Legrand, and William Giraud. 2023. 'D4.4 – Model Validation'. *MANIFESTS Project*, 1–45. https://manifests-project.eu/documents/24/MANIFESTS_D4.4_-_Models_validation.pdf.

Oke, Timothy R. 2002. *Boundary Layer Climates*. Second edition. Routledge.

Oke, T.R. 1987. 'Boundary Layer Climates, Methuen & Co'. *Ltd, London,*.

Olsen, Jan Erik, Dorien Dunnebier, Emlyn Davies, Paal Skjetne, and John Morud. 2017. 'Mass Transfer between Bubbles and Seawater'. *Chemical Engineering Science* 161: 308–15.

Poole, Colin. 2005. *Gas Chromatography*. 2nd ed. Elsevier.

Price, K.S, G.T. Waggy, and R.A. Conway. 1974. 'Brine Shrimp Bioassay and Seawater BOD of Petrochemicals'. *Journal of Water Pollution Control Federation* 46: 63–77.

World Health Organization. 2005. 'Butyl Acetates.' *Concise International Chemical Assessment Document 64*. https://www.inchem.org/documents/cicads/cicads/cicad64.htm.

Annexes

4.1. Wind tunnel methanol

4.1.1. Pure 60 mL

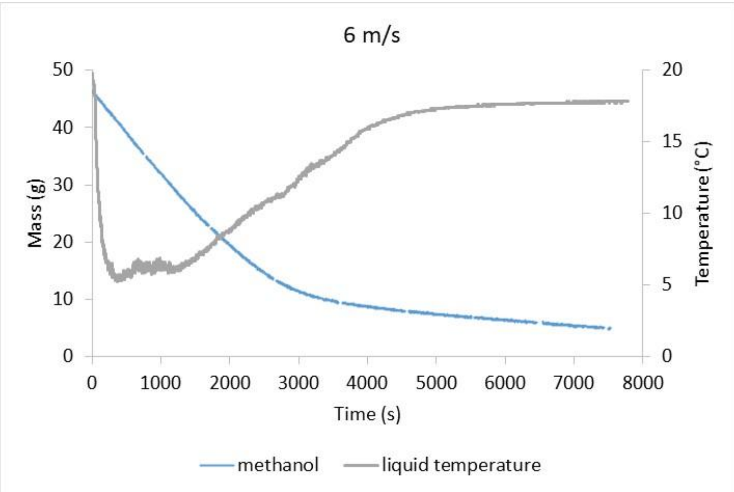

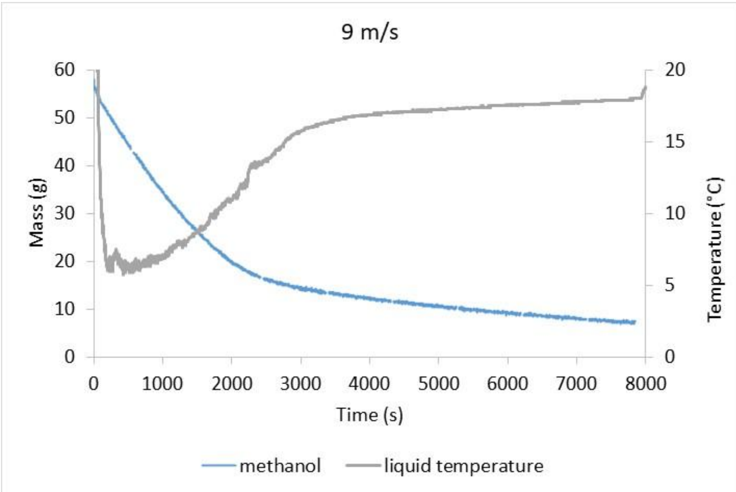

Figure 53. Evaporation of pure methanol at 6 and 9 m/s.

4.1.2. 150 mL on seawater

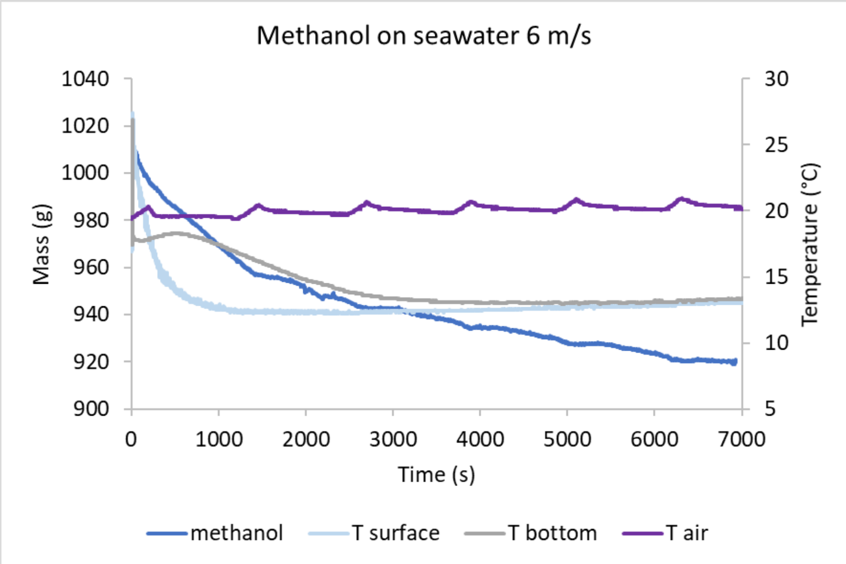

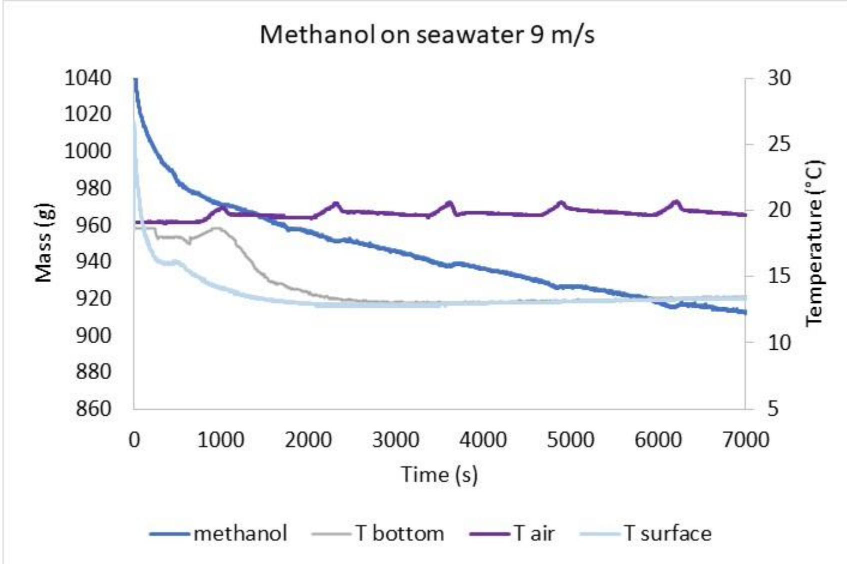

Figure 54. 150 mL of methanol released on seawater at 6 and 9 m/s.

4.1.3. 60 mL on seawater

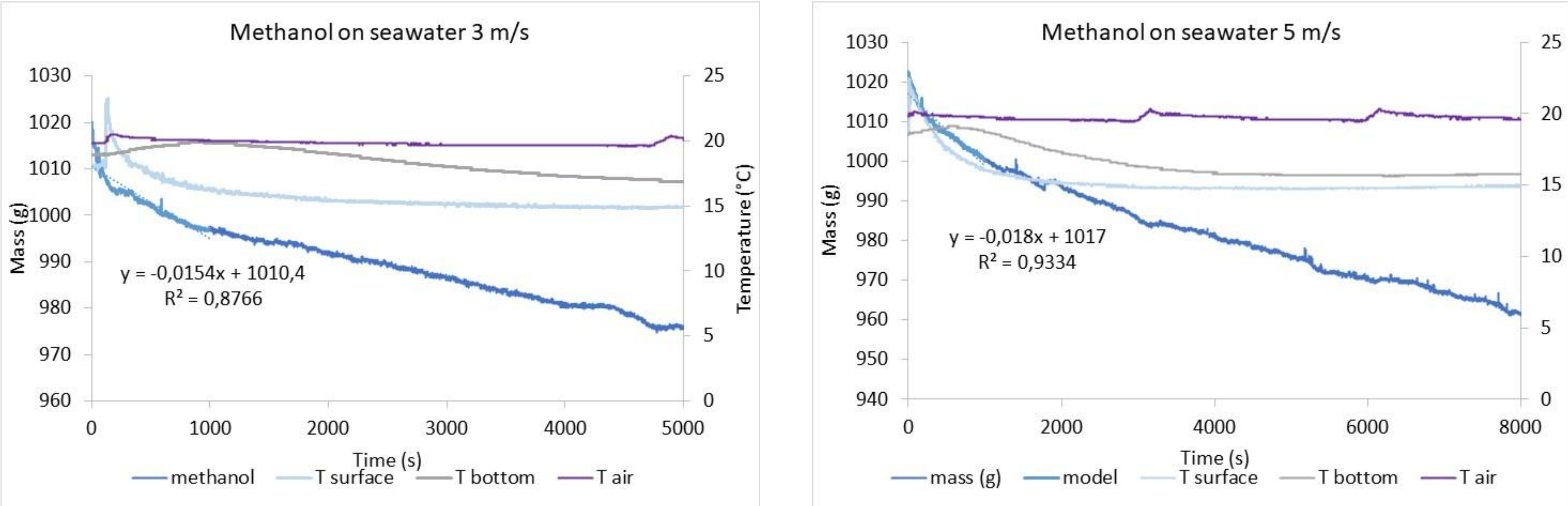

Figure 55. 60 mL of methanol released on seawater at 3 and 5 m/s.

4.1.4. 60 mL on freshwater

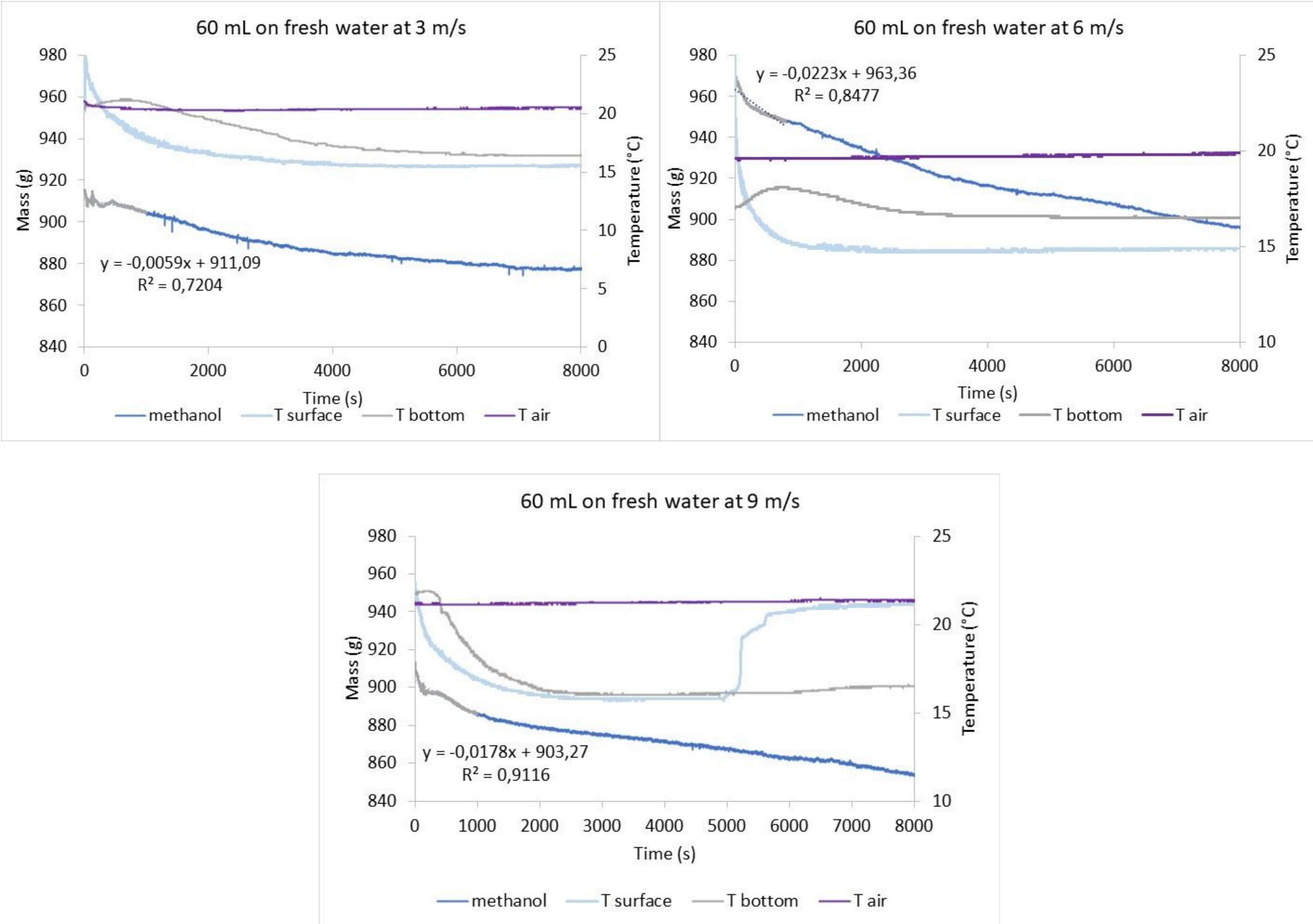

Figure 56. 60 mL of methanol released on freshwater at 3, 6 and 9 m/s.

4.2. Wind tunnel cyclohexane

4.2.1. Pure 60 mL

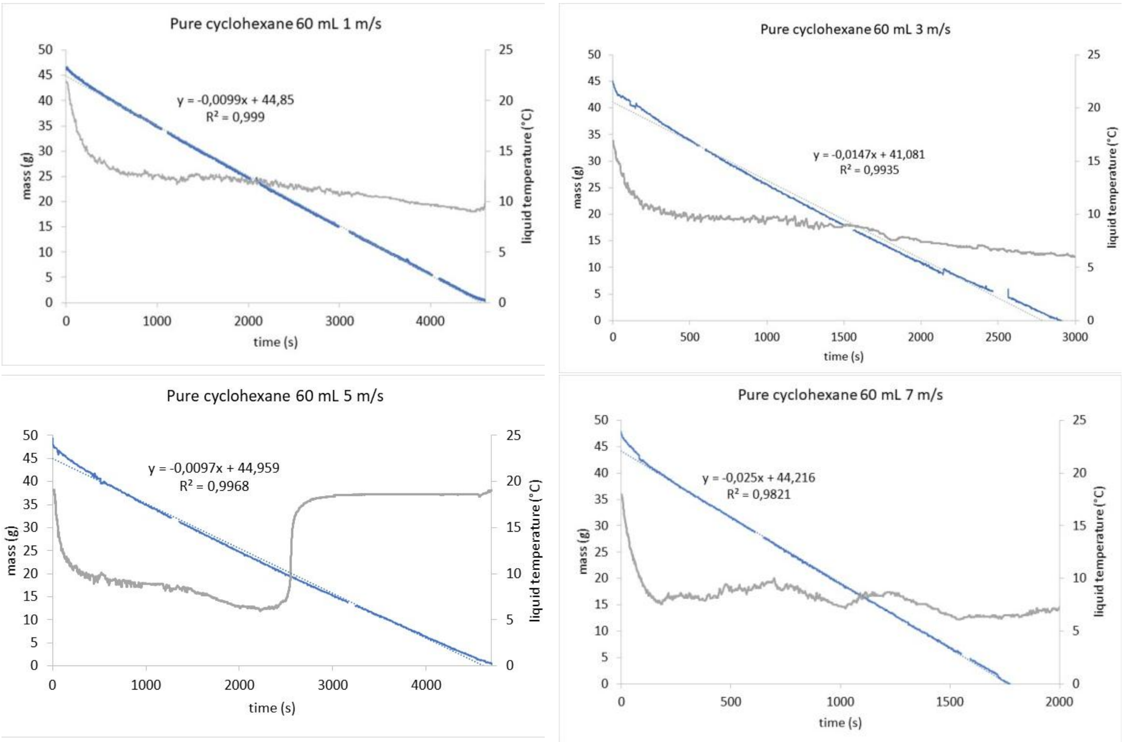

Figure 57. Evaporation of 60 mL of pure cyclohexane at different wind speeds.

4.2.2. 60 mL on seawater

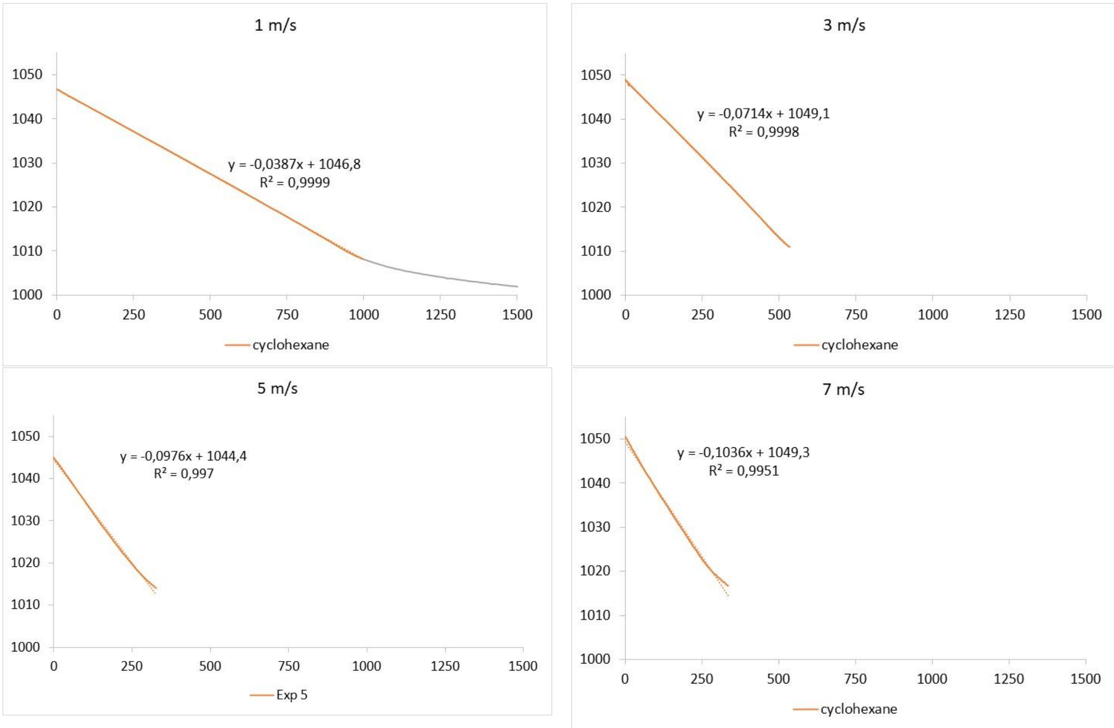

Figure 58. Evaporation of 60 mL of cyclohexane on seawater at different wind speeds.

4.2.3. 150 mL on seawater

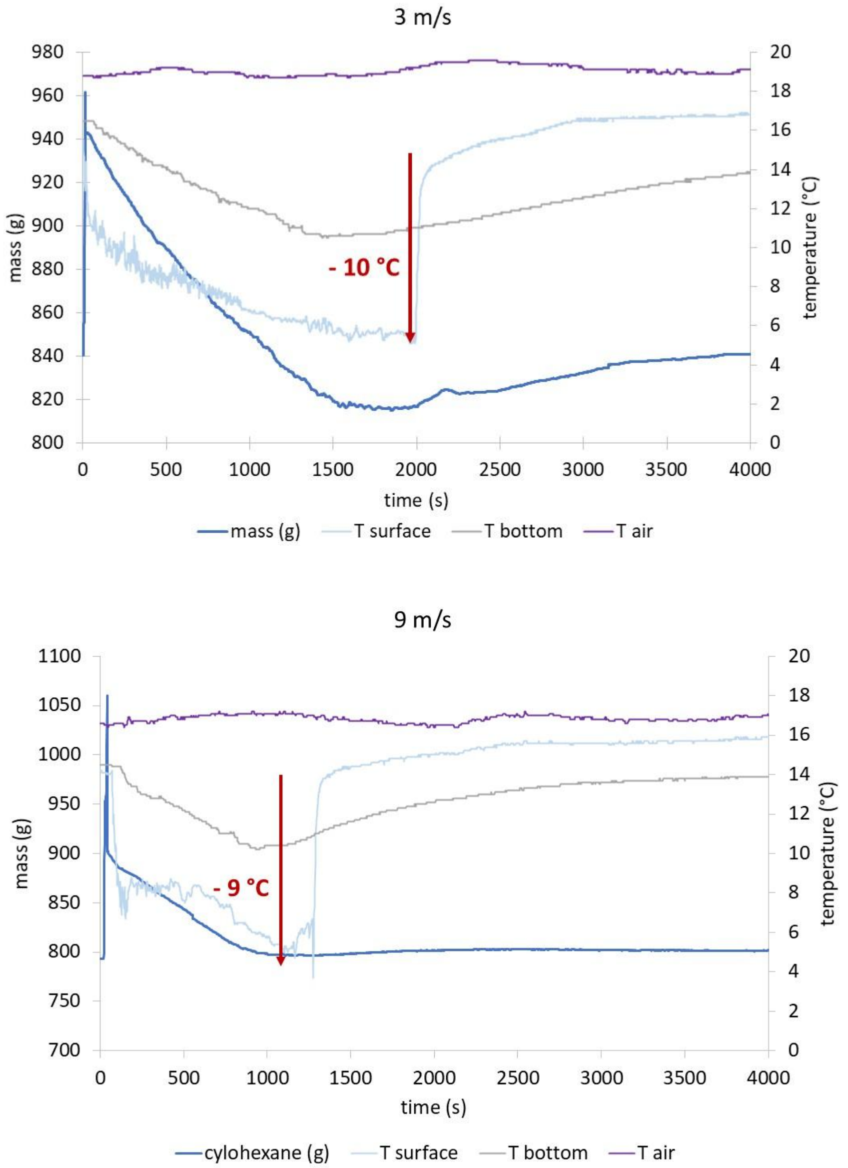

Figure 59. 150 mL of cyclohexane released on seawater at 3 and 9 m/s.

4.3. Wind tunnel butyl acetate

4.3.1. Pure 10 mL

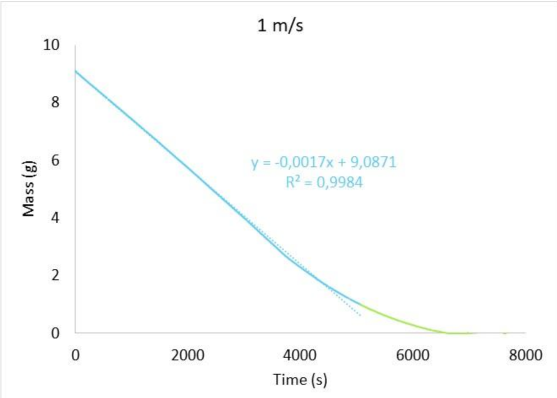

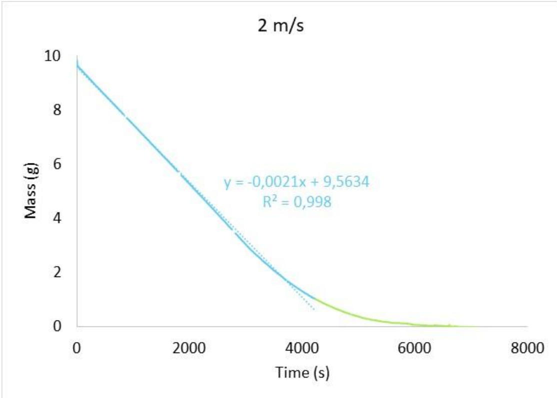

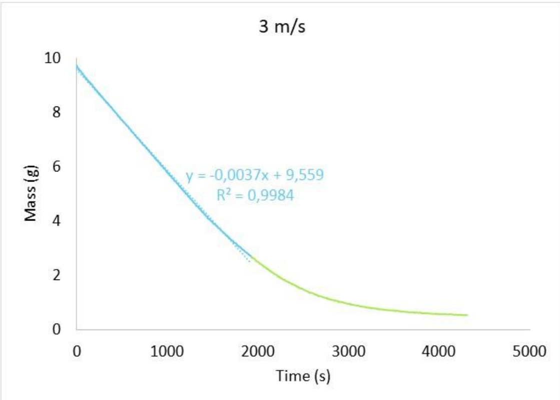

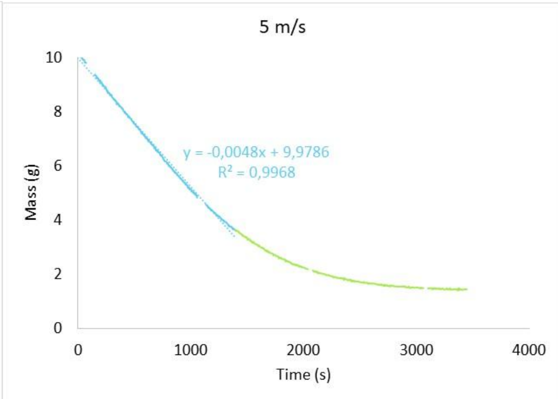

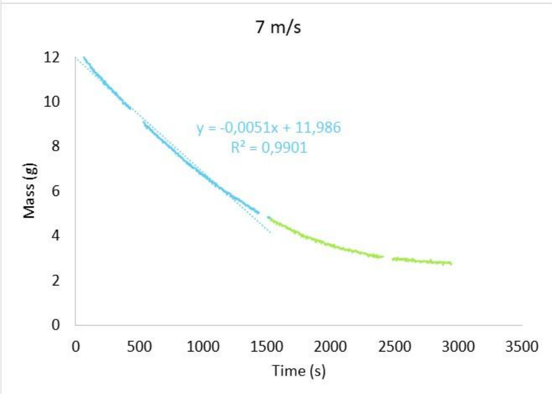

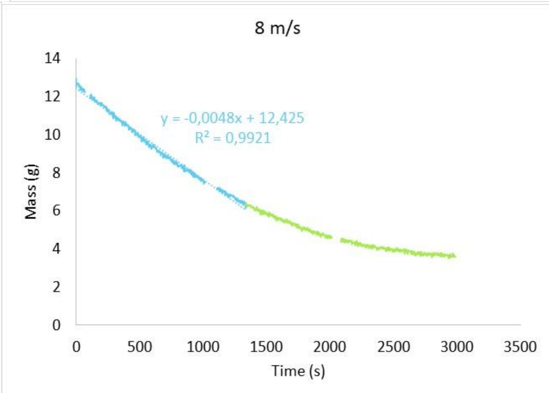

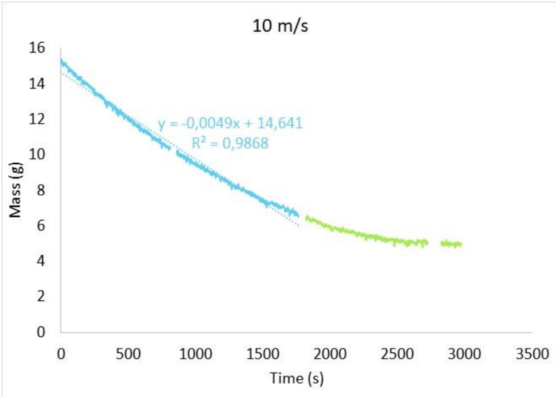

Figure 60. Pure butyl acetate evaporation.

4.3.2. 60 mL on seawater

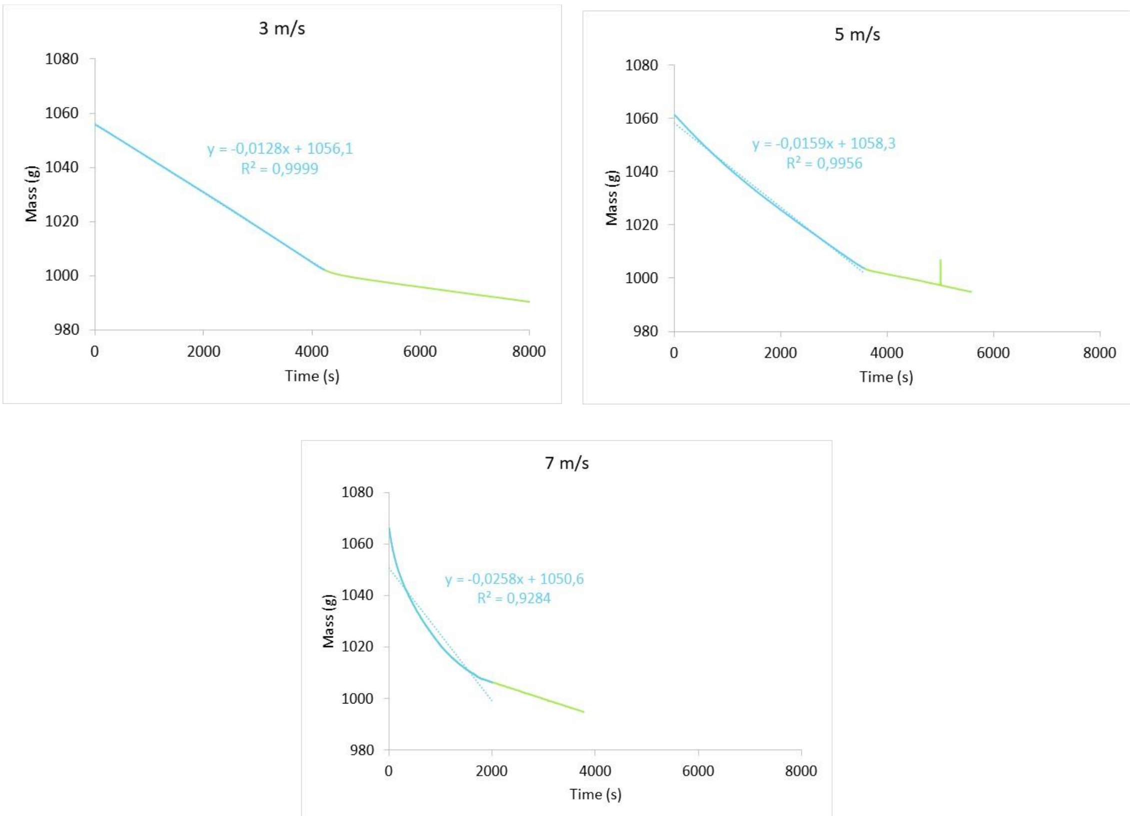

Figure 61. Evaporation of butyl acetate (60 mL) on seawater.

4.3.3. 150 mL on seawater

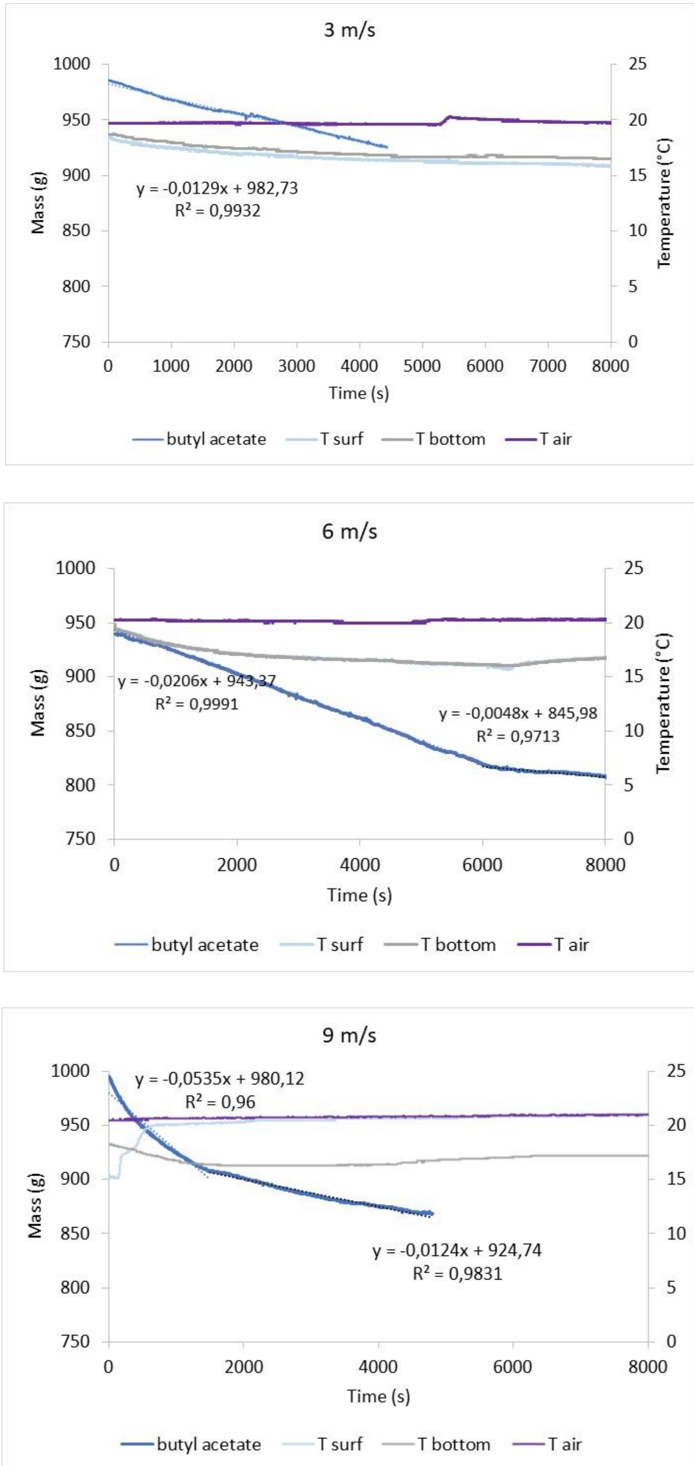

Figure 62. 150 mL of butyl acetate poured on seawater.

4.4. Wind tunnel ammonia

4.4.1. Ammonia solutions released in freshwater

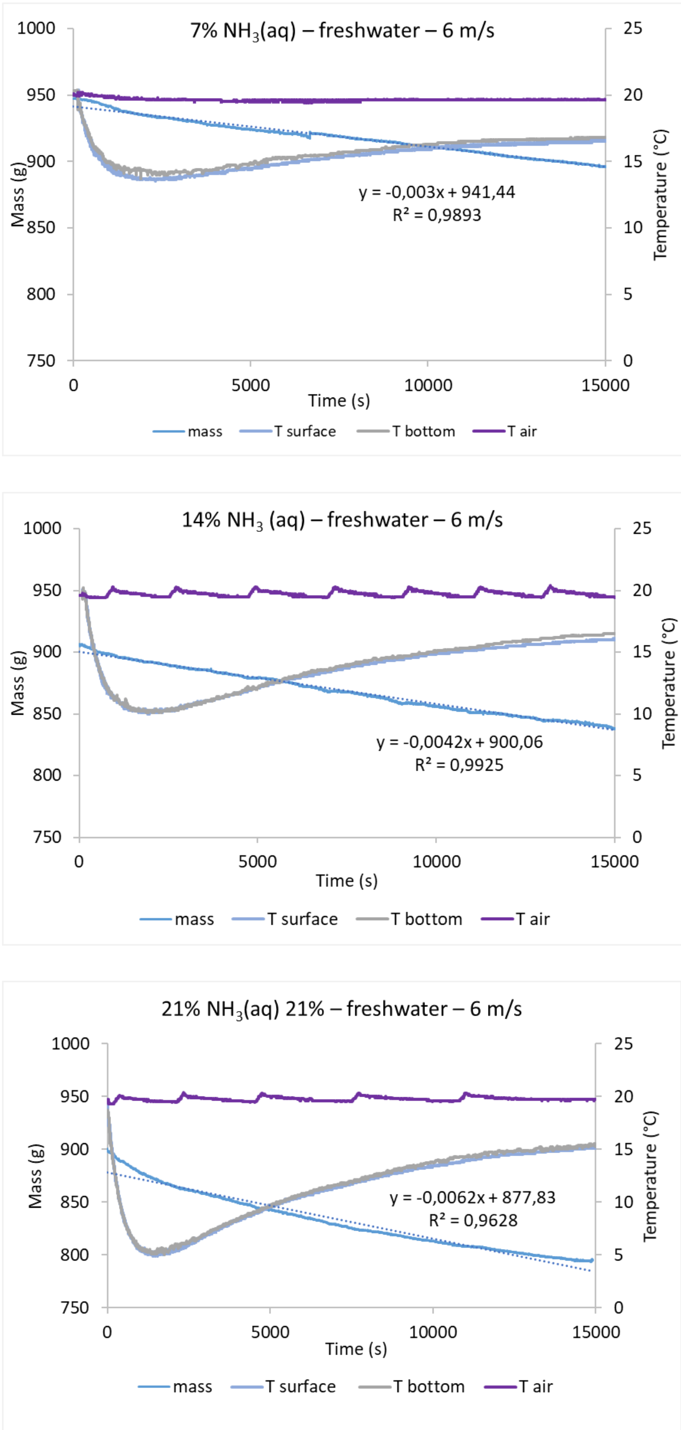

Figure 63. Evaporation of aqueous ammonia solutions (7, 14 and 21%) in freshwater at 6 m/s and associated liquid and air temperatures.

4.4.2. Ammonia solutions released in seawater

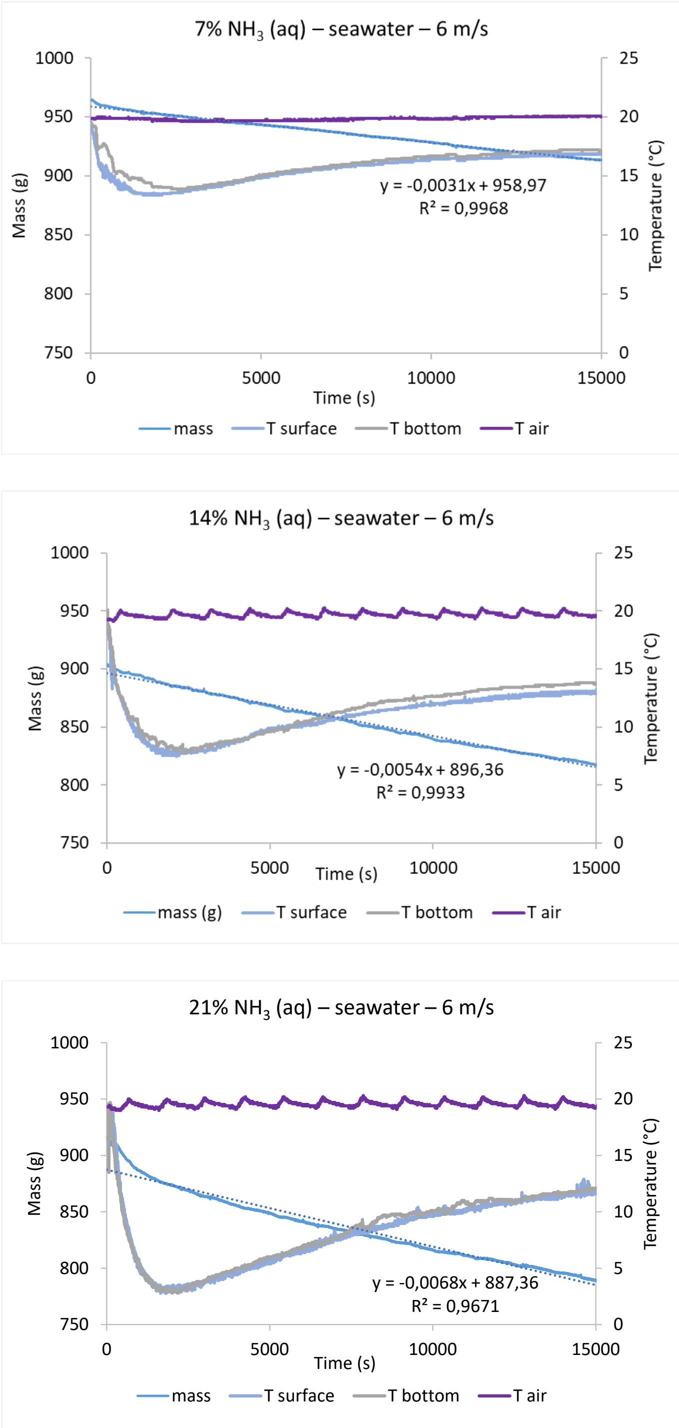

Figure 64. Evaporation of aqueous ammonia solutions (7, 14 and 21%) in seawater at 6 m/s and associated liquid and air temperatures.

4.5. Chemistry bench cyclohexane

Table 23. Cyclohexane concentrations in water. 150 mL cyclohexane in 80 L seawater at 15 °C.

0 m/s	Sampling	Time afer spill	Surface Concentration (mg/L)	Middle Concentration (mg/L)	Bottom Concentration (mg/L)
	1	30 s	0,05	0,08	0,07
	2	5 min	0,21	0,07	0,02
	3	15 min	0,17	0,25	0,23
	4	30 min	0,02	0,02	0,14
	5	1 h	0,02	0,02	0,33
	6	2 h	0,01	0,12	0,15
	7	3 h	0,06	0,13	0,16
	8	4 h	0,02	0,10	0,20
	9	5 h	0,02	0,15	0,19
	10	6 h	0,02	0,18	0,21
	11	7 h	0,04	0,13	0,16
	12	8 h	0,06	0,12	0,15
3 m/s	Sampling	Time afer spill	Surface Concentration (mg/L)	Middle Concentration (mg/L)	Bottom Concentration (mg/L)
	1	30 s	0,01	0,03	0,05
	2	5 min	0,02	0,01	0,02
	3	15 min	0,03	0,02	0,02
	4	30 min	0,01	0,02	0,03
	5	1 h	0,03	0,04	0,05
	6	2 h	0,03	0,03	0,03
	7	3 h	0,03	0,03	0,03
	8	4 h	0,02	0,02	0,02
	9	5 h	0,01	0,03	0,03
	10	6 h	0,02	0,03	0,03
	11	7 h	0,01	0,03	0,03
	12	8 h	0,03	0,03	0,03
6 m/s	Sampling	Time afer spill	Surface Concentration (mg/L)	Middle Concentration (mg/L)	Bottom Concentration (mg/L)
	1	30 s	0,02	0,02	0,02
	2	5 min	0,02	0,02	0,03
	3	15 min	0,03	0,06	0,08
	4	30 min	0,03	0,05	0,05
	5	1 h	0,03	0,05	0,04
	6	2 h	0,03	0,04	0,04
	7	3 h	0,03	0,07	0,04
	8	4 h	0,03	0,05	0,05
	9	5 h	0,01	0,03	0,04
	10	6 h	0,01	0,04	0,02
	11	7 h	0,02	0,01	0,04
	12	8 h	0,02	0,03	0,03

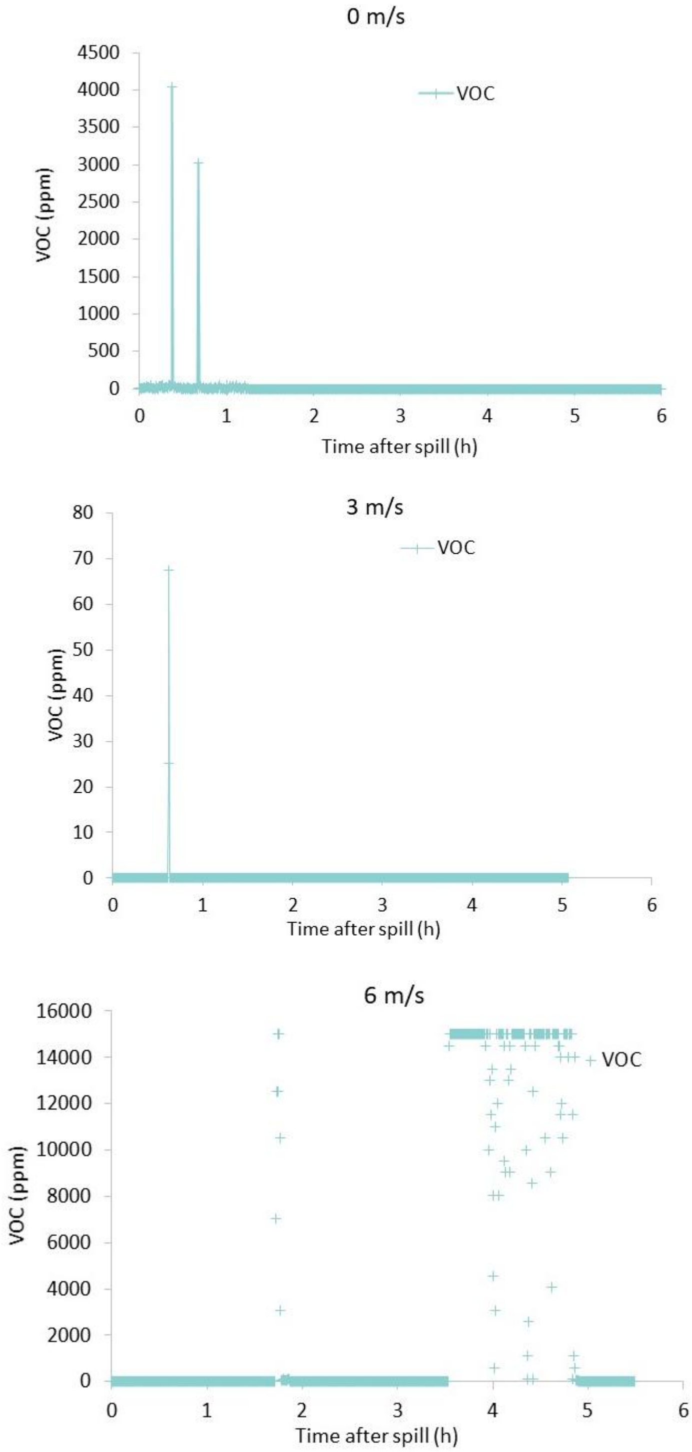

Figure 65. Cyclohexane concentration in the air (ppm) at 0, 3 and 6 m/s.

4.6. Chemistry bench butyl acetate

Table 24. Butyl acetate concentrations in water. 150 mL butyl acetate in 80 L seawater at 15 °C.

0 m/s	Sampling	Time afer spill (h)	Surface Concentration (mg/L)	Middle Concentration (mg/L)	Bottom Concentration (mg/L)
	1	30 s	589,50	1,24	0,2855
	2	5 min	76,63	1,42	1,00
	3	15 min	45,35	5,03	5,32
	4	30 min	46,43	5,71	1,91
	5	1 h	78,94	10,10	4,98
	6	2 h	68,63	13,62	11,63
	7	3 h	65,24	42,96	32,99
	8	4 h	41,61	44,42	26,19
	9	5 h	55,35	53,94	37,77
	10	6 h	51,82	55,86	26,24
	11	7 h	48,57	45,57	41,93
	12	8 h	82,70	45,63	31,17
3 m/s	Sampling	Time afer spill (h)	Surface Concentration (mg/L)	Middle Concentration (mg/L)	Bottom Concentration (mg/L)
	1	30 s	205,04	0,43	11,88
	2	5 min	14,65	2,45	23,96
	3	15 min	28,50	13,68	23,76
	4	30 min	55,97	35,33	37,19
	5	1 h	44,45	52,94	38,65
	6	2 h	54,11	44,70	23,63
	7	3 h	44,96	30,71	79,87
	8	4 h	48,24	54,96	51,20
	9	5 h	63,25	59,96	56,85
	10	6 h	65,97	61,21	57,65
	11	7 h	67,56	58,99	58,06
	12	8 h	59,93	62,73	44,52
6 m/s	Sampling	Time afer spill (h)	Surface Concentration (mg/L)	Middle Concentration (mg/L)	Bottom Concentration (mg/L)
	1	30 s	421,61	0,66	13,75
	2	5 min	39,17	17,27	26,34
	3	15 min	48,20	59,12	72,82
	4	30 min	36,73	80,25	104,84
	5	1 h	82,59	55,74	53,86
	6	2 h	115,00	22,90	101,51
	7	3 h	78,85	86,89	102,21
	8	4 h	135,05	83,85	76,15
	9	5 h	72,35	80,22	84,20
	10	6 h	63,52	64,83	61,70
	11	7 h	54,36	57,18	55,73
	12	8 h	45,98	50,48	50,06

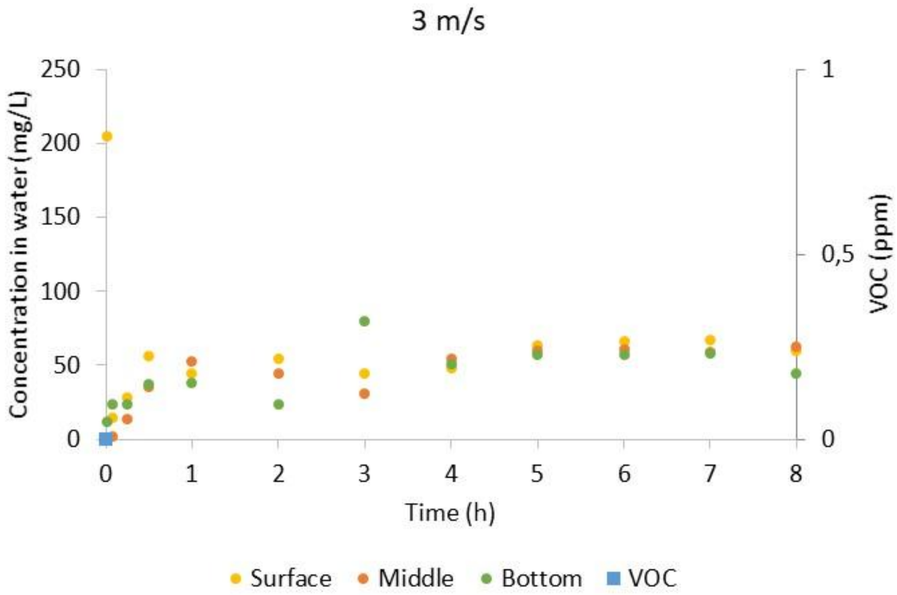

Figure 66. Water and air concentrations of 15 mL butyl acetate at 3 m/s in the chemistry bench. Concentrations in water homogenise 4 hours after the spill around 51 mg/L.

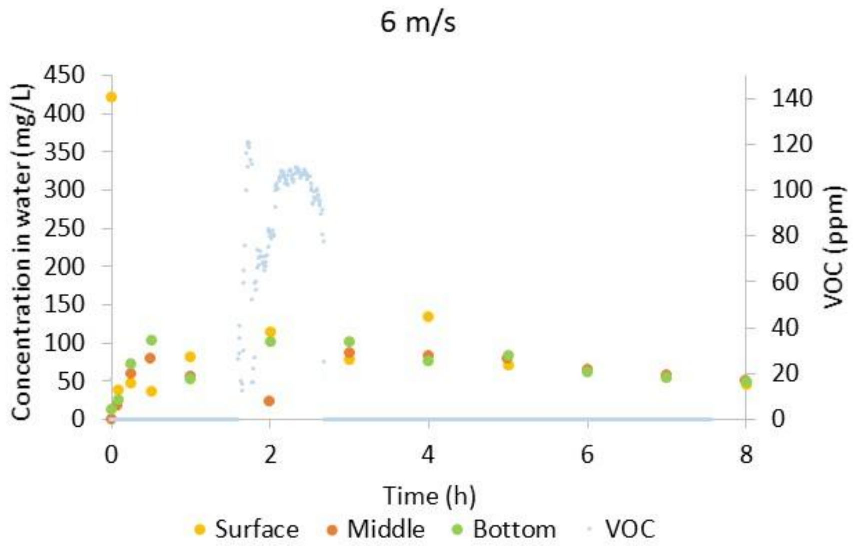

Figure 67. Water and air concentrations of 15 mL butyl acetate at 6 m/s in the chemistry bench. Concentrations in water homogenise 5 hours after the spill around 79 mg/L.

4.7. Chemistry bench methanol

Table 25. Methanol concentrations in water. 15 mL methanol in 80 L seawater at 15 °C.

0 m/s	Sampling	Time afer spill (h)	Surface Concentration (mg/L)	Middle Concentration (mg/L)	Bottom Concentration (mg/L)
	1	30 s	35	34	35
	2	2 min	935	38	38
	3	4 min	635	53	36
	4	6 min	538	142	35
	5	8 min	376	35	34
	6	15 min	601	35	34
	7	30 min	728	36	34
	8	1 h	914	34	34
	9	2 h	1115	40	37
	10	4 h	523	40	42
	11	6 h	1110	42	42
	12	8 h	1159	44	40
3 m/s	Sampling	Time afer spill (h)	Surface Concentration (mg/L)	Middle Concentration (mg/L)	Bottom Concentration (mg/L)
	1	30 s	124	150	158
	2	2 min	442	35	40
	3	4 min	226	101	74
	4	6 min	206	34	34
	5	8 min	137	38	56
	6	15 min	360	35	34
	7	30 min	260	34	34
	8	1 h	175	106	34
	9	2 h	233	120	148
	10	4 h	180	207	159
	11	6 h	128	131	184
	12	8 h	127	169	135,00
6 m/s	Sampling	Time afer spill (h)	Surface Concentration (mg/L)	Middle Concentration (mg/L)	Bottom Concentration (mg/L)
	1	30 s	259	167	121
	2	2 min	606	46	34
	3	4 min	392	34	35
	4	6 min	316	34	34
	5	8 min	365	41	38
	6	15 min	166	89	92
	7	30 min	140	283	160
	8	1 h	188	178	196
	9	2 h	167	173	180
	10	4 h	167	178	171
	11	6 h	173	172	165
	12	8 h	169	200	147,89